An Initial Electrochemical Study Into the (Bio)Leaching of Chalcopyrite

by

Mpho Namane
BSc. (Hons) Chemistry
University of Cape Town
Rondebosch
7701
2008

Approved:

J.Petersen
_____
Thesis Adviser

S.T.L Harrison
_____
Thesis Adviser

J-P. Franzidis
_____
Thesis Adviser

A Thesis submitted to the
Faculty of Engineering and Build Environment,
University of Cape Town in fulfilment of the
requirements for the degree of
MASTER OF SCIENCE
Major Subject: CHEMICAL ENGINEERING
December, 2011

I know the meaning of plagiarism and declare that all the work in the document, save for that which is properly acknowledged, is my own.

Signature: _____ Date: 22 December 2011

Dedicate to my
mother,
Madikotsi Pauline Namane,
brothers,
Moahlodi Vincent Namane,
and the late
Lehlohonolo Irish Namane
for being my pillars of strength,
always inspiring greatness,
seeing the potential in me,
and
for always being the driving force in pursue of my dreams”

Acknowledgements

First and foremost, I would like to thank my Ultimate Creator for the strength that I had towards the work presented here and throughout my whole career.

I would like to express my greatest gratitude to my supervisor, Jochen Petersen for being such an instrumental figure for the work presented in this thesis, for his advice and encouragement throughout the project. From where we started the project to this document presented herein, it has been a journey that I can proudly say was worth every moment and experience. A very big thank you is also extended to the Minerals to Metals Research Initiative's Jean-Paul Franzidis for securing funding for this work. Much admiration to Thebe Mokone for his continued guidance and input throughout this journey, even at the last stages, he still came through for me.

Also would like to express my heartfelt gratitude to the CeBER research group for providing lab space for the experimental work. To Frances Pockock, for her constant assistance in the labs, I would like to thank her from the bottom of my heart. I would like to also acknowledge the Minerals to Metals and CeBER research groups and colleagues.

I would like to extend appreciation to Annie Potter and Kelly-Ann Whitehead for their work on the chrono-amperometric data from their final year thesis project.

I would also like to acknowledge the electrical workshop, mechanical workshop staff from both Chemical Engineering and Geology department.

Finally I would like to put forward my gratitude to my family and friends for their constant support throughout the duration of my studies.

Abstract

Hydrometallurgical methods are increasingly considered as alternatives to conventional pyrometallurgical techniques for extraction of metals from mineral ores. Chalcopyrite is a key copper mineral due to its abundance on earth. However, due to its refractory nature in sulfate leaching systems, a viable hydrometallurgical route for its extraction remains elusive. Sulfate leaching systems for dissolution of chalcopyrite would be attractive due to their simplicity and relatively low cost, especially in heap systems. The key concern encountered in these kinds of systems is that they show very slow leaching kinetics, which are thought to be caused by the formation of a passivation layer on the surface of the mineral. Chalcopyrite dissolution has also been shown to follow electrochemical corrosion type reactions. Electrochemical techniques can thus be employed as a fundamental tool to assist in understanding dissolution of chalcopyrite. Specific techniques that are commonly employed include voltammetry, and current-time studies at different potentials, known as chrono-amperometry. These studies are significant in elucidating the behaviour of the pre-passive and/or passive behaviour during chalcopyrite dissolution.

The work in this present thesis is presented as an initial study to commission the potentiostat instrument, investigate the common trends that are observed in running potential controlled (voltammetric) studies of chalcopyrite and compare them to those reported in literature, and investigate the electrochemical behaviour under different reaction conditions. At first electrodes were designed to new specifications and the previously acquired potentiostat was tested and commissioned by performing reproducibility studies in acidic media. These studies were then continued to further investigate the effect of scan rate during linear sweep voltammetry (LSV) on the observed curves. It was observed that the slowest scan rate (5, 2, 1 mV/s) studied showed much clearer and detailed curves, and more defined peaks in sweeps.

Subsequently the electrochemical behaviour of chalcopyrite electrodes in acidic iron oxidizing media was investigated. Different conditions, viz. total iron concentration (0.5, 2, 5 g/L), temperature (25, 45, 65 °C) and ratio of Fe^{3+}/Fe^{2+} (10:1, 5:1, 2:1, 1:1, 2:1, 5:1, 10:1) were investigated in sweeps in both the anodic and cathodic

directions . The anodic peak was shown to increase with an increase in Fe^{2+} ions in solution and temperature. Higher Fe^{3+} ions in solution in turn showed effects on the starting point of the anodic direction sweeps, where the starting point of the sweeps was observed to be starting at cathodic current densities even though the potential was arbitrarily started at 0 V. This was attributed to the Fe^{3+} reduction reactions occurring at lower potentials. For the three total Fe concentrations studied, it was observed for 5 g/L total Fe concentration the peaks observed started to decrease, suggesting a critical concentration at which these studies can be performed (between 0.5 – 5 g/L).

It is suggested that multiple discreet reactions occur at the same time around the main anodic peak. These reactions are predicted by the Fe-OH and chalcopyrite Pourbaix diagrams to suggest formation of secondary copper sulfide minerals and iron precipitates. Furthermore, anodic peaks disappeared when the anodic direction sweep was started at the open circuit potential (OCP) of the chalcopyrite electrode. The passivation potentials of chalcopyrite were investigated by chrono-amperometry at different potential steps. It was found that there is a transient dependence of current density on the potential at the passivation region due to slow formation of the passivation layer

Sweeps performed in the cathodic direction served as a good introduction to observe the general trends in this region, as according to the Pourbaix diagram there are other products that can form in this region, but were not investigated in further detail in the present study

For further studies, it is suggested from this work that due to the transient nature of the sweeps, LSV sweeps should be performed at the slowest scan rate possible to eliminate any effects from the potentiostat. Since inclusion of Fe^{2+} showed effects on the chalcopyrite electrochemical reactions, it was further suggested that this effect be investigated much closer by continuously adding Fe^{2+} to the system. For the larger scope of the project, it is recommended that in biotic systems the surface of the mineral should also be monitored by a technique such as electrochemical impedance spectroscopy. A batch experiment should also be performed with an apparatus that would allow LSV and chrono-amperometry to also be utilised at time intervals during a longer batch study.

Contents

List of Figures

List of Tables

1 INTRODUCTION

World copper demand has doubled between 1984 and 2006 to 18 Mt, reported by the Australian Bureau of Agricultural and Resource Economics (ABARE). It is also reported by the International Copper Study Group that there will be even a further increase in copper demand in the future (International Copper Study Group, 2010). Thus, there is an overwhelming demand for more and more copper resources. Chalcopyrite is the most important and abundant primary copper sulfide mineral. Conventionally copper is extracted through milling and flotation to form high grade concentrate, which is then processed by pyrometallurgical methods which include thermal treatment of the ore in order to bring about a physical and chemical change in the mineral (Prasad and Pandey, 1998). Low grade ores such as chalcopyrite thus require large amounts of ore to be crushed and milled per ton of copper produced, thereby in turn requiring high amounts of energy (Rhodes, 2008). Energy costs are likely to rise in the future and ore grades are likely to drop, thus potentially making the cost of producing concentrate prohibitive. The high energy consumption of low grade ore pre-treatment is also indirectly associated with environmental impacts from pyrometallurgical processing. Pyrometallurgy involves methods such as smelting and roasting, which are exothermic reactions that oxidise chalcopyrite into copper, iron sulfides, sulfates and oxides. The production of dust, gases of sulfur and trace metals, especially arsenic, are a cause for major environmental concerns (Kawatra, 2010; Prasad and Pandey, 1998). Hydrometallurgy is being considered as an alternative process route to pyrometallurgy. This technology has been explored for the past 50 years through tank/agitated leaching (atmospheric and under pressure) followed by solvent extraction and eletcrowinning (Brierley and Brierley, 2001). Tank leaching is has been recently shown to be comparable to pyrometallurgical processes from an environmental and economic view point, but do not offer any clear advantages as the concentrate still has to produced, and low capital costs in the leaching section are offset by higher operational costs in the electrowinning step (Lusinga, 2011).

Another hydrometallurgical process that has been explored and found to offer some advantages is heap/dump leaching, whereby the ore is coarsely crushed, stacked, and drip irrigated (and aerated) with leaching solution. Heap leaching does not require milling of the ore, and hence requires comparatively less capital cost to operate (Watling, 2006). Processing of low grade ores has been given a lot of attention in recent years and that of chalcopyrite has been found to be in the forefront. Unlike most base metal sulfide minerals, chalcopyrite has been shown to be refractory to conventional ferric sulfate leaching systems at atmospheric pressure. Most research has been conducted to assist in the understanding of this drawback but there has not been any generally accepted justification of this phenomenon (Córdoba et al., 2008; Antonijevic and Bogdanovic, 2004; Hiroyoshi et al., 2000; Hackl et al., 1995; Dutrizac, 1978). Over many years of study, numerous theories have been put forward to try describe this phenomenon, where most point to a surface layer that forms on or in the surface of the mineral; known as a passivating layer (Córdoba et al;. 2009; Hackl et al., 1995; Biegler and Horne, 1985; Warren et al., 1982). To enhance the rates of chalcopyrite leaching, microbially assisted leaching has been found to show some promise. It has been proposed that certain types of bacteria and archea enhance chalcopyrite leaching, although it is unclear in what way their presence affects the process (Watling, 2006; Petersen and Dixon, 2003; Barret et al. 1993). These microorganisms are categorised according to the way they adapt to different temperatures, and are thought to have some interactions with the said passivating layers (Brandl, 2005).

There are two main ways of studying chalcopyrite (bio)leaching, that is, by performing leach tests or by studying the electrochemical responses of the mineral in a leach environment (Petersen, 2009; Hiroyoshi et al., 2001; Jáuregui and Reyes, 1987; Jackson, 1986; Biegler and Horne, 1985; Biegler and Swift, 1979). The latter is the focus of the present study, relying on the fact that leaching reactions exhibit corrosion-type behaviour and, that sulfide minerals are semi-conductors, and thus electrochemical techniques can be utilized on pure mineral surfaces. These types of studies have an advantage in that one can work with small samples, measuring even the smallest progress through currents at micro- and even nano-ampere level, and that test work can rapidly analyse for the effects of a large variety of factors, and allow to directly relate the observed trends to surface phenomena.

A larger objective of an ongoing research project is to gain a comprehensive understanding of the effect of micro-organisms on the interaction at the mineral surface during the bioleaching of chalcopyrite. The specific objective of the current study is limited to providing an initial study of electrochemical reactions that might occur at the surface of chalcopyrite and the formation of the passivation layers in an abiotic environment. This is performed by exploring various electrochemical techniques to characterize these. The main techniques utilized in the present work are open circuit potentials, linear sweep voltammetry and chrono-amperometry. The aim of the present study is to provide recommendations for a systematic study in biotic systems and provide a set of benchmark data for alternative chalcopyrite leaching techniques. The approach taken in this study was firstly to establish a suitable electrode preparation method, to commission the potentiostat and conduct a set of reproducibility studies. A more comprehensive study was then undertaken using linear sweep voltammetry, open circuit potential measurements and chrono-amperometry. Different conditions were then studied using these techniques, that is, scan rate effects, temperature, total iron concentration and the ferric to ferrous ratio.

1.1 Outline of thesis

This thesis is an embodiment of 6 chapters. Chapter 1 introduces the reader to the significance of the present study within the scope of electrochemical chalcopyrite leaching. Chapter 2 covers the background of the current study by examining the literature on chalcopyrite leaching (chemical and biochemical), electrochemical consideration of chalcopyrite leaching and finally the techniques for performing these types of studies. Chapter 3 covers the materials utilized for the experiments, experimental procedures and consideration, as well as the experimental setup. Chapter 4 presents a full discussion of the results obtained from the commissioning of the potentiostat, reproducibility studies and finally the electrochemical implications of the experiments performed. Chapter 5 then draws important conclusion on the experiments performed on chalcopyrite, and finally Chapter 6 outlines recommendations for future work.

2 LITERATURE REVIEW

2.1 Chalcopyrite

2.1.1 Physical properties and structure

Chalcopyrite is the most common copper ore mineral. Though this mineral ore contains the least amount of copper in terms of atoms per molecule, 25% – 34% by mass, compared with other copper sources such as chalcocite, cuprite, covellite and bornite (with 80%, 80%, 67%, 50% by mass respectively), chalcopyrite is by far the most abundant copper resource and is found in almost all the sulfide deposits around the world. It has a brassy-yellow colour, tarnishes blue, red and purple, and has metallic lustre. The mineral has opaque crystals, a tetragonal crystal system with tetrahedral disphenoidal faces (Figure 2.1a). It is found widely distributed in metal veins, hydrothermal veins, disseminations and massive replacements. In nature it is found associated with other minerals such as pyrite, galena, calcite, and various other minerals. This mineral contains copper (Cu), iron (Fe), and sulfur (S) with the chemical formula, $CuFeS_2$ and chemical composition; 34.5% Cu, 35% Fe and 35.5% S by mass.

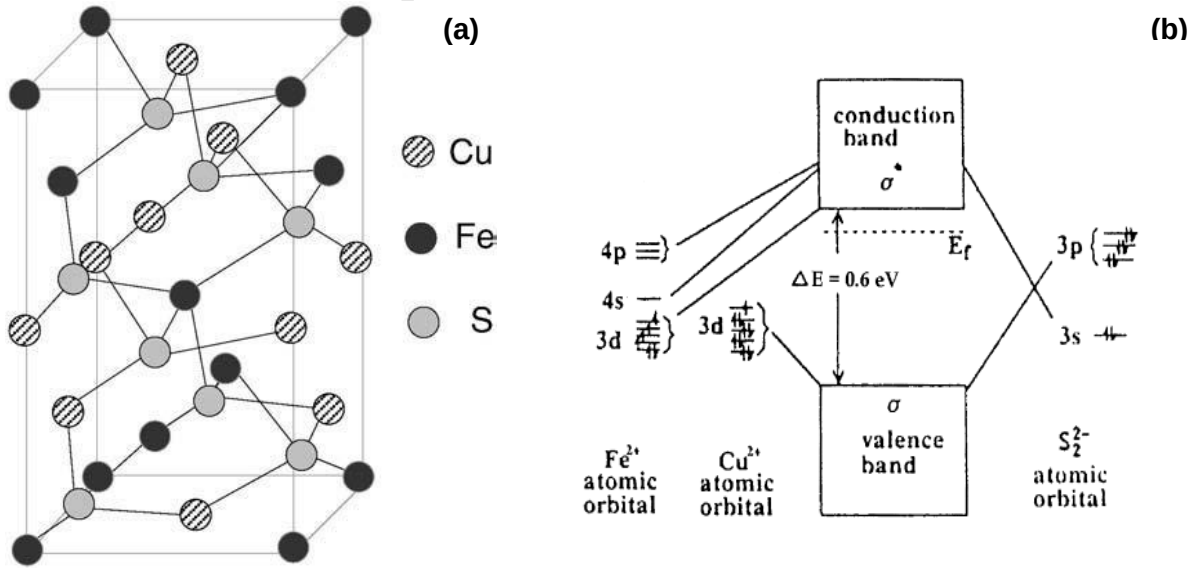

Figure 2.1. (a) Tetragonal crystal lattice structure of chalcopyrite (Betejtin, 1977); (b) Electronic band diagram for chalcopyrite (Sand et al., 2001).

Like all other sulfide minerals, chalcopyrite possesses semiconductor properties, due to its bonding valence band being derived from both the copper and sulfur atomic orbitals (Figure 2.1(b)) (Córdoba et al., 2008; Sand et al., 2001). In this electron band diagram, the electronic character of the lower band (conduction band), is given by iron's 3d orbitals, and that of the upper band (valence band) is given by copper 3d and sulfur 3p orbitals. The valence band electrons of chalcopyrite can thus be easily removed by ferric ions and protons, which cause the breaking of the bond/s between the sulfur and copper moiety of the mineral. Compared to other metal sulfides, such as pyrite, tungstenite, etc, which are insoluble in acid, chalcopyrite is more or less soluble in acid. The degree of solubility in acid is due to its configuration of the valence band's copper and sulfur electron configuration, whereby these two are bonded together.

2.1.2 Metal Extraction from Chalcopyrite

2.1.2.1. Pyrometallurgical processes

Traditionally, copper extraction from chalcopyrite has been treated by pyrometallurgical processes. In these processes, mineral ores are thermally treated to bring about physical and chemical transformations in the minerals in order to enable recovery of the valuable metal. This includes methods such as roasting of sulfide concentrate, smelting, converting and fire refining. The process of roasting comprises exothermic reactions that oxidize the ore concentrate to a mixture of copper and iron sulfates, oxides and sulfides (unoxidized material) (Kawatra, 2010). The roasting products then go through a smelter, whereby copper is reduced in part by iron sulfide into a copper-iron matte that melts and separates from the rest of the other products. This copper-iron matte (blister copper) is then oxidised in the conversion step to form a metallic copper, an iron oxide slag and sulfur dioxide. The copper from the converting step contains considerable amounts of dissolved oxygen. Oxygen is then removed in the fire refining by reduction with hydrocarbons to form metallic copper. After the fire refining step copper that is 99.5% pure is obtained.

Pyrometallurgical methods have been under scrutiny in recent years due to their environmental impacts. The major disadvantage of these pyrometallurgical processes is the production of environmentally hazardous gases, dust and oxides as impurities.

2.1.2.2. Hydrometallurgical processes

A potentially more cost effective and environmentally friendly method of extracting metals from low grade ores such as chalcopyrite is by hydrometallurgical processes. These are extractive metallurgy processes that involve the use of aqueous chemistry for recovery of metals from their ore concentrates or minerals at much lower temperatures. Hydrometallurgy uses leaching for mineral dissolution, precipitation for removal of impurities and solvent extraction and electrowinning for separation and production of metals (i.e. cathode copper in the case of chalcopyrite). Waste materials produced by hydrometallurgical processes are found to have less environmental impact, because they can further be treated to nontoxic material (Liew, 2009), and there are much less of them than in pyrometallurgy as no fluxing agents are needed. Sulfur emissions from hydrometallurgical processes are also presented in a form of stable sulfates such as gypsum or elemental sulfur. Hydrometallurgical processes involve the following stages, leaching, solution concentration and purification, and metal recovery. Leaching reactions, i.e. the dissolution of metal values from minerals, can be broken down into two types; chemical leaching and microbial assisted leaching. There are different kinds of leaching reactors employed in the industry, primarily either, tank/autoclave leaching or heap/dump leaching. Solution concentration and purification include precipitation, cementation, solvent extraction or ion exchange of the leached solution to remove impurities or any other unwanted metals. The final step for hydrometallurgical processes is metal recovery which utilizes the method of electrowinning by electrodeposition of the metal at the cathode.

Through hydrometallurgical processes, an increase in copper production has been observed in the past 15 years, with production increasing from 0.8 to 2.0 Mt, in the period between 1993 to 1997, primarily due to the introduction of solvent extraction

and electrowinning (Watling, 2006). In 2001 alone, the combined production of copper in America and Chile was 2.1 Mt and 0.16 Mt from other countries (Rohwerder et al., 2003; Bartos, 2002). The new development of bacterially assisted heap leaching of low grade minerals has proved to be successful (Watling, 2006; Rohwerder et al., 2003). In the case of copper sulfide minerals, success has been shown for secondary minerals of copper sulfide, such as chalcocite, covellite, etc. However, since chalcopyrite presents itself as a refractory primary copper sulfide, heap bio/leaching of this mineral has not yet been established at an industrial scale.

2.2 Leaching of chalcopyrite

2.2.1 Chemical leaching of chalcopyrite – Alternative systems

Chemical copper leaching dates back to the 18th century at Rio Tinto (Halelva, Spain) (Watling, 2006). Here, copper was extracted by cementation with metallic iron in sulfate solutions, and subsequent evaporation of the solution. Cementation is an electrochemical reaction involving the precipitation of one metal ion from solution by another more electronegative metal according to reaction 2.1, in general (Lamya and Lorenzen, 2005);

$$M + N^{2+} \rightarrow N + M^{2+} \qquad (2.1)$$

Previously, hydrometallurgical processing of chalcopyrite has been broken down and grouped into three processes; i.e. (i) thermal treatment, (ii) direct electrochemical leaching, and (iii).direct leaching, and these are discussed below.

The thermal treatment, also known as the roast-leach-electrowin process of chalcopyrite is process whereby copper extraction is achieved by altering the mineralogical composition of the ore mineral. Copper is converted into its soluble metal sulfates, iron into insoluble metal oxides, and sulfur into sulfur dioxide (Prasad and Pandey, 1998; Venkatachalam, 1991). A sulfation step is introduced in this process, which results in the above mentioned copper sulfate intermediates. The calcine obtained is then ground and the iron intermediates washed out using

counter current treatment. Solvent extraction and electrowining are then utilized to obtain copper metal from the purified leach liquor. This process requires the use of both oxides and sulfides of copper ores.

Direct electrochemical leaching can be obtained in two ways, whereby the copper is obtained by direct electrochemical reaction of an oxidant in solution with the chalcopyrite, where both electrochemical half reactions (anodic and cathodic) take place on the same surface. This process is attractive because the ore concentrate is used as it is, without any pre-treatments. Secondly, direct electrochemical leaching can also be obtained by galvanic interactions. In galvanic dissolution, two minerals of different rest potentials are brought into electric contact with each other in a corrosive (i.e. oxidising) solution. The mineral with the lower rest potential will be anodically dissolved while the one with a higher potential will be cathodically protected, facilitating the reduction of the oxidant. Thus, in the case of chalcopyrite and pyrite, pyrite will act as a cathode and chalcopyrite as the anode. Chalcopyrite oxidation by this method, results in dissolved copper and other copper sulfides (2.2) (Venkatachalam, 1991). Anodic dissolution of chalcopyrite will be discussed in detail in subsequent sections.

$$CuFeS_2 + O_2 + 4H^+ \rightarrow Cu^{2+} + Fe^{2+} + 2S^0 + 2H_2O \qquad (2.2)$$

The third hydrometallurgical processing method for chalcopyrite is direct leaching. This involves reacting mineral concentrates with various lixiviants without prior pre-treatment. Leaching of the mineral requires strong oxidizing agents, due to its strong lattice. Various reagent systems have been explored for the process of leaching chalcopyrite; these include oxygen, sulfuric acid, chloride, nitric acid, and acid-ferric systems[1] and these will be discussed below.

[1] Bacterially assisted leaching is also seen as a form of direct leaching process, which uses mostly acidic ferric systems. Discussion of this method will be covered individually in the next section.

2.2.1.1. Sulfuric acid system

According to Prater et al. (1970), as cited in Prasad and Pandey (1998), it is possible to directly dissolve chalcopyrite in strong sulfuric acid. To achieve this, a chalcopyrite concentrate is first baked at temperatures of between 220 – 230 °C in 93% sulfuric acid for a certain length of time. This allows for chalcopyrite to be converted into water soluble copper and iron sulfates, which can be subsequently purified, and copper can be obtained (2.3). Large amounts of iron enter the leach solution in this process (2.4)[2]; therefore iron needs to be precipitated before the copper leached step. Industrial processes, such as the Sherritt-Cominco[3] Copper Process, have been utilized to reduce the production of iron prior to the oxidation leach of copper (Prasad and Pandey, 1998).

$$CuFeS_2 + 2H_2SO_4 \rightarrow CuSO_4 + FeSO_4 + 2H_2S \quad (2.3)$$

$$H_2S + H_2SO_4 \rightarrow S^0 + SO_2 + 2H_2O \quad \text{(fast reaction)}$$

$$2FeSO_4 + 2H_2SO_4 \rightarrow Fe_2(SO_4)_3 + SO_2 + 2H_2O \quad (2.4)$$

2.2.1.2. Chloride systems

Chloride leaching of chalcopyrite occurs with utilization of a number of chloride salt solutions. Ferric chloride leaching has been shown to be more effective that its sulfate salt counterpart (Dutrizac, 1981). This method of copper extraction has yields of greater that 95% from chalcopyrite (Liddicoat and Dreisinger, 2007). An added advantage to the use of chloride salt is that they are inexpensive, readily available and easily regenerated. Chloride ions are also known for ease of forming highly stabilized soluble complexes with a number of transition metals, and in the case of chalcopyrite this is further advantageous, because the cuprous and cupric

[2] Reactions represented by this author are questionable as H_2SO_4 is not a very strong oxidizing agent. But it is worth noting that these reactions are performed at high temperatures (220 – 230 °C) according to (Prasad and Pandey, 1998).

[3] This process was utilized by the company Sherritt Gordon Mines and Cominco Limited. (Swinkels, G.M. et. al., 1978), but is no longer operational.

ion couple can exist in chloride media while cuprous ions are not stable in sulfate media. Three main reactions occur when mixed solutions of ferric chloride and cupric chloride are utilized for chalcopyrite dissolution (2.5 – 2.7). In the first stage, both cupric and ferric ions act as oxidizing agents for chalcopyrite dissolution, with copper in a cuprous chloride form. This product solution is further subjected to precipitation, purification, drying and hydrogen reduction to form elemental copper.

$$4FeCl_3 + CuFeS_2 \rightarrow 5FeCl_2 + CuCl_2 + 2S^0 \quad (2.5)$$

$$3CuCl_2 + CuFeS_2 \rightarrow 4CuCl + FeCl_2 + 2S^0 \quad (2.6)$$

$$6CuCl_2 + S^0 + 4H_2O \rightarrow 6CuCl + H2SO_4 + 6HCl \quad (2.7)$$

The only process that has been observed thus far to utilize chloride leaching has been the Duval Corporation's CLEAR process[4], which operated for a period of 6 years. This process has since been shut down due to economic and technical reasons (Liddicoat and Dreisinger, 2007). These included a complication in downstream separation of complexes formed due to Cl^- high affinity for most transition metals, corrosiveness of Cl^- ions, and hydrochloric acid being expensive.

2.2.1.3. Nitric acid systems

Nitric acid has also been found to be a good lixiviant that plays an important role in the leaching of chalcopyrite due to its oxidizing effect. Reactions of chalcopyrite leaching were performed at temperatures of 95^0C for 2.5 hours (Bjorling et al., 1976). Two methods have been proposed for nitric acid leaching, in which a low concentrated and high concentrated acid is utilized. In the low concentrated acid process, nitric acid acts as a catalyst, and there is not much information regarding this process. In the other process, where nitric acid is concentrated, there is an evolution of nitrogen oxide gases, which are collected outside the leaching reactor (2.8 – 2.10).

[4] This is a prototype commercial scale process that is not yet fully commercial.

$$6CuFeS_2 + 10HNO_3 + 15H_2SO_4 \rightarrow 6CuSO_4.+ 3Fe_2(SO3)_3 + 10NO + 12S^0 + 20H_2O \quad (2.8)$$

$$2CuFeS_2 + 10HNO_3 + 5H_2SO_4 \rightarrow 2CuSO_4 + Fe_2(SO4)_3 + l0NO_2 + 4S^0 + 10H_2O \quad (2.9)$$

$$2NO + 1.5O_2 + H_2O \rightarrow 2HNO_3 \quad (2.10)$$

This type of system has been found to have a number of disadvantages, that is, nitric acid is expensive, regeneration of the acid from the product gas nitrogen dioxide is very difficult, and copper recovery from nitrate solutions is known to be difficult (Venkatachalam, 1991). This process has been modified and utilized by Kennecott Copper Corporation (Davies et al., 1978), where sulfate salts of iron and copper are separated by co-crystallization, dissolved in water and iron rejected as goethite in an autoclave.

The last system for leaching of chalcopyrite considered here is utilization of acidic ferric sulfate media (also in bacterial system). This is the most commonly used method for chalcopyrite leaching and will be discussed in much more detail, as studies presented here will be performed in acid ferric media. Discussion of this system will also be further reviewed to introduce some basic concepts of microbial assisted leaching of chalcopyrite.

2.2.2 Chemical leaching of chalcopyrite – Acid iron sulfate systems

Acid ferric sulfate leaching is by far the most commonly utilized method of leaching chalcopyrite. This system has been applied in tank, heap/dump leaching of chalcopyrite. Utilization of ferric/ferrous sulfate system is found in processes tested at laboratory, pilot and commercial scales. Mechanisms and kinetics of utilization of the iron sulfate systems in acid media have been extensively researched (Córdoba et al., 2008; Munoz, et al., 1979). These systems have low corrosion tendencies and the acid used can be regenerated in the electrowinning step. The acid that is utilized

for iron systems is usually sulfuric acid. This system also requires oxidizing agents, and oxygen (O_2) and solutions of ferric (Fe^{3+}) sulfates have been found to be the most effective (Córdoba et al., 2008). O_2 is the primary oxidizing agent in leaching reactions, but direct leaching by oxygen is very slow at low temperatures. Thermodynamics of chalcopyrite leaching in acidic media have been elucidated and represented on a Pourbaix diagram (Figure 2.2). This diagram shows that dissolution of chalcopyrite in acidic media takes place through solid transformations of chalcopyrite to secondary sulfide mineral intermediates, which are richer in copper. The diagram also shows that at pH values of less than 4 and potentials of more +0.4 V (vs SHE) are essential for dissolution of chalcopyrite.

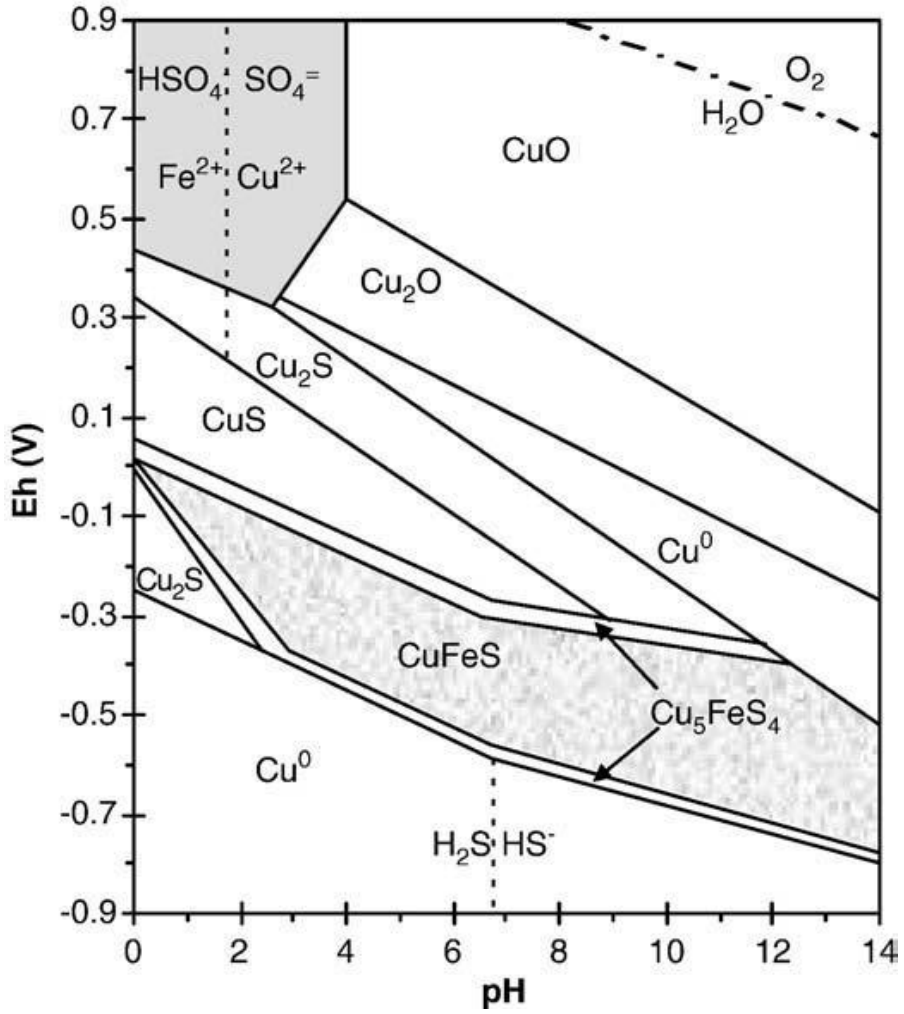

Figure 2.2. Pourbaix diagram for dissolution of chalcopyrite in a $CuFeS_2$-H_2O system in acidic media (Garrels and Christ, 1965).

Sulfate media leaching of chalcopyrite has also been observed to be slower than in any other lixiviant media, and rates of chalcopyrite dissolution have been observed to decline rapidly as time progresses. This decline has been attributed to a passivating layer that forms on the mineral surface during dissolution of the mineral. In the presence of ferric ions in acidic solutions, the bulk of chalcopyrite dissolves to form elemental sulfur, ferrous and cupric ions by the reaction (2.11) and the rest by reaction (2.12) [5] (Dutrizac and MacDonald, 1974).

$$CuFeS_2 + 4Fe^{3+} \rightarrow Cu^{2+} + 5Fe^{2+} + S^0 \quad (2.11)$$

$$CuFeS_2 + 4Fe^{3+} + 3O_2 + 2H_2O \rightarrow Cu^{2+} + 5Fe^{2+} + 2H_2SO_4 \quad (2.12)$$

Most research has been conducted to understand the refractory nature of chalcopyrite dissolution in sulfate media (Antonijevic and Bogdanovic, 2004; Hiroyoshi et al., 2000; Hackl et al., 1995; Dutrizac, 1978). Different components with the leaching environment have been found to have different effects on the dissolution of the mineral. These include temperature, the type of iron media, inclusion of additives, concentration of iron in solution, pH, etc.

2.2.2.1. Effects of the type of ferric salt

Two ferric salts have been considered important in the dissolution of chalcopyrite; ferric sulfate ($(Fe_2(SO_4)_3$) and ferric chloride ($FeCl_3$) (Córdoba et al., 2008). It has been shown that $FeCl_3$ is a better leaching/oxidizing agent than $Fe_2(SO_4)_3$. Dissolution of chalcopyrite by using $Fe_2(SO_4)_3$offers an advantage in that, the acid is inexpensive, readily available and can be recovered. Considering that to date pyrometallurgical processes are still utilized, and H_2SO_4 can be produced cheaply from SO_2 generated during this process. Thus, the type of ferric salt that can be used for dissolution of chalcopyrite is dependent on a lot of factors, but

[5] This reaction is unusual as both oxidants (Fe^{3+} and O_2) appear as reactants and there is no clarity from the authors as to why this is so. In essence it is known that one can have either Fe^{3+} or O_2 as an oxidant. This reaction is a combination of reactions that shows that $Fe^{3+}$is a redox catalyst and can be regenerated with O_2 by the reaction: $4Fe^{2+} + O_2 + 4H^+ \rightarrow 4Fe^{3+} + 2H_2O$.

$Fe_2(SO_4)_3$leaching is still by far the most effective and most researched lixiviant. The only disadvantage of $Fe_2(SO_4)_3$ solution leaching is the decreased kinetics that are observed over a period of time during dissolution, attributed to the rapid formation of a passivating layer that forms on the mineral surface.

2.2.2.2. Effects of pH

pH has a strong influence in the dissolution of chalcopyrite. It has been observed that very low pH values prove to be unfavourable for dissolution of chalcopyrite (Córdoba et al., 2009; Antonijevic and Bogdanovic, 2004). pH values of less than 0.5 have also been shown to have a negative effect on the dissolution of chalcopyrite as this aggravates formation of the sulfur passivating layer due to deficiencies in iron on the surface of chalcopyrite (Antonijevic and Bogdanovic, 2004). By performing studies at pH values between 0.5 – 2 Córdoba et al. (2009) observed a marked increase in the dissolution of chalcopyrite at higher pH values. At pH 2, these authors also observed precipitation and nucleation of the passivating layer of jarosite, visualized on scanning electron microscopy (SEM) micrographs. The most predominant ferric species found to exist at pH values between 0 – 2 was $Fe(SO_4)_2^-$ and other Fe^{3+} species played an insignificant role.

2.2.2.3. Concentration of ferric ions

Ferric ion concentration is observed to have an effect on the dissolution of chalcopyrite only at low levels, 0.001 to 0.1 M, and the effect tends to be negligible at concentrations higher than these limits (Córdoba et al., 2009; Antonijevic and Bogdanovic, 2004; Hirato, et al., 1987). Antonijevic and Bogdanovic (2004) studied the influence of the concentration of ferric ions on dissolution of chalcopyrite between 1 – 20 g/dm^3. In their studies the authors found non-dependence of the rate of chalcopyrite dissolution and dissolved copper on the ferric concentration. A zero order reaction rate related to ferric concentration was also observed by Munoz et al. (1979). Improvements in chalcopyrite dissolution were only observed with

ferric concentrations in the range of 0.001 – 0.1 M (Hirato et al., 1987). According to thermodynamic data, the only species that are concerned with chalcopyrite dissolution were found to be Fe^{3+} and $FeHSO_4^{2+}$. These species were found to only exist up until the 0.1 M concentration limit, and above this value, $FeSO_4^{+}$ species prevailed.

2.2.2.4. Temperature

Chalcopyrite dissolution rate and temperature have been shown to have a direct relationship in the temperature range between ambient and 70 °C (Córdoba et al., 2008; Tshilombo et al., 2002). Higher temperatures have been shown to provide more energy needed to break the bonds of chalcopyrite crystal lattice. Effects of temperature on the leaching rate of chalcopyrite have been attributed to the semiconductor nature of chalcopyrite. Effects of temperature on the dissolution of chalcopyrite are affected by the type of leach media, whereby chloride is preferred to sulfate media (Córdoba et al., 2008).

2.2.3 Biological leaching of chalcopyrite

Biologically assisted leaching (bioleaching) of copper sulfide minerals is an emerging technology that has been found to be reasonably efficient in leaching of secondary copper sulfide minerals (bornite, covellite, chalcocite, etc) (Vilcáez, et. al, 2008; Rohwerder et al., 2003; Sand et al., 2001; Schippers and Sand, 1999). This technology is still in development for bioleaching of chalcopyrite, and thus far operations exist only for bioleaching of secondary copper sulfide minerals (Table 2.1). The refractory nature of chalcopyrite in sulfate media is also observed for bioleaching reactions, with similar passivation effects, although good rates are possible with certain thermophilic organisms.

Industrially, during heap bioleaching of sulfide minerals, the ore is crushed and agglomerated with acidic water, to bind fines to larger particles (Barret et al., 1993).

Heap bioleach systems are utilized for ores with lower copper grade. The ore is stacked into a heap of 6 – 10 m. The heap is then drip irrigated with slightly acidic water, while air is provided from the bottom of the heap. The microorganisms propagate and reproduce to reach *ca* 10^7 cells per gram of ore and per millilitre of solution (Brierley and Hill, 1993). In these heaps, solutions of copper (or other metals) are removed at the bottom of the stack by another pipe system as it accumulates, and recovered by methods of precipitation, solvent extraction and electrowinning.

Table 2.1. Shows the historical and present processes that utilizes bioleaching of copper ores (Watling, 2006).

Region/mine	Operation reserves (t)	Ore processed (t/day)	Cu production (t/year)
Lo Aguirre, Chile 1980–1996	Heap bioleach 12×10^6 at 1.5% Cu	Oxides/chalcocite 16×10^3	$14–15\times10^3$
Cerro Colorado, Chile 1993–	Heap bioleach 80×10^6 at 1.4% Cu	Chalcocite, covellite 16×10^3	100×10^3
Ivan Zar, Chile 1994–	Heap bioleach 5×10^6 at 2.5% Cu	Oxides/sulphides 1.5×10^3	12×10^3
Quebrada Blanca, Chile 1994–	Heap/dump bioleach 85×10^6 at 1.4% Cu 45×10^6 at 0.5% Cu	Chalcocite 17.3×10^3	75×10^3
Punta del Cobre, Chile 1994–	Heap (bio)leach 10×10^6 at 1.7% Cu	Oxides/sulphides –	$7–8\times10^3$
Andacollo, Chile 1996–	Heap/dump bioleach 32×10^6 at 0.58% Cu	Chalcocite 15×10^3	21×10^3
Dos Amigos, Chile 1996–	Heap bioleach 2.5%	Chalcocite 3×10^3	–
Zaldivar, Chile 1998–	Heap/dump bioleach 120×10^6 at 1.4% Cu 115×10^6 at 0.4% Cu	Chalcocite 20×10^3	150×10^3
Lomas Bayas, Chile 1998–	Heap/dump 41×10^6 at 0.4% Cu	Oxides/sulphides 36×10^3	60×10^3
Cerro Verde, Peru 1977–	Heap bioleach —at 0.7% Cu	Oxide/sulphide 32×10^3	54.2×10^3
Escondida, Chile	Heap bioleach 1.5×10^9 at 0.3–0.7%	Oxides, sulphides	200×10^3
Lince II, Chile, 1991–	Heap leach 1.8% Cu	Oxides, sulphides	27×10^3
Toquepala, Peru	Heap leach	Oxides, sulphides	40×10^3
Morenci, Arizona 2001–	Mine for leach 3450×10^6 0.28% Cu	Chalcocite, pyrite 75×10^3	380×10^3
Equatorial Tonopah, Nevada, 2000–2001	Heap bioleach 0.31% Cu	25×10^3	25×10^3
Gunpowder Mammoth Mine, Australia, 1991–	In situ (bio)leach 1.2×10^6 at ~1.8% Cu	chalcocite and bornite –	33×10^3
Girilambone, Australia 1993–2003	Heap bioleach — at 2.4% Cu	Chalcocite/chalcopyrite 2×10^3	14×10^3
Nifty Copper, Australia, 1998–	Heap bioleach — at 1.2%	Oxides/chalcocite 5×10^3	16×10^3
Whim Creek and Mons Cupri, Australia 2006–	Heap bioleach 900×10^3 at 1.1% Cu 6×10^6 at 0.8% Cu	Oxides/sulphides	17×10^3
Mt Leyshon, Australia 1992–1997	Heap bioleach — 0.15%	Chalcocite 1.3×10^3	750
S&K Copper, Monywa, Myanmar, 1999–	Heap bioleach 126×10^6 at 0.5% Cu	Chalcocite 18×10^3	40×10^3
Phoenix deposit, Cyprus, 1996–	Heap (bio)leach 9.1×10^6 at 0.78% Cu 5.9×10^6 at 0.31% Cu	Oxide/sulphide –	8×10^3
Jinchuan Copper, China 2006–	240×10^6 at 0.63% Cu	Chalcocite, covellite, enargite	10×10^3

In bioleaching processes, ferric ion containing salts are used and reactions 2.11 and 2.12 principal reactions occur. There are two additional reactions that occur when microorganisms are involved (2.13 and 2.14) (Figure 2.3).

$$4Fe^{2+} + 4H^{+} + O_2 \rightarrow 4Fe^{3+} + 2H_2O \quad (2.13)$$

$$2S + 3O_2 + 2H_2O \rightarrow 2H_2SO_4 \quad (2.14)$$

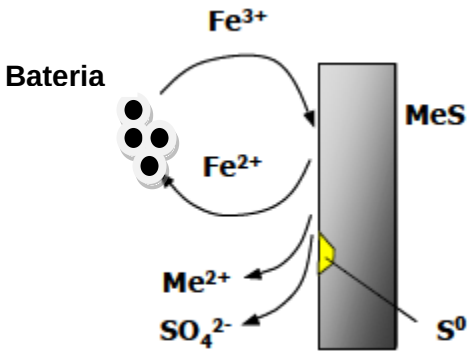

Figure 2.3 Schematic representation of a bioleaching process on mineral grain scale (Petersen, Dixon 2003).

In these reactions, the microorganisms concerned regenerate the oxidizing agent and the acid. The two reactions are respectively named the acid consumption and ferric regeneration (2.13), and acid regeneration (2.14) reactions (Vilcáez et al., 2008). Ferric and sulfuric acid are hence by-products of bioleaching, and they are both reused in the process (2.11 and 2.12). The microorganisms involved in bioleaching utilize products from the chalcopyrite dissolution (i.e Fe^{2+} and S^0) reactions as sources of energy. They are chemolithotrophic; i.e. they fix carbon dioxide from the atmosphere as their carbon source. All other nutrient requirements for the microorganisms are fulfilled from the bioleach environment. Bioleaching microorganisms present themselves in three different classes of species according the temperature range in which they exist (mesophiles, moderate thermophiles and thermophiles), and have been isolated from acid mine drainage (AMD) environments, existing heap and dump leach operations and some also from sulfur lakes. Since these microorganisms thrive in such harsh conditions, they have been classified as acidophilic (acid-loving) bacteria. Being acidophilic in nature, bacteria utilized in bioleach environments survive under extremely low pH (0.5 - 4) (Watling, 2006).

It is essential for the microorganisms to be allowed to adapt to chalcopyrite. Methods of inoculation have been proposed by a number of authors for both heap and dump bioleaching (discussed by Watling (2006)). The methods discussed involve;

- Inoculating with a tailored bacterial culture that grows particularly well on a specific mineral (e.g. chalcopyrite) and feeding the culture from a storage pond to the heap (Hunter, 2002),
- Inoculating a biological contactor with iron oxidising strains and feeding the ferric-rich stream (also containing some microorganisms washed out) to the heap (Hunter, 2001).

Classification of these species of bacteria has been in accordance to their survival at different temperatures, pH, and the type of the chemical component they oxidize (Table 2.3). At moderately low temperatures of less than 40 °C, mesophilic bacteria (mesophiles) predominate. The second class of bacteria are called moderate-thermophiles, and these are adapted to temperature between 45 °C and 65 °C. At temperatures higher than 65 °C, the third class of bacteria involved in bioleaching, called thermophiles (extremophiles) exist. Most bioleaching microorganism species have also been named in accordance with the chemical component they oxidize, that is sulfur or iron. The most common iron oxidizing bacterial species that are found in chalcopyrite bioleach environments are *Acidothiobacillus ferrooxidans* (*A. ferrooxidans* formerly called *Thiobacillus ferrooxidans*); *Leptospirillum ferriphilum* and *Leptospirillum ferrooxidans, and* both iron and sulfur oxidizing *Acidithiobacillus thiooxidans*. These species of bacteria are both gram-negative, autotrophic and they are mesophilic in nature. *A. ferrooxidans* species are inhibited by very high ferric concentrations, whereas their *L. ferriphilum* counterparts are not, and *L. ferriphilum* allows for growth at high temperatures up to ~ 45 °C and low pH (Pradhan et al., 2008; Brandl, 2005). The most commonly found moderate-thermophilic bacterial species are sulfur oxidizing *Acidithiobacillus caldus*., *Metallosphaera* and *Sulfolobus* species, which are found to be become more and more abundant as temperature increase (Brandl, 2005) . These species are found to exist at preferentially extreme temperatures as high as 95 °C. They have been found to be more efficient than

using mesophiles, but exhibit some level of sensitivity to copper and high pulp densities in agitated systems.

They lack a rigid peptidoglycan cell wall and fluidity of the cellular membrane increases with temperature (Konig, 1988). A combination of these factors results in a potential for bacteria to be sensitive to shear (Nemati et. al, 2000; Kelly and Deming, 1988).

2.2.3.1. Factors affecting bioleaching

Bioleaching of chalcopyrite, like any other process that involves living organisms, is influenced by environmental, physico-chemical and biological factors, which in turn affect the rate and yield of metal dissolution. Optimal conditions for the microorganisms have to be established for maximum process efficiency. Physical and chemical parameters, biological parameters and ore characteristics should be considered for maximum chalcopyrite dissolution (Table 2.2).

Table 2.2. Factors and parameter affecting bioleaching and metal recovery (Pradhan et al., 2008).

Factor	Parameters affecting bioleaching
Physical and chemical parameters	Temperature, pH, redox potential, CO_2 and O_2 content, nutrient availability, oxygen availability, homogenous mass transfer, Fe (III) concentration, presence of inhibitors, etc
Biological parameters	Microbial diversity, population density, microbial activities, metal tolerance, spatial distribution of microorganisms, attachment to ore particles, adaptation abilities of microorganisms, and inoculum
Ore characteristics	Composition, mineral type, acid consumption, grain size, mineral dissemination, surface area, porosity, hydrophobic galvanic interactions, and formation of secondary minerals

Table 2.3. Shows a list of iron and sulfur oxidizing bacteria, with their temperature classification and survival pH.(Watling, 2006).

Organism	Reported growth substrates	Characteristics
Acidianus ambivalens	S oxidation and reduction	Hyperthermophiles
Acidianus brierleyi	Sulphides	pH opt 1.5–2.5
Acidianus infernus	Poor, if any, Fe oxidation	
"Acidianus tengchongensis "		
Acidimicrobium ferrooxidans	Mixotroph Fe oxidation and reduction Sulphides (poor)	Moderate thermophile pH opt 2
Acidiphilum spp	Obligate heterotrophs	Mesophiles
Acidiphilium SJH	S oxidation Fe(III) reduction	pH opt ~2–3
Acidiphilium acidophilum	Facultative autotroph S oxidation Fe(III) reduction	Mesophile pH opt ~2–3
Acidithiobacillus albertensis	Autotrophs	Mesophiles
Acidithiobacillus ferrooxidans	S oxidation, sulphides	pH range 2–4
Acidithiobacillus thiooxidans	(*Af*, Fe(II) oxidation; Fe(III) reduction as a facultative anaerobe)	
Acidithiobacillus caldus	Mixotroph 3S oxidation, sulphides	Moderate thermophile pH opt 2–2.5
Acidolobus aceticus	Heterotroph S reduction to H_2S	Hyperthermophile pH opt 3.8
Alicyclobacillus spp	S oxidation, sulphides	Mesophiles — moderate thermophiles
"Alicyclobacillus disulfidooxidans"	(*Ad*, facultative autotroph,;	pH 1.5–2.5
"Alicyclobacillus tolerans"	At, mixotroph, Fe(III) reduction)	
"Ferrimicrobium acidiphilium"	Heterotroph Fe(II) oxidation, sulphides Fe(III) reduction	Mesophile pH opt 1.7–1.8
Ferroglobus placidus	Fe oxidation	Thermophile pH neutral
"Ferroplasma acidarmanus"	Possibly autotroph	Moderate thermophiles
"Ferroplasma cyprexacervatum"	Iron oxidation	pH range< 1–2
Ferroplasma acidophilum	Pyrite oxidation poor	
Ferroplasma MT17		
Hydrogenobaculum acidophilus	S, H oxidation to produce sulphuric acid	Thermophile pH opt 3–4
Leptospirillum ferriphilum	Fe oxidation	Mesophiles, some thermo-tolerant strains
Leptospirilum thermoferrooxidans	Pyrite	pH range 1.6–1.9
Leptospirillum ferrooxidans	Fe oxidation, pyrite	Mesophile pH opt 1.5–1.7
Metallosphaera sedula	S oxidation	Thermophiles
Metallosphaera prunae	Sulphides	pH 1–4
"Metallosphaera hakonensis"		
Sulfobacillus acidophilus	Fe(II) oxidation; Fe(III) reduction, Sulphides	Moderate thermophiles
Sulfobacillus thermosulfidooxidans	S oxidation	pH 1–2.5
Sulfolobus metallicus	Strict chemolithoautotroph	Hyperthermophiles
"Sulfolobus rivotincti"	S oxidation, sulphides	Various pH in range 1–4.5
Sulfolobus shibatae		
"Sulfolobus tokodaii		
Sulfolobus yangmingensis		
"Sulfolobus" JP2 and JP3		
Sulfolobus acidocaldarius	Heterotrophs	Hyperthermophiles
Sulfolobus solfataricus	Not S oxidation	pH 2–4.5
Sulfurococcus yellowstonensis	S and Fe oxidation	Hyperthermophile
Thiobacillus prosperus	S and Fe oxidation sulphides	Mesophile, halophile pH opt 2
Thiomonas cuprina	S oxidation, sulphides	Mesophile pH opt 3–4

Das et al. (1999) reviewed various factors that affect the kinetics of bioleaching reactions and identified them as follows;

***Activity of the microorganisms*:** Microbial activity is indirectly measured in terms of iron and sulfur oxidation rates. Differences are observed from strain to strain, and rate differences are due to characteristics such as change in morphology, nutrient metabolism, tolerance of organic material, etc. The activity can be increased by methods such as adaptation onto the minerals, which helps bacteria grow and survive in foreign conditions. Adaptation also decreases the lag period before the onset of bacterial growth, which in turn improves the rate of leaching.

***pH and Fe (III) concentration*:** During oxidation of ferrous iron to ferric, acidophilic microorganisms take up protons as nutrient. Bacterial growth is initiated at low pH and is not affected by an increase in pH as the bacteria grow. Suitable pH maintenance (strain specific) is required for increased bacterial activity, which in turn increases the bioleaching rate. High ferric concentration shows competitive inhibition of ferrous oxidation. This is due to the depletion of oxygen uptake by microorganisms at high ferric concentrations.

***Aeration of the heap*:** Bioleaching processes are aerobic in nature, requiring sufficient supply of O_2 and CO_2. In the heap, CO_2 is obtained from the surrounding air, and that is sufficient for microorganism biomass production. On the other hand, air needs to be supplied from the outside, as due to the height and packing density, CO_2 and O_2 are rapidly consumed within the network of the heap (Pradhan et al., 2008). The air is supplied from the bottom of the heap in an upward direction. Around the bottom of the heap O_2 is in ample supply. As the air rises within the heap around the spaces between the particles in the bed, microorganisms utilize oxygen for oxidation reactions. This gas uptake from gas phase to liquid phase is a mass transfer step, which is governed primarily by temperature (Petersen and Dixon, 2007). It is worth noting that copper dissolution is directly related to oxygen consumption, which in turn is related to microbial activity and the rate of aeration.

2.2.3.2. The bioleaching model

For bioleaching to occur, the bacteria have to be in close proximity with the mineral. Two mechanisms have been identified for bioleaching, viz. the indirect and contact leaching mechanisms (Sand et al., 2001). In the indirect mechanism ferrous and sulphur species that result from ferric oxidation, are further oxidized to ferric and sulfates. Bacterial action in this mechanism does not necessarily require direct attachment of the microorganisms to the mineral surface (Figure 2.4). On other sites of the mineral, direct attachment can be achieved, but microorganism do not directly react with mineral, as previously envisaged in the so-called 'direct' mechanism where microorganisms were thought to oxidise the mineral by direct enzymatic attack, although this has by now been completely discredited. During bioleaching microorganisms convert ferrous to ferric, while oxygen is converted to water via an electron transport chain (Bard and Faulkner, 1980).

$$2Fe^{2+} + \frac{1}{2}O_2 + 2H^+ \rightarrow 2Fe^{3+} + H_2O \qquad (2.15)$$

Figure 2.4. Indirect mechanism of bacterial leaching.

The bacterial species produce a highly oxidizing environment to oxidize ferrous into ferric. Ferric ions in turn assist in the oxidative dissolutions of the chalcopyrite. Elemental sulfur produced during dissolution reactions is further oxidized by sulfur specific bacterial species, such as *Acidothiobacillus ferooxidans*. The indirect mechanism of chalcopyrite leaching is further broken down into two other sub-mechanisms; the thiosulfate and polysulfide mechanism (Figure 2.5), which are specific to the electronic structure of the mineral (Schippers and Sand, 1999).

Minerals such as chalcopyrite follow the polysulfide mechanism, because this mechanism is specific for minerals that are soluble in acidic media. Conversely, the thiosulfate mechanism is specific for minerals such as pyrite, molybdenite, tungstanite, etc. These minerals are insoluble in acidic media, which is caused by a difference in electronic structure. The valence band of pyrite type minerals does not contribute to the bonding between the metal and sulfur (see section 2.1.1 for chalcopyrite electronic structure). Thus dissolution of these types of minerals can only be achieved by oxidative dissolution reactions, whereas chalcopyrite type minerals can undergo both acidic and oxidative dissolution reactions.

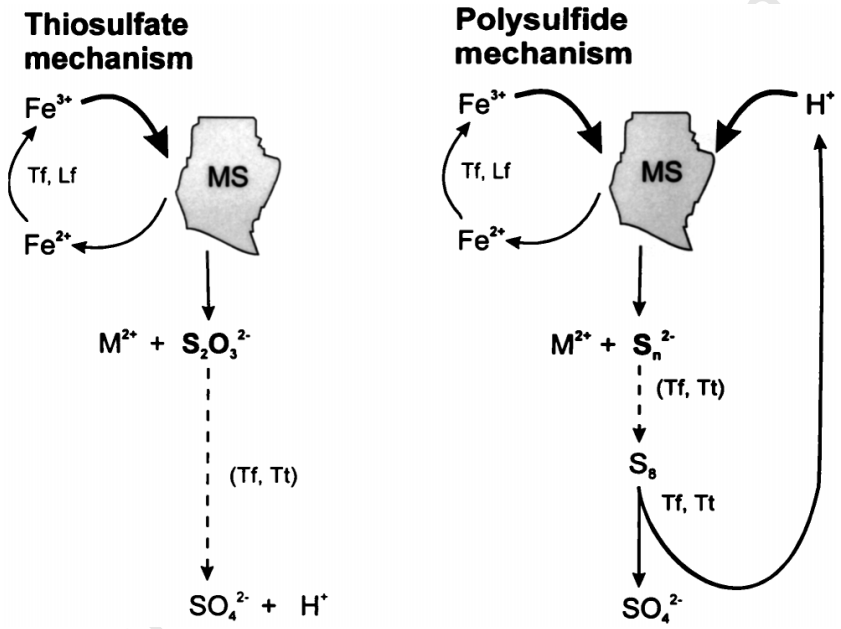

Figure 2.5. The thiosulfate mechanism of pyrite type and polysulfide mechanism of chalcopyrite type minerals (MS). Tf and Lf indicate the bacterial species (Schippers and Sand, 1999)

The polysulfide mechanism produces sulfur radicals that eventually polymerize to form polysulfide compounds. Elemental sulfur produced from these polysulfide compounds is further metabolized by the bacteria to produce sulfates. Third et al. (2000) studied the role of iron oxidizing bacteria (mesophile and thermophiles) in stimulation/inhibition of chalcopyrite bioleaching. They reported that large volumes of inoculated bacteria have negative effects on bioleaching. They observed less copper extraction in 50% (v/v) of the total solution volume, but maximum leaching in 10% (v/v) of inoculums. They attributed this to the continuous oxidation of ferrous by the bacteria, which increases the potential, whereas the potential stayed constant for

200 hours in the 10% inoculums. Conclusions from their studies were that bioleaching of chalcopyrite is not a typical straight forward bioprocess, because an increase in the biomass is disadvantageous to the dissolution reaction. As mentioned a continual oxidation of ferrous when there is a large biomass results in an increase in the potential of the system, therefore in this regard potentials shift the mineral into passivation.

Recent studies have identified a layer that forms on various sites on the surface of the mineral during bioleaching. This layer is composed of extracellular polymeric substances (EPS) (Rohwerder et al., 2003; Sand et al., 2001; Gehrke et al., 2001; Rodriguez-Leiva and Tributsch, 1988). These substances are secreted by microorganisms to form a biofilm attached to the semi-surface of the mineral, which assists in bioleaching. It is a more or less type of an indirect mechanism of bioleaching, and has been given the name contact mechanism (Rohwerder et al., 2003). EPS have been shown to be composed of sugars of glucose, mannose, rhamnose, fucose, and xylose; saturated fatty acids of lengths between C_{12} –C_{20}; glucuronic acid and ferric ions (Gehrke et al., 2001). Bacterial cells are not directly attached to the surface of the mineral, nor do they directly leach the mineral. Attachments of bacteria to the mineral surface have been found to be mainly due to electrostatic forces brought by formation of stable complexes between ferric and glucuronic acid moiety of the cell and the negatively charged ore (Solari et al., 1992). Attachments have been reported to be preferential for sites where there is evidence of surface imperfections (Sanhueza et al., 1999; Edwards et al., 1998; Shrihari et al., 1995). Imperfect sites are those where dissolution of the mineral has already occurred, that is sites where there are signs of pitting, cracks, scratches, etc. Other bacteria have been shown to possess chemosensory systems that are specific for these imperfect sites and also react positively with Fe^{2+}/ Fe^{3+} and thiosulfate gradients (for pyrite, whereby this would prefer polysulfide compounds for chalcopyrite) (Meyer et al., 2002). Dissolution of the mineral takes place within the EPS space. The proposed EPS mediated mechanism (Figure 2.6) is not very well established. Two assumptions have been proposed to explain the redox reactions in the EPS space. The first employ the theory of electron tunnelling (Sand et al., 2001; Medvedev and Stuchebruhov, 2001), and the second uses the fact that there is

preferential complexation of glucorunic acid to ferric compared to ferrous (Rohwerder et al., 2003). These mechanisms follow that within the EPS space, discrete local electrochemical (anode and cathode) sites are created where dissolution takes places. Anodic sites have been shown to be preferable for attachment of microorganisms, and these are sites where the metal is leached. In the same vicinity, there are also cathodic sites, where ferric/ferrous redox reactions occur (shown in Figure 2.6 for the case of pyrite). Thus the contact leaching mechanism occurs in such a way that bacterial cells are attracted to dissolution sites by their chemostatic sensory system and thus determine the anodes and cathodes on the metal sulfide surface to become permanent (Rohwerder et al., 2003). This mechanism of leaching brings insight in that it be can envisaged that for direct chemical leaching, oxidative and reductive reactions are competing with each other. Oxidative reactions in chemical leaching when compared to bioleaching may mask the cathodic reactions because there are no specific cathodic sites that a created on the mineral surface, hence the observed slow dissolution rates.

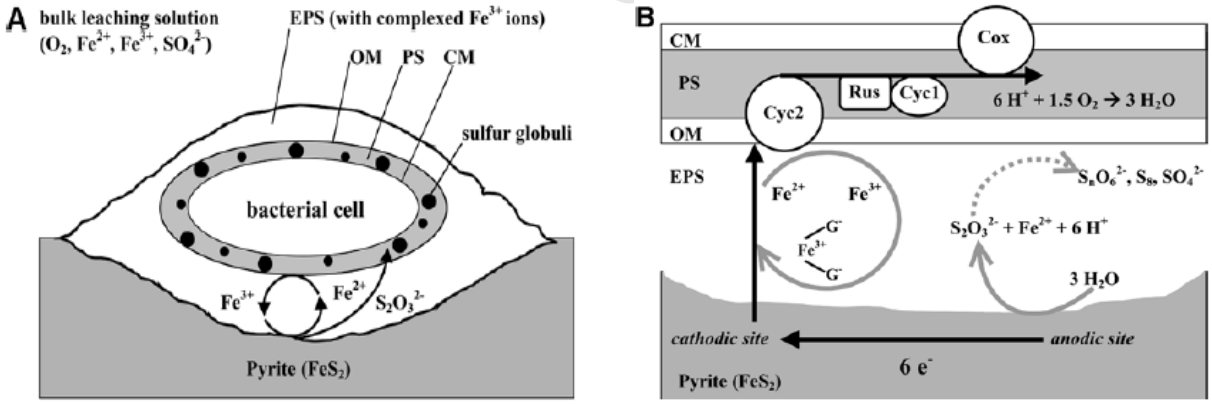

Figure 2.6. Model for the contact leaching mechanism of pyrite. (A) Shows the bacterial cells surrounded by the EPS layer (CM - Cytoplasmic membrane, PS - periplasmic space, OM - outer membrane). (B) Shows the electrochemical reacitions that occur during bioleaching at anodic and cathodic sites and the electron transport chain from ferric to oxygen (Rohwerder et al., 2003).

Thermophilllic bacteria have been shown to provide more enhancements during chalcopyrite bioleaching compared to chemical leaching (Vilcáez et al., 2008; Parker et al., 2003; Nemati et al., 2000; Jordan et al., 2006). The higher capacity of utilization of thermophilic bacterial during bioleaching has been attributed to a high affinity of the bacteria to the reaction that oxidizes sulfur species (2.14), compared to

the ferrous oxidation one (2.13) (Vilcáez et al., 2008). This prevents formation of ferric species (jerosite) and sulfur species that form on the surface of the mineral. As mentioned earlier, the hydrodynamic and structural factors of thermophiles are the only drawback during bioleaching (Kelly and Deming, 1988; Nemati et al., 2000). Factors found to have the most detrimental effects on thermophiles have been found to be the high concentrations of ore, physical attrition, chemical toxicity and unfavourable mass-transfer properties (Clark and Norris, 1996; Brierley and Brierley 1986). Enhancement of chalcopyrite dissolution by thermophiles have also been attributed to retardation of jerosite precipitation when there is enough supply of protons produced by bacterially catalyzed acid generation reaction (2.14) to the acid consumption reaction (2.13) (Vilcáez et al., 2008).

2.3 Electrochemical studies of chalcopyrite

2.3.1 General electrochemical concepts

Electrochemical processes are electron transfer reactions whereby a substance is oxidized by donating electrons and another is reduced by accepting electrons. An overall electrochemical reaction is given by two half reactions (2.16 and 2.17). These reactions are termed reduction/oxidation (redox) reactions. The site where an oxidation reaction occurs is referred to as the anode and that where a reduction reaction occurs as the cathode. These reactions always occur in pairs during electrochemical processes as there is no net generation or consumption of electrons.

$$MS \rightarrow M^{2+} + S^0 + 2e \qquad \text{(Anodic)} \qquad (2.16)$$

$$Ox + 2e \rightarrow Red \qquad \text{(Cathodic)} \qquad (2.17)$$

$$MS + Ox \rightarrow M^{2+} + S^0 + Red \qquad \text{(Overall)} \qquad (2.18)$$

Redox reactions give rise to a reversible electrochemical potential, E, which is described by the Nernst equations (Eq. 2.1 or Eq. 2.2);

$$E\ (V) = E^0 - \frac{RT}{nF} \ln \frac{a_{red}}{a_{ox}} \qquad \text{(Eq. 2.1)}$$

$$E\ (V) = E^0 - \frac{RT}{nF} \ln \frac{[Red]}{[Ox]} \qquad \text{(Eq. 2.2)}$$

where E^0 is the standard reversible potential of the electrode couple, R is the universal gas constant, T is the temperature, F is the Faraday constant, n is the charge number of electrons, [ ] signifies concentration of the reduced and oxidized species, a_{red} and a_{ox} are the chemical activities which appear on the reduced and oxidized sides of the electrode reactions, respectively. Equation 2.2 is mostly utilized in electrochemical reactions, because it applies formal potentials, which are measured potentials when the ratio $\frac{[Red]}{[Ox]}$ is unity and concentrations of other solution species are specified and fixed. The thermodynamics of an electrochemical process can be determined by the Gibb's free energy equation, where potential can be related to the change in Gibb's free energy (G_R) by the following equation (Eq. 2.3);

$$-\Delta G_R = nF\Delta E \qquad \text{(Eq. 2.3)}$$

Biegler and Swift (1979) showed that chalcopyrite dissolution to be an electrochemical corrosion process, that is, in this processes electron transfer drives the dissolution of the mineral. Generally, in a heterogeneous dissolution process a soluble oxidant is reduced at the mineral surface, which therefore acts as the cathode. At the same time the mineral dissolves and therefore also behaves as an anode. In the anodic reaction of chalcopyrite sulfide sulfur and sometimes iron are oxidized to a higher oxidation state. The principal overall electrochemical reaction for complete chalcopyrite dissolution is as follows;

$$CuFeS_2 + 4Fe^{3+} \rightarrow Cu^{2+} + 5Fe^{2+} + 2S^0 \qquad (2.19)$$

With the following half reactions in a acidic ferric oxidizing media;

Anodic: $CuFeS_2 \rightarrow Cu^{+2} + Fe^{2+} + 2S^0 + 4e$ (2.20)

Cathodic: $4e + 4Fe^{3+} \rightarrow 4Fe^{2+}$ (2.21)

It is known that for an oxidative process to be effective, the potential difference between the two half-reactions should be at least 0.2 V (Jackson, 1986). The overall reaction 2.19 is thermodynamically favorable, with ΔG^0 = - 101.5 kJ/mol (determined from -172 kJ/mol and -70.5 kJ/mol for the half reactions 2.20 and 2.21 at standard conditions, respectively) (Sokić et al., 2009). Thus, the potential of the combined reactions from the above ΔG values is 0.263 V. Since some redox reactions involve exchange of protons, the Nernst equation can be expanded to show a relationship between potential and pH (Eq. 2.4).

$$\mathbf{E\ (V) = E^0 - 2.303\ \frac{RT}{nF}\ pH - 2.303\ \frac{RT}{nF}\ log\ \frac{[red\}}{[ox\}}} \quad \text{(Eq. 2.4)}$$

This equation shows the relationship between the redox potential, solubility and speciation equilibria of ionic species in solution. Evaluation of this modified Nernst equation, solubility data and hydrolysis constants can be summarized in an Eh-pH diagram (also known as Pourbaix diagram, Figure 2.2). Eh-pH diagrams show the thermodynamic stability areas of different species (i.e. dissolved ion, condensed oxides, hydroxides and oxides, etc.) of the same metal in aqueous solutions. The upper and lower stability limits of water are shown with dotted lines on the Eh-pH diagram (2.22 and 2.23). The lines in the Eh-pH diagram can also be represented by their respective chemical equations (Roine and Anttila, 2009), where

a. Horizontal lines represent reactions that represent electron transfer but are independent of pH
b. Vertical lines represent reactions that involve either H^+ or OH^- ions, but are independent of electron transfer

c. Diagonal lines of negative and positive slopes represent reactions that involve both electrons and H^+ or OH, i.e. which are plots of the Nernst equation (Eq. 2.4)

During an electrochemical reaction current flows spontaneously in the direction of the more negative half reaction potential. Current is a measure of rate of the cathodic and the anodic reactions taking place at the electrode surface, as it represents the flow of electrons per unit time (1 A = 1C/s). In electro-kinetics studies, current is usually expressed in terms of current per unit area of the electrode, known as current density i,. Cathodic currents are defined as negative and anodic currents are positive (Enos and Scribner, 1997).

It is possible, however, to change the direction of the current by applying an external source to force a reaction against the spontaneous direction (this is the case in electrowinning) (consider Figure 2.7). The voltage that is applied over the cell is a combination of the potential difference between both electrodes and solution, with the voltage drop across the cell, thus;

$$V_{cell} = E_a + E_s + E_c \qquad \text{(Eq. 2.5)}$$

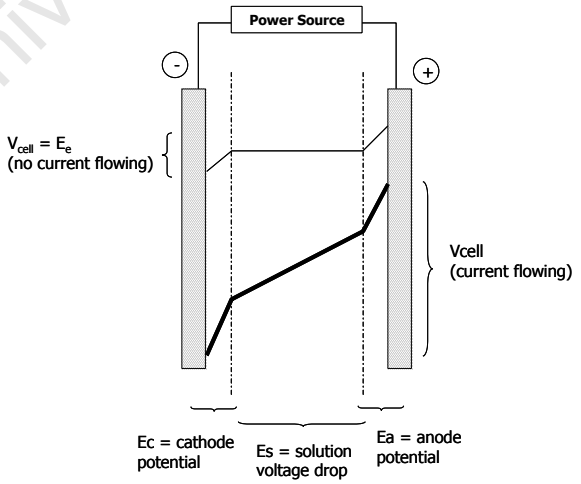

Figure 2.7. Potential and voltage drops in a typical cell arrangement (Petersen, 2009).

When there is no current flowing, the potential of an individual electrode is determined by Nernst equation (Eq. 2.2). Under these conditions equilibrium prevails which means that forward and reverse reactions occur at the same rate and hence no net change occurs.

In a system where there is current flow due to the applied potential, current flow in one direction will be larger than that in the other and hence a net anodic or cathodic reaction occurs. The relationship between current (or current density) and potential, E, is described by the Butler-Volmer (BV) equation (Petersen, 2009, Zhang et al., 2009):

$$i = i_0 \left\{ \exp\left[(E - E_e) \frac{1-\alpha}{RT} F \right] - \exp\left[(E - E_e) \frac{-\alpha}{RT} F \right] \right\} \quad \text{(Eq 2.6)}$$

anodic contribution — cathodic contribution

where i_0 is the exchange current density, which is a characteristic parameter of the half-cell reaction, E_e is the rest potential, α is a symmetry factor related to the nature of electron transfer. At equilibrium when no net current flows the potential is the equilibrium potential and the cathodic and anodic current densities, i_a and i_c respectively, are the same as the exchange current densities. The exchange current density is hence a measure of the kinetic activity of the half-cell reaction at equilibrium. Values of i_0 vary from the order of 10^{-7} to 10^{+5} mA/m^2 (Table 2.4, last column). This large variation in exchange current density values makes them important, but these are seldom reported in literature when studying mineral dissolution electrochemistry. Simplifications of the BV equation result in the Tafel equations (represented by Eq. 2.7) for the anodic and cathodic reactions.

$$\eta_a = b \log_{10}\left(\frac{i_a}{i_0}\right)$$

$$\eta_c = b \log_{10}\left(\frac{i_0}{i_a}\right) \qquad \text{where } b = 2.303\frac{RT}{(1-\alpha)F} \quad \text{(Eq 2.7)}$$

$\eta_{a \text{ or } c}$. is the overpotential of the anode and cathode, and a and b represent the Tafel slopes.

Table 2.4 Electrochemical Parameters of some reactions, 25 °C (Petersen, 2009).

Reaction	Electrode	E^0 (V)	Solution	Tafel Slope (mV)	i_0 A/m^2
$2H^+ + 2e \rightarrow H_2$	Hg	0	1M H+	120	5.10^{-9}
"	Zn	0	"	120	1.10^{-6}
"	Ni	0	"	120	1.10^{-3}
"	Pt	0	"	30	1.0
Ni^{2+} _ 2e → Ni	Ni	-0.26	1M $NiSO_4$	120	2.10^{-5}
Zn^{2+} +2e → Zn	Zn	-0.76	1M $ZnSO_4$	40	0.2
"	Zn		1M ZnCl	30	3
$Cu^{2+} + 2e \rightarrow Cu$	Cu	0.34	1M $CuSO_4$	40	0.2
$Ag^+ + e \rightarrow Ag$	Ag	0.80	0.1M Ag^+	60	1.10^{+4}
$2H_2O \rightarrow O_2 + 4H^+ + 4e$	Pt	1.23	1M H_2SO_4	120	1.10^{-4}
"	αPbO_2	1.23	"	120	1.10^{-8}
Fe^{3+} e → Fe^{2+}	Pt	0.77	0.1M $Fe^{2+,3+}$	120	2.10^{+3}

2.3.2 Oxidative dissolution of chalcopyrite

Study of electrochemistry assists in the understanding of the nature of the redox reactions that take place at the surface of chalcopyrite during dissolution. Oxidative (or anodic) dissolution of chalcopyrite has been studied extensively over the last three decades (for example (Burkin, 2001; Hiroyoshi et al., 2001; Jáuregui and Reyes, 1987; Warren et al., 1982; Biegler and Horne, 1985;Biegler and Swift, 1979). Their studies have been performed in different types of media (acidic or basic) with different oxidizing solutions (ferric, cupric, sulfate or chloride, etc.). In most of these studies, a lot of focus had been dedicated to H_2SO_4 acidic media with ferric as an oxidizing agent. All these studies were aimed to contribute towards understanding

the mechanisms and kinetics during dissolution of chalcopyrite for copper metal extraction. They based their studies on the fundamental premise that the reactions that occur during dissolution of chalcopyrite in oxidizing media are essentially electrochemical in nature.

During anodic reactions at the surface of chalcopyrite, the sulfide component of the mineral is oxidized by loss of electrons to give the product copper ions. The rate of this reaction has been observed to be slow (Córdoba et al., 2008). Most authors agree that the rate of the dissolution reaction is strongly influenced by a passivating layer that forms on the surface of the mineral as the reaction takes place (Hackl et al., 1995; Warren et al., 1982; Biegler and Horne, 1985). The formation of this layer hinders access to the mineral surface for further oxidation reactions to take place. The presence and nature of the passivating layer has been the root for vigorous research on the dissolution of chalcopyrite, in order to explain the refractory nature of the mineral. Understanding of how this layer forms, will offer insight on the mechanism observed for chalcopyrite dissolution and potentially point to a way to overcome it. The reaction for chalcopyrite oxidation at the anode has been widely accepted as the one shown in reaction 2.19. Some authors have also elucidated the mechanism of oxidative dissolution of chalcopyrite stoichiometry to be a combination of two reactions (2.22 and 2.23) (Warren, 1978).

$$CuFeS_2 \rightarrow Cu^{2+} + Fe^{3+} + 2S + 5e \quad (2.22)$$

$$CuFeS_2 + 8H_2O \rightarrow Cu^{2+} + Fe^{3+} + 2SO_4^{2-} + 16H^+ + 17e \quad (2.23)$$

Considering the anodic reactions and the passivating film that forms during the dissolution of chalcopyrite, Biegler and Swift (1979) observed that equimolar amounts of Cu^{2+} and Fe^{2+} were present in solution after leaching. They also observed that the ratio of sulfur to sulfate produced in reactions (2.22 and 2.23) was about 6:1. They concluded that the passivating layer that forms during chalcopyrite dissolution is predominantly composed of elemental sulfur. At a later stage Biegler and Horne (1985), also studying the same reactions in a different study, they observed the ratio of copper to ferrous in the products to be 4:1. In their studies they concluded that the layer that forms on the chalcopyrite surface was a mixture of

elemental sulfur and CuS solid phase. They proposed the reaction (2.24), with the thickness of the passivating layer observed to be 2.9 nm formed from a 3.7 nm thick layer of the mineral that reacted.

$$CuFeS_2 \rightarrow 0.75CuS + 0.25Cu^{2+} + Fe^{2+} + 1.25S^0 + 2.5e \quad (2.24)$$

Warren et al. (1982) studied the effects of the passivating film using current density measurements (Chrono-amperometry, discussed in detail in the sections that follow). Reporting on chalcopyrite from different sources, the authors observed that decay in the current density over time is affected by potentials between 0.59-0.84 V, for purer chalcopyrite samples. At a potential between 0.9-1.04 V, they observed no current decay (fig 2.8). This decay in current density was then associated with the progressive thickening of the passivating layer. In addition, the authors observed that ferrous ions had a positive contribution on the overall leaching of chalcopyrite (also later observed by Hiroyoshi et al. (2001).

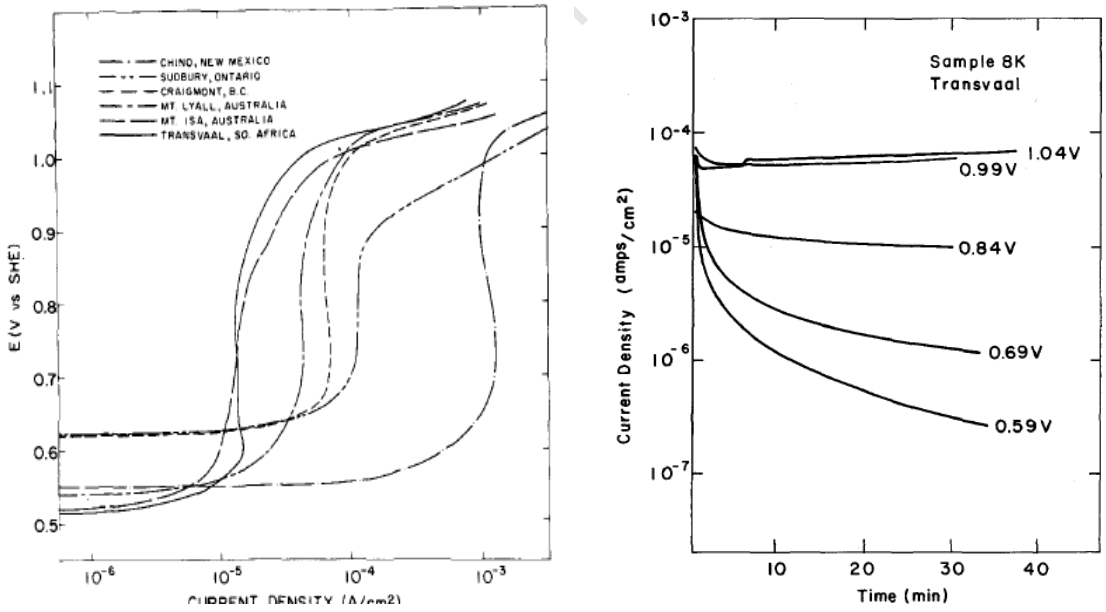

Figure 2.8. Anodic polarization scans (left) for chalcopyrite sample from different sources, and current density vs. time scans at specific potentials for one of the samples as observed by (Warren et al., 1982).

Addition of ferrous ions resulted in an increase in current density in the lower potential region, the passivating region. The conclusion drawn from these studies was that there are other solid phases that are present at the passivating layer at low potentials. This resulted in the suggestion that leaching of chalcopyrite goes through intermediate solid phases which allow it to be more susceptible to dissolution. These intermediates were observed to be bornite ($CuFeS_4$) and covellite (CuS), in support of reaction (2.24). (Parker at al., 1981) suggested that the passivating layer formed was due to a copper-rich polysulfide which had different semiconductor properties to chalcopyrite. The metal polysulfide was concluded to slow down the transport of ions and transfer of electrons between oxidizing agent and chalcopyrite. Subsequent and recent reports (Córdoba et al., 2008; Hiroyoshi et al., 1997; Hackl et al., 1995) closely agree with older studies on the layers that form during anodic reactions taking place at the surface of chalcopyrite during leaching in acidic and ferric media.

Hence in all studies on oxidative dissolution of chalcopyrite that have previously been performed, it is agreed that there is a passivating layer that forms on the surface of the mineral. Disagreements only come up when trying to describe what constitutes this layer, how and the level at which this layer forms, and also on descriptions on its effect on the rates of chalcopyrite dissolution. Electrochemical corrosion studies have also been shown to be a useful tool in trying to understand the mechanisms that take place at the anodic sites during chalcopyrite dissolution. Studies at these sites have resulted in a number of observations that have caused substantial debate between different research groups which has not been resolved to this day.

An alternative approach could be to turn away from the anodic reactions and focus attention on the cathodic reactions. These reactions are important, because they take up electrons for mineral dissolution to take place and the overall rate of a redox reaction is determined by both cathodic and anodic parts – to ensure electro-neutrality they both have to proceed at the same rate, which is determined by the slower of the two half reactions. As mentioned, cathodic reactions are important in the contact leaching mechanism. In this mechanism microorganisms create discrete

cathodic sites within the EPS layer. Virtually no attention is given in the literature to the cathodic counter-reaction at the surface of chalcopyrite (usually the reduction of ferric to ferrous), especially in the context of a passivation layer forming on the mineral surface which could interfere with this reaction. Prevention of a passivation layer, as could potentially be achieved locally by attached micro-organisms, could ensure continued support of the cathodic rather than anodic reaction, and therefore further study of the cathodic reduction of ferric on the surface of chalcopyrite may be if some interest.

2.3.3 Reductive dissolution of chalcopyrite

Anodic dissolution of sulfide minerals in sulfate media has been extensively studied as a primary method of treatment for copper leaching. Due to the slow kinetics of chalcopyrite dissolution, alternative methods for mineral decomposition need to be considered. An alternative approach to treatment of chalcopyrite would be to perform a reductive dissolution of the mineral. In comparison to oxidative dissolution, little attention has been focused on this method of leaching. In an electrochemical sense, reductive dissolution also possesses the anodic and cathodic half reactions, where the anodic reaction is the oxidation of the reductant, and reduction of chalcopyrite is the cathodic portion, which is thought of as the collapse in its crystal structure. Different reducing agents can be utilized, for example, metallic copper, iron or hydrogen in acid solutions (Fuentes-Aceituno et al., 2008; Dreisinger and Abed 2002). Generally, reductive decomposition in effect transforms chalcopyrite to a much more reactive secondary copper sulfides (e.g. chalcocite), which can in turn allow for further oxidative dissolution in a secondary step (Fuentes-Aceituno et al, 2008; Dreisinger and Abed, 2002; Elsherief, 2002). Products of the reductive reactions of chalcopyrite in acidic media have been observed to be hydrogen sulfide, ferrous, secondary copper sulfides, and trace amounts of elemental copper and sulfur.

During reductive dissolution with a transient (non-atomic) hydrogen as a reducing agent, principal reactions (2.25 – 2.27) were proposed (Fuentes-Aceituno et al., 2008). These are multi-step reactions where the transient hydrogen is first produced, reduces chalcopyrite to chalcocite, hydrogen sulfide and ferrous oxidised to sulfur and ferric, respectively.

$$2CuFeS_2 + 2H\bullet + 4H^+ \rightarrow Cu_2S + 3H_2S + 2Fe^{2+} \quad \text{(cathodic)} \quad (2.25)$$

$$H_2S \rightarrow S^0 + 2H^+ + 2e$$

and (both anodic) (2.26)

$$Fe^{2+} \rightarrow Fe^{3+} + e$$

$$2CuFeS_2 + 6H^+ \rightarrow Cu_2S + 3S^0 + 2Fe^{3+} + 3H_2 \quad \text{(overall)} \quad (2.27)$$

Finally the transient hydrogen can then be converted to molecular hydrogen in another separate step at the cathode (not shown), resulting in the products in the overall reaction (2.27). These reactions are not very well established in practice; however it is thought that pre-reduction of chalcopyrite with this method would result in a solid product that may then further be treated with an additional oxidant, hydrogen peroxide, which oxidizes the chalcocite, thereby allowing the copper to dissolve (Fuentes-Aceituno et al., 2008). Ferric ion obtained in the cathodic reaction could serve as an oxidant for Cu_2S, however its formation has been observed to be disadvantageous in the chalcopyrite reduction stage.

Dreisinger and Abed (2002) studied reductive dissolution of chalcopyrite utilizing metallic iron as a reducing agent in acidic media. Advantages in using iron as a reductant are because of its low price, availability, and full compatibility with the leach solution. In their studies, the authors aimed to establish an understanding of the physical chemistry of the reductive leaching of chalcopyrite (2.28). During dissolution of the mineral, there is also a second competing reaction (2.29, termed hydrogen evolution reaction) that was observed, but to simplify kinetic calculations,

they assumed that these two reactions are identical. Metallic iron as a reducing agent was found to have a direct effect on the conversion of chalcopyrite not beyond twice the stoichiometric amounts of reaction 2.28, because the competing reactions (e.g. 2.29) would start taking effect. Electrochemical half reactions that occur during this process were not very well established.

$$2CuFeS_2 + Fe_{(s)} + 6H^+_{(aq)} \rightarrow Cu_2S + 3Fe^{2+}_{(aq)} + 3H_2S_{(g)} \quad (2.28)$$

$$Fe_{(s)} + 2H^+_{(aq)} \rightarrow Fe^{2+}_{(aq)} + H_{2(g)} \quad (2.29)$$

On another study, Elsherief (2002) studied the cathodic scan limit, and effect of ferrous and cupric ions on the effect of reductive dissolution of chalcopyrite in H_2SO_4 using a carbon paste electrode. The authors used this study to predict the reactions and products that form at cathodic currents during chalcopyrite dissolution. The major products that were observed were hydrogen sulphide and ferrous ion together with the solid phases – bornite, chalcocite and elemental copper, formed in the order with decreasing potential (2.30 – 2.33). These reactions were observed to occur at different cathodic potentials, where at -245 mV_{SHE}, reactions (2.30) and (2.31) occurred, resulting in talnakhite and bornite, respectively. At higher cathodic potentials approx. -700 mV_{SHE}, reaction (2.32) formed chalcocite with a complete removal of iron from the chalcopyrite lattice. Further reduction of chalcocite was observed at potentials above -1000 mV, and these potentials were also thought of as sufficient for elemental copper to be obtained, shown in reaction (2.33) (Batlett et al., 1986).

$$9CuFeS_2 + 4H^+ + 2e \rightarrow Cu_9Fe8S_{16} + Fe^{2+} + 2H_2S \quad (2.30)$$

$$5\ CuFeS_2 + 12H^+ + 4e \rightarrow Cu_5FeS_4 + 4Fe^{2+} + 6H_2S \quad (2.31)$$

$$2CuFeS_2 + 6H^+ + 2e \rightarrow Cu_2S + 2Fe^{2+} + 3H_2S \quad (2.32)$$

$$2Cu_2S + 4H^+ + 4e \rightarrow 4Cu + 2H_2S \quad (2.33)$$

Liberation of H_2S from all reactions can be assumed to reduce the level of formation of the passivating layer. Thus cathodic reactions might prove to have a positive effect on the leaching of chalcopyrite by production of intermediates that show better oxidative dissolution than chalcopyrite, by evolution hydrogen sulfide instead of forming elemental sulfur, and by producing elemental copper. Reactions in ferric solutions are also reported to have a positive effect on the dissolution of the mineral due to the oxidations of ferrous to ferric, which has been shown increase dissolution of chalcopyrite (Elsherief, 2002).

2.4 Theory and practice of electro-analytical methods in the dissolution of chalcopyrite

As already stated, mineral dissolution is an electrochemical corrosion process, thus electrochemical analysis methods can be utilized for fundamental understanding of this process. These electro-analytical techniques have been utilized to assist in understanding the slow rates observed for chalcopyrite leaching. Electro-analytical methods for corrosion studies require a potentiostat. A potentiostat is an electronic instrument that controls the electrical potential between the working and reference electrodes of a three-electrode cell. The three electrode system comprises of the reference electrode (RE), working electrode (WE) and the auxiliary/counter electrode (AE or CE) (Figure 2.9). A potentiostat applies the desired potential between the working electrode and the reference electrode. Current required to sustain electrolysis at the working electrode at the desired potential is provided between the auxiliary and the working electrodes. This type of set-up prevents large currents that could change the potential passing through the reference electrode. This system is a controlled circuit, whereby current is controlled in such a way that potential is maintained at a target level. It also permits one to minimize voltage errors due to Ohmic (IR drop) loss through the solution by placing the reference electrode physically close to the working electrode surface. To study the current and potential responses using a potentiostat, there are different methods that can be employed.

Examples include coloumetry, chrono-potentiometry, chrono-amperometry, voltammetry, and many more. For the purposes of the present study, only concepts of chronoamperometry and voltammetry are reviewed.

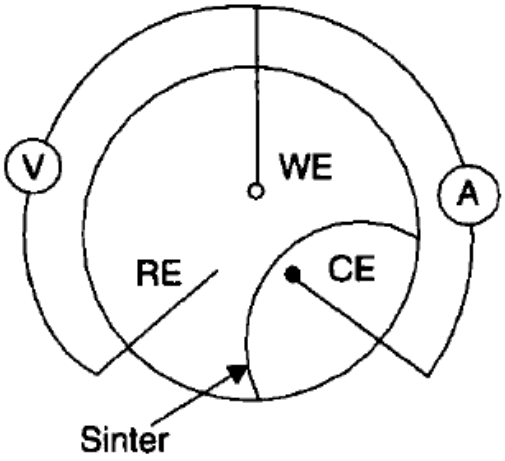

Figure 2.9. The three-electrode electrochemical cell system utilized in potentiometric studies (Monk, 2002)

2.4.1 Voltammetry

In voltammetry potential applied across the working and the reference electrodes can be considered an excitation signal. The resulting signal is a triangular waveform, which sweeps the potential of the electrode between two values (Figure 2.10b) (Kissinger and Heineman 1983). The potential of the working electrode is ramped at a certain scan rate, *v*. The current can be considered as the response signal to the potential excitation signal. The resultant plot of potential I (or i), versus current E is termed a voltammogram, and since potential varies linearly with time, the horizontal axis can be thought of as a time axis. There are linear sweep voltammetry (LSV) and cyclic voltammetry (CV). During linear sweep voltammetry, the potential of the working electrode is ramped from initial potential E_i to a final potential E_f, usually at slow scan rates. The resulting current trace is plotted as a function of scan rate $\left(\frac{E-E^0}{v}\right)$, that is, the overpotential (η).

The other type of voltammetry, which is commonly utilized in electrochemical analysis, is cyclic voltammetry. The potential is similarly ramped from an initial to a final potential, but instead of stopping at the end of the linear sweep, the potential scan is reversed (Figure 2.11a). The sweep is usually performed in cycles. The current response at different scan rates allows conclusions about the various electrochemical reactions taking place at any point during the sweep.

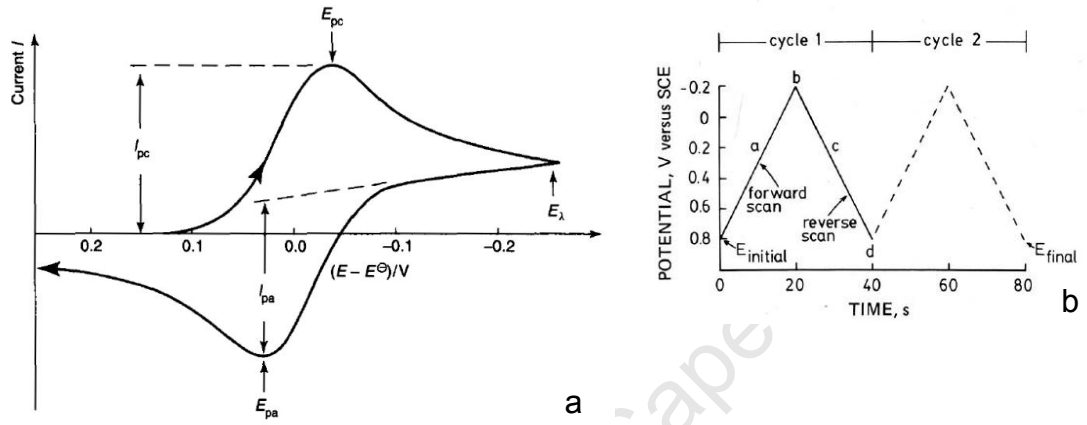

Figure 2.10. (a)A typical cyclic voltammogram for the reduction (forward scan) reaction and oxidation (reverse) of the electrochemically active species. The potential in this cyclic voltammogram is shown as overpotential. (b) Shows an excitation signal, that is, the potential plotted against time, in LSV (until point b) and CV (until point d). Two CV cycles (second cycle is dotted) are shown in the insert; where the switching potential is at b (Monk, 2002; Kissinger and Heineman, 1983).

In the beginning of a CV scan, an electrochemically active species is chosen at a certain concentration of a solution that acts as a supporting electrolyte. An initial potential is chosen to avoid any reactions that occur between the electrolyte and the electrode, prior to starting the sweep. The electrode is scanned at negative (or positive) potentials; forward scan, until the potential is sufficient to reduce/oxidize the electrochemically active species. At this stage the electrode is acting as a strong oxidant (or reductant) to convert the electrochemically active species. The current increases rapidly until the concentration of the electrochemically active species at the electrode surface are substantially diminished, causing the current to peak. The current then decays as a result of the solution surrounding the electrode being depleted due to the electrolytic conversion of the reductant to an oxidant (or vice versa). The potential at which the reverse scan occurs is known as the switching potential, E_λ. At this stage the potential is still sufficiently negative (or positive)

enough to reduce (or oxidize) the electrochemically active species. The electrode then becomes a strong oxidant (if the forward scan was oxidation) or reductant (if the forward scan was reduction). A current peak is observed for this reverse scan for similar reasons as stated for the forward scan. The cycle is complete when the potential reaches the initial potential at the beginning of the scan. The scan can then be repeated (if more than 1 cycle is required). Thus, CV is capable of rapidly generating a new oxidation state during the forward scan and probing its fate on the reverse scan. It is essential to apply initial potentials that do not allow for undesired electrolysis of the electrochemically active species as a result of applying the initial potential. In voltammetry anodic scans are represented by a positive potential; oxidation reactions, and cathodic scans by negative potentials; reduction reactions. This technique can be understood by considering the Nernst equation and the changes in concentration that occur in the solution adjacent to the electrode during electrolysis. The scan rate between the initial potential, E_i, and the switching potential, E_λ in CV, is the same as that from the switching potential to the final potential E_f (which might be at the initial potential) in the reverse scan. A cyclic voltammogram is the result of such a scan and this is characteristic for an electrochemical couple that is reversible in the thermodynamic sense. Electro-reversibility of an electrochemical couple has the following diagnostic features;

- $I_{pc} = I_{pa}$
- Peak potential E_{pc} and E_{pa} are independent of the scan rate
- $E^{0'}$ is positioned midway between the two peak potentials so that $E^{0'} = \frac{E_{pa}+E_{pc}}{2}$
- I_p is directly proportional to $\sqrt{v}$
- Separation between E_{pa} and E_{pc} is $\frac{59}{n}$ mV for an n-electrode process.

If the electrode reaction is reversible, the peaks of the forward and the reverse scan in the cyclic voltammogram will be similar in shape and magnitude. The peak positioning in cyclic voltammetry of a fully reversible system contains thermodynamic information, since the two peaks are positioned on either side of the formal electrode potential $E^{0'}$ (equals $\frac{E_{pc}+E_{pa}}{2}$), which is ultimately the same as the standard electrode potential $E^{\ominus}$. This technique is essential for studying dynamic electrochemistry and

useful for discerning kinetics and mechanisms, in addition to thermodynamic parameters which are usually obtained at equilibrium.

Voltammetry has been utilized as the method of choice for electrochemical studies of chalcopyrite for many years. Ever since dissolution of a mineral was observed to be a corrosion process, voltammetry has been utilized. LSV and CV have been utilized in chalcopyrite dissolution to elucidate the reactions that occur at specific potentials, to establish the irreversibility of the chalcopyrite electrochemical dissolution reaction, and effects of scan rate (Hiroyoshi et al., 2008; Nava and González, 2006; Hiroyoshi et al., 2004; Gómez et al., 1996; Biegler and Horne 1985; Warren et al., 1982; Biegler, 1977). A general consensus for anodic voltammetric studies of chalcopyrite dissolution is that polarization curves show a region where current depends steeply on potential, sometimes with several steps or inflections, and an approach to a limiting current at high potentials. Classical research on the anodic dissolution of chalcopyrite by using voltammetry as a method of choice showed that there was a prewave region in the beginning stages of the scan on a freshly polished electrode. This prewave (also known as the activation of dissolution) region is regarded as the portion of the voltammogram where the main chalcopyrite electrochemical reactions occur (Warren et al., 1982, Biegler, 1977). Variation in the position of the prewave has been observed, and these have been attributed to origin of the chalcopyrite source, the electrode polishing method used, time delay between starting electrode preparation and starting the voltammetric sweep, and many more. The dissolution region on a voltammogram is followed by a passive region, where there is current does not show any dependence on the increasing potential. Lastly voltammetric studies have also shown a region that is called the transpassive region where current increases steeply at higher potentials (regions shown in Figure 2.11). Generally voltammetric sweeps show this typical behaviour according to most research that has been performed.

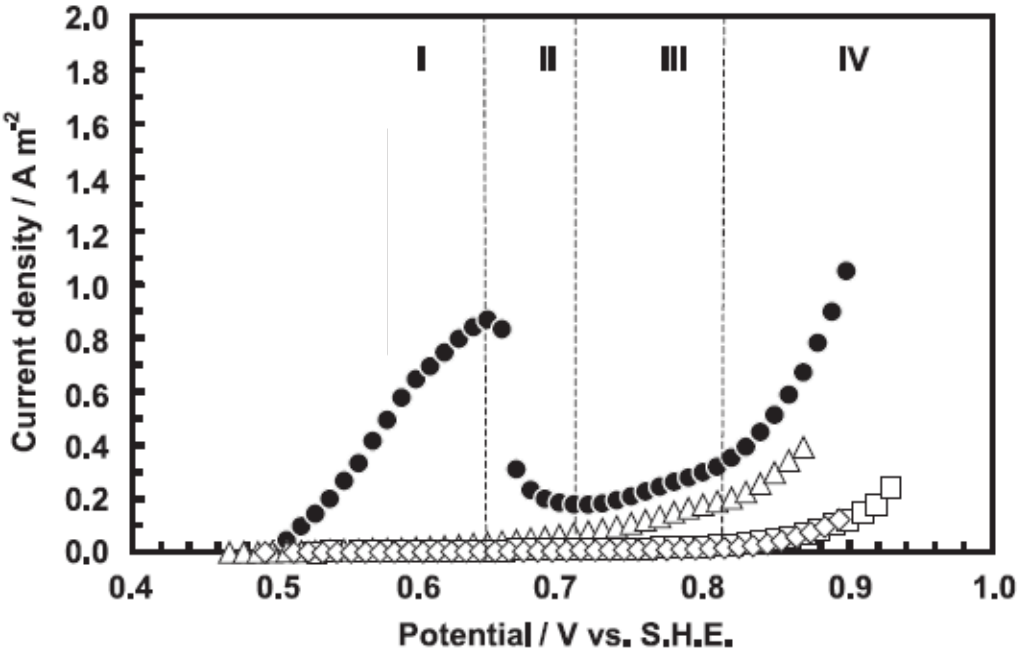

Figure 2.11. A typical LSV curve showing (I, active region; II, transient region; III, passive region; IV, trans-passive region (Hiroyoshi et al, 2004).

2.4.2 Chrono-amperometry

Generally in a chrono-amperometric experiment, potential is stepped to a target potential and then maintained there for a certain length of time. This is done to monitor current changes from the time of the step potential to the end of the experiment. A plot of current against time is obtained, whereby a rapid rise in current is followed by a gradual decline, is usually observed. Current declines smoothly after the rise time until, eventually reaching a final level that might approach zero (Figure 2.12). This process can take up to a time that is set for the step potential. At the beginning, before the target potential is stepped, the electrode is surrounded by the solution ion, the concentration of which is similar throughout the solution. After the potential is stepped, redox reactions occur at the surface and very soon the solution surrounding the electrode contains only the electrochemically modified product. A quantitative description of how the current trails with time in a chronoamperometric study is given by the Cottrell equation (Eq 2.8).

$$I_{lim} = nFAc_{analyte}\sqrt{D/\pi t} \quad \text{(Eq. 2.8)}$$

Where I_{lim} is the limiting current, A is the area of the electrode, $c_{analyte}$ is the concentration of the analyte, and D is the diffusion coefficient. Application of the Cottrell equation relies in the current being limiting, which means that the potential must be stepped to an extreme overpotential to ensure that I_{lim} is proportional to $c_{analyte}$. The Cottrell equation is based on a model that assumes that electrons have to diffuse through a growing, semi-infinite layer at the surface of the electrode. Application of the Cottrell equation has the following experimental and instrumental limitation (Bard and Faulkner, 1980);

- Potentiostatic limitations; the Cottrell equation predicts high currents for short periods of time, but actual maximum current may depend on the current voltage output characteristics of the potentiostat.
-

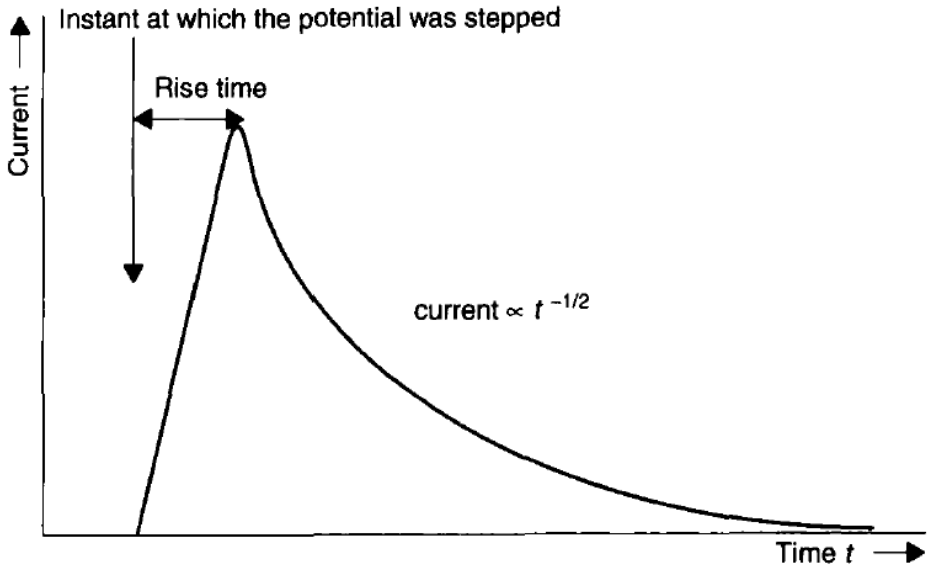

Figure 2.12 A chronoamperometric plot of current against time. Insert shows a potential step plot from E_1, when the analyte is electroinactive to E_2, where the analyte is converted to an electrochemically modified product. (Monk, 2002).

Chronoamperometric studies with regards to chalcopyrite dissolution have mostly been performed in the anodic region (Hiroyoshi et al., 2004; Lu et al., 2000; Warren et al., 1982). In their studies, researchers used this method for qualitative studies to observe different regions during anodic dissolution of chalcopyrite. This method,

when used in conjunction with other electro-analytical methods has been demonstrated to be a valuable tool for explaining potentials where the passive region occurs during dissolution. Hiroyoshi et al. (2004) utilized this technique to observe different changes in current density at potentials where their polarization curves showed interesting results. They further went on to determine that the rate determining step during dissolution is a surface reaction in the low anodic potential region, or a diffusion reaction in the passive region. Disagreements exist over explaining the trans-passive region, where some authors observe an increase in current, whereas others still observe a decrease in current. A decrease (which takes a longer period of time) in current has been connected with both the surface and diffusion reactions taking place at the same time on the electrode (Hiroyoshi et al., 2004).

2.5 Enhancement of chalcopyrite oxidative reaction by additional ions in solution

Recent studies by Hiroyoshi and co-workers have shown that addition of different ions in solution enhance anodic dissolution of chalcopyrite (Hiroyoshi et al., 2007; 2001, 2002, 1997). The first of these series of experiments studied ferrous sulfate systems instead of the commonly utilized ferric sulfate leaching (Hiroyoshi et al., 1997). Different sample of chalcopyrite from different locations were utilized in these studies and it was found that only one out of four sample showed a higher leaching of copper in ferric media after 168 hours, whereas the other three showed higher leaching with ferrous media. In the same study it was shown that an increase in ferrous concentration further enhanced copper recovery. In another study led by the same author, oxidative leaching of chalcopyrite was studied in normal ferric media with addition of Fe^{2+} ions in solution (Hiroyoshi et al., 2000). Ferrous ions containing cupric ions in solutions were shown to increase copper extraction. The authors proposed a model that suggested that chalcopyrite leaching is an electrochemical process, which is mainly controlled by the redox potential of the solution, and that extraction was enhanced at lower potential regions. This model suggested that

chalcopyrite is firstly reduced by Fe^{2+} ions in the presence of Cu^{2+} to form Cu_2S (2.34), followed by ferric oxidation of Cu_2S to obtain copper (2.35); where *x* represents a mole of Cu_2S oxidized by Fe^{2+} per mole of Cu_2S formed in reaction 2.34.

$$CuFeS_2 + 3Cu^{2+} + 3Fe^{2+} \rightarrow 2Cu_2S + 4Fe^{3+} \quad (2.34)$$

$$2(1 - x).Cu_2S + 8\,(1 - x)Fe^{3+} \rightarrow 4(1 - x).Cu^{2+}\ 8(1 - x)Fe^{2+}\ 2(1 - x)S \quad (2.35)$$

As discussed earlier, this model provided more information towards the proposal that chalcopyrite dissolution goes through intermediate sulfide minerals, which are easier to oxidize.

Work performed by Hiroyoshi and colleagues was novel in studying the effect of inclusion of Fe^{2+} ions into leaching studies, but these types of studies have not been explored in electrochemical sense.

2.6 Objectives of research

As covered extensively in the preceding literature review, chalcopyrite is known for its refractory nature in ferric sulfate media in the interim range of potentials. This behaviour of chalcopyrite is attributed to a formation of surface layers, bringing about the passivation phenomenon. Previous research has shown that surface layers that form during chalcopyrite dissolution might be in a form of a mixture of secondary copper sulfides and/or sulfur species. In the electrochemical sense these surface layers can be thought of as restricting the flow of dissolved ions from the surface of the mineral and thus create an electrical resistance. It would be logical to postulate that formation of these surface layers also inhibits the cathodic reaction (2.21), although this effect does not seem to have been studied in isolation. Thermophillic microorganisms potentially offer a way around this issue, that is, by creating cathodic 'islands' on the mineral surface, through which the flow of electrons from the mineral

is less inhibited, thus facilitating a higher rate of anodic dissolution outside these 'islands', even in the presence of passivating layers. It would therefore be of interest to study the cathodic ferric reduction reaction in the context of anodic dissolution of chalcopyrite. A conventional method of studying anodic dissolution of chalcopyrite has been shown to be by utilizing electrochemical techniques. Previous studies have generally not focused any attention on the simultaneously occurring ferric reduction reaction on the surface of the mineral. Therefore, putting some focus into this reaction could assist in a further elucidation and understanding of the passivation/de-passivation behaviour in ferric sulfide media. The electrochemical techniques of choice are linear sweep voltammetry and chrono-amperometry. Utilization of these two methods can offer different pieces of information in terms of electrochemical studies on chalcopyrite dissolution.

The present study is aimed as preliminary work towards a larger objective of research. It is aimed as an initial study for development of methodologies, testing the electrochemical techniques mentioned above and confirming trends observed in literature. The most important part of the present work hones in on the novel work that has been given special attention by Hiroyoshi and co-workers. In this project, the type of work by Hiroyoshi is expanded, whereby the effect of the ratio between ferric/ferrous ions in solution is investigated for anodic dissolution of chalcopyrite (by polarization studies). These studies are performed under different temperature and total iron concentrations. The larger objective of the present study was to set precedence for a more advanced study that would investigate more closely the effect of the cathodic reaction of attached microorganisms. The present study is limited, however, to investigating the effect of dissolved iron on the polarization of chalcopyrite in abiotic ferric sulfate systems.

3 EXPERIMENTAL

3.1 Apparatus

3.1.1 Experimental set-up

A 50 ml thermostatically jacketed titration vessel was purchased from Metrohm South Africa (Pty) Ltd, shown in Figure 3.1. The vessel consisted of an air tight sealable top lid with 5 stoppable openings on top. Rubber fittings were prepared to be able to fit the three electrodes. The other openings of the lid were kept closed with the stoppers that came with the vessel. A recirculation pump waterbath was used for heating the reaction vessel during experiments.

Figure 3.1. Thermostatically jacketed reaction titration vessel that was used as a rection vessel for experiments and its lid (Metrohm SA (Pty) Ltd)

Connections between the potentiostat and electrodes were achieved by direct connection onto the hardware with colour coded crocodile clips. Electrode colour codes were as follows;

- White – Reference electrode
- Red (counter) and Orange (counter-balance) – Counter electrode
- Green – Working electrode

The reaction vessel was attached to a retort stand, to ensure that the vessel was stable. The complete experimental set-up is shown in Figure 3.2. The reference electrode used for all experiments was a SCE, and a platinum wire was used as a counter electrode.

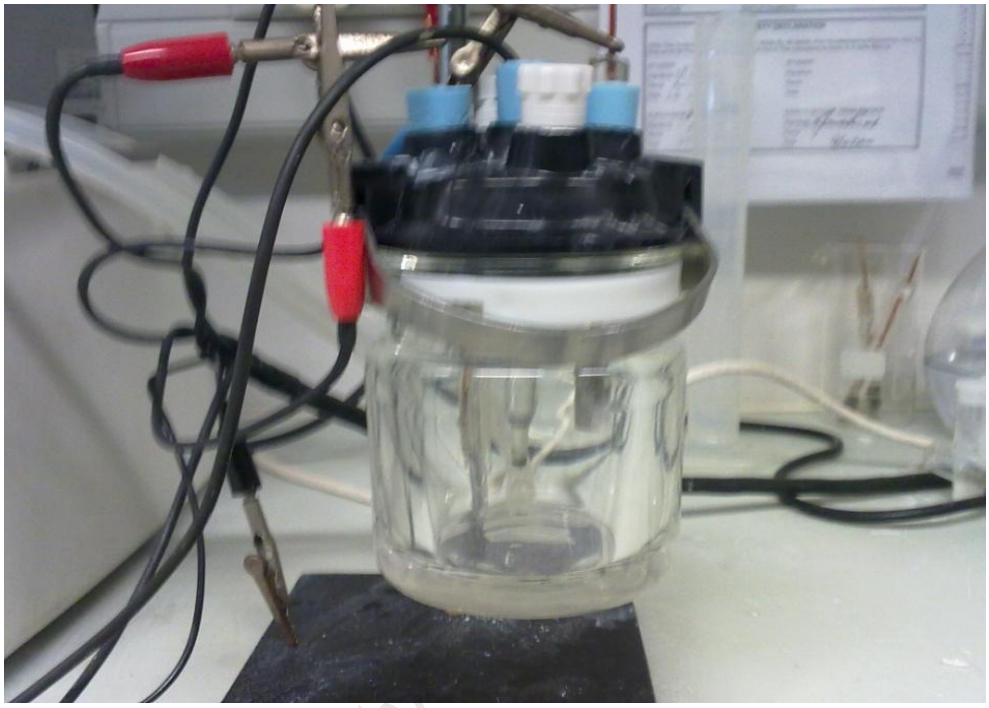

Figure 3.2. Experimental set-up for all experiments that were performed.

3.1.2 **Potentiostat** (Gamry Instruments 1990 - 2008)

The potentiostat utilized for running experiments was obtained from Gamry Instruments. For electrochemical studies performed, a Series G300 potentiostat model was utilized. This potentiostat is usually suited for small current measurements, due to the size of the electrodes used in the experiments for this work. The PHE200™ Physical Electrochemistry software was utilized for taking measurements. This software, also from Gamry Instruments, has multiple electrochemistry experimental methods, eg CV, LSV, chono-potentiometry, chrono-amperometry, coloumetry, etc. With this software the following specifications were obtained for all experimental protocols:

- Min. Scan Rate: 0.0175 µV/s
- Sampling Period: 3.3 µs-600 s
- Min. Step Height: 12.5 µV
- Max. Points per Data File: 262,143
- iR Drop Compensation

The PHE200™ used Framework™ for data acquisition and Echem Analyst™ for data analysis.

3.2 Chalcopyrite ore and chemicals

3.2.1 Chalcopyrite ore

Research grade chalcopyrite ore was obtained from VWR International: WARD's Natural Science. Two different localities were required and at the time ore minerals were obtained only stock from Durango, Mexico and Ontario, Canada were available. These mineral ores were promised to be of high purity from the supplier. The purity of the two specimens was confirmed with XRD, and it was found that the Durango sample contained 100% chalcopyrite. However, the Ontario sample was observed to contain 75% chalcopyrite, 13% Pyrite and 12% Quartz (Figure 3.3), which may significantly influence the behaviour of the mineral in the test work. As the XRD analysis was done towards the end of the study it was unfortunate that a larger portion of the study had focussed on the less pure Ontario material, but by then it was too late to repeat test work with the Durango electrode

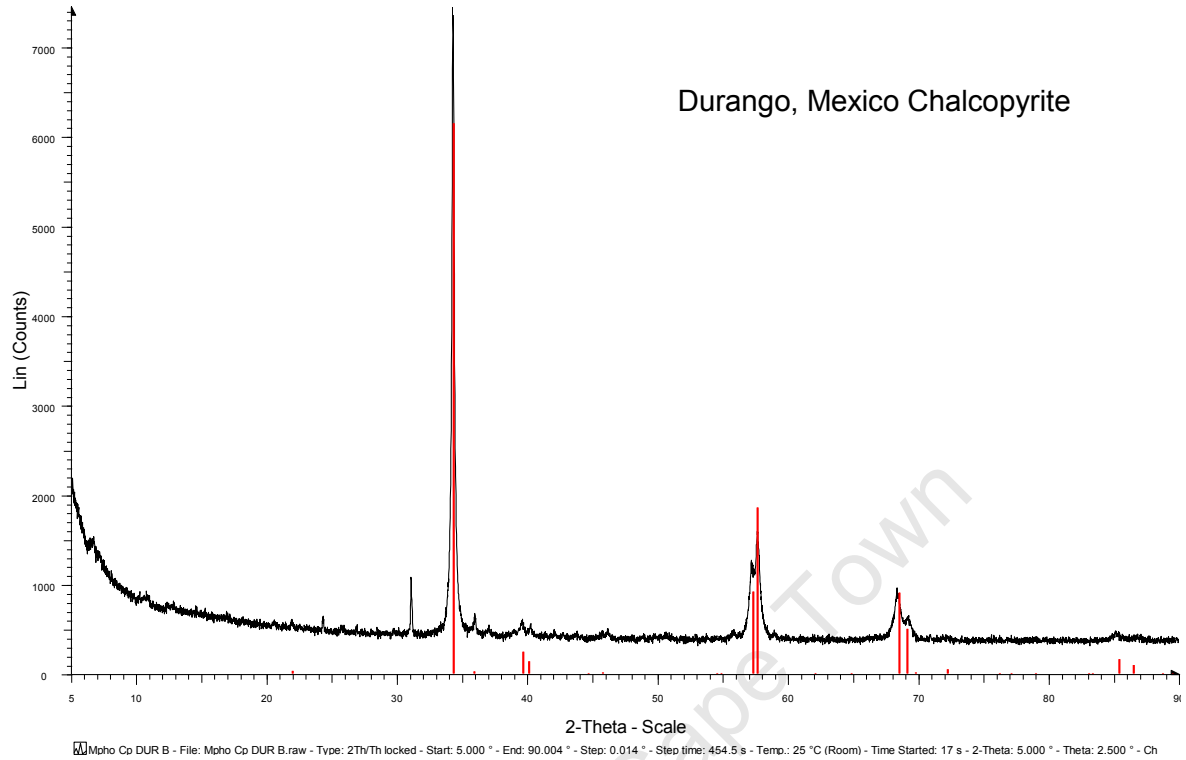

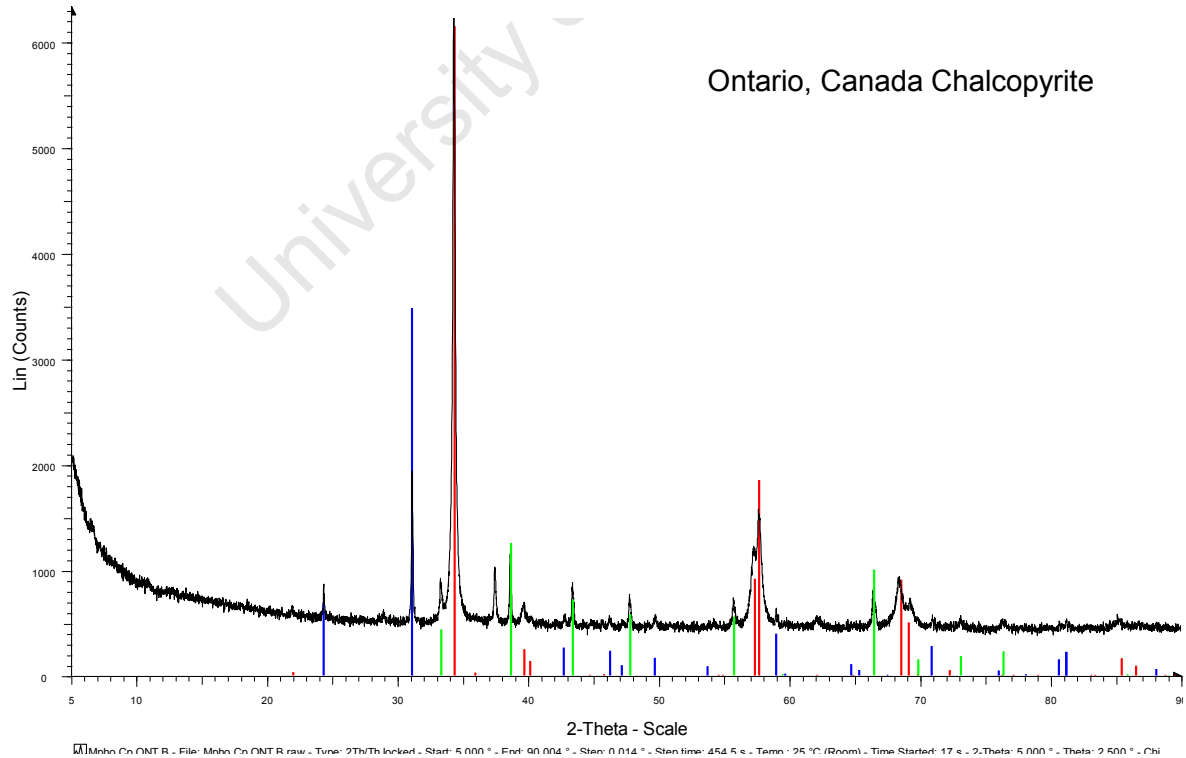

Figure 3.3. XRD analysis data plots for the chalcopyrite samples. The red spikes represent chalcopyrite, blue represent quartz, and green represent pyrite distribution.

3.2.2 Chemicals

Analytical-grade reagents were used for all the experiments. A SpeciFix epoxy resin and a SpeciFix-20 curing agent were obtained from IMP Scientific and Precision (Pty) Ltd. Epoxy resin and the curing agent were mixed at the following ratios, 7:1 (w/w) or 26:5 (v/v). After mixing the solution was stirred for 3 minutes, ensuring that there are no air bubbles that form. The mixture was allowed to sit for *approx*. 5 minutes to set and then used for mounting. SpeciFix-20 curing agents are known to harden for a maximum period of 8 hours, but were left overnight. Ease Release spray, used as an adhesive substance was utilized to allow for easier removal of the mounted material from any surface, and this was obtained from AMT composites. 98% H_2SO_4 that was utilized in all experiments, whereby it was diluted using deionised water to required concentrations (mostly 0.1 M, unless otherwise stated). pH was adjusted using 98% H_2SO_4.

3.2.3 Electrode design

The working mineral electrodes were designed and prepared by cutting up the bulk chalcopyrite mineral particle into small cylindrical shaped forms, with a diameter of 5mm and a 20 mm height. The cut ore was then placed in a small single open ended glass tube of 10 – 12 mm outside diameter. An epoxy release spray was sprayed into the glass tube. Epoxy resin was used to mount the cut mineral ore into the glass tube, resulting in the bottom part of the specimen shown in Figure 3.4. This initial mounting phase was performed because in previous cases, attempting to drill a hole on the mineral itself before mounting resulted in it either cracking or breaking. After the epoxy had cured and hardened, the glass tube was placed in boiling water and the mounted piece removed. A small hole was drilled a quarter to half way into the mineral on the exposed surface using a 0.75 mm diamond drill bit. A copper wire of approx. 180 mm was inserted into the hole. Silver conducting paint was used as an adhesive agent for the copper wire and also to increase contact of

the mineral with the copper wire for increased conductivity. These were left for 24 hours to dry (Figure 3.4).

The resulting material was placed in a release agent pre-treated glass tube of 10 – 12 mm outside diameter and 150 mm height. Final epoxy mounting was performed. The cured material was removed from the glass tube as above; the final specimen shown is in Figure 3.5(a). Carbide paper was used to file down excess epoxy at the bottom as to expose a flat mineral surface (Figure 3.5 (b)).

The surface of the mineral was characterized by utilizing ImageJ software. This software requires images of the surface to be taken before processing. Also, a scale was set by taking the image of the surface with a ruler, and calibrated with the software. For processing of the image a line was drawn around the exposed surface, and finally the image processed. Surface area measurements were then obtained straight from the software already corrected to the scale previously set. The surface area for the mineral specimen was in the range 0.2 – 0.25 cm^2.

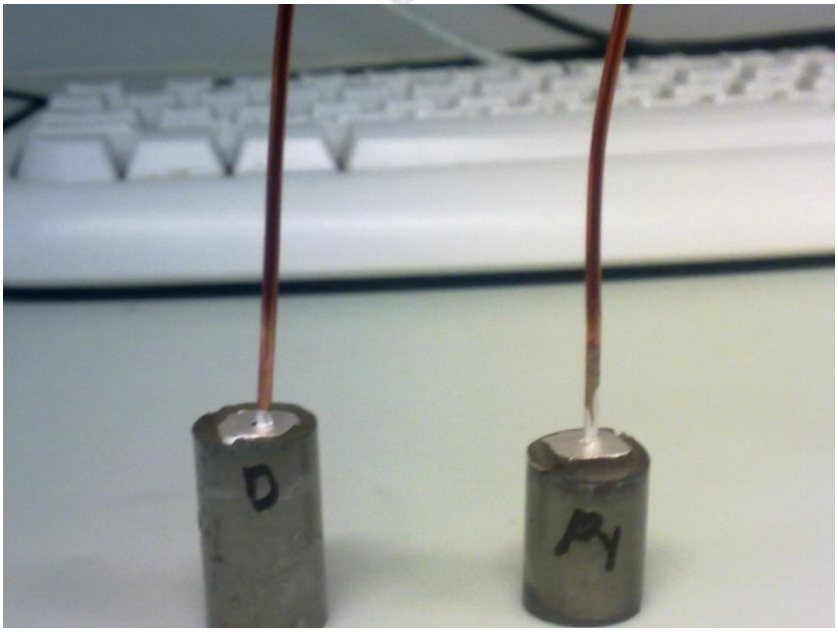

Figure 3.4. The resulting initial mounting of the mineral

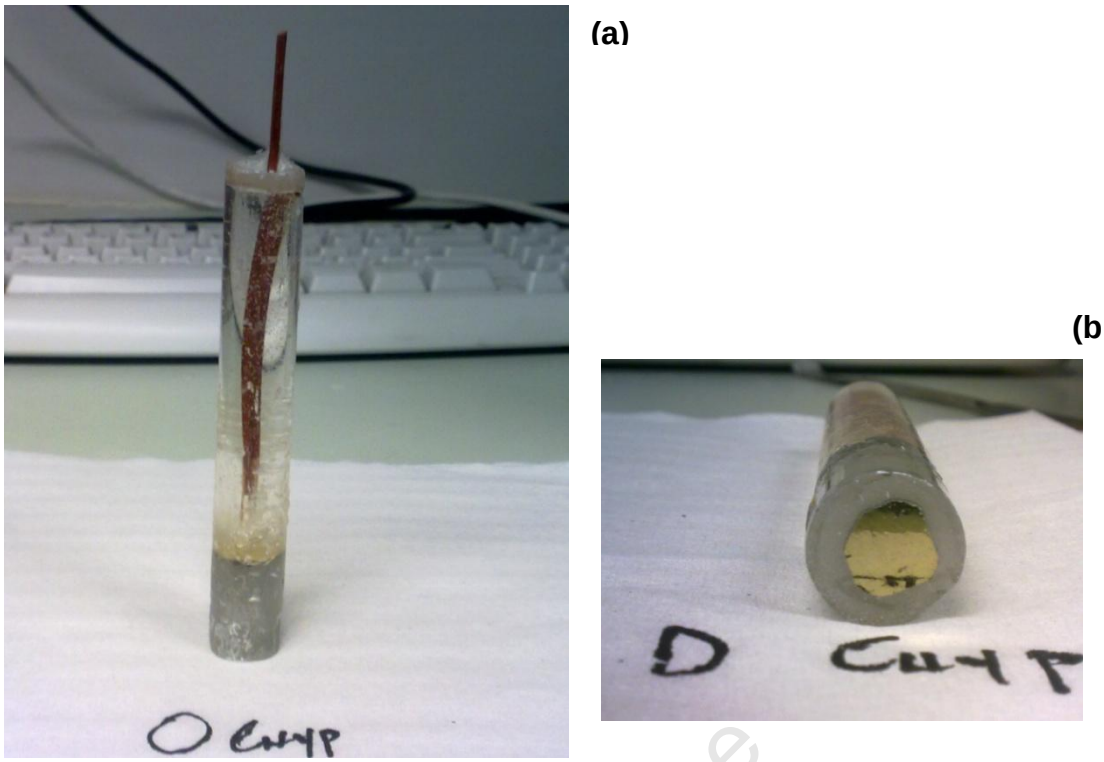

Figure 3.5. The completed working electrode. (a) The complete mounted mineral ore; (b) exposed mineral surface

Mineral electrodes were polished for each and every run; where polishing was performed on pressure sensitive adhesive (PSA) polishing cloths with high purity aluminium powder of sizes 1 micron (Type B), 0.3 micron (Type C) and 0.05 micron (Type A), all obtained from Metallurgical Supply Company Inc. Freshly renewed electrode refers to the electrode surface being polished on a carbide paper, polished with different size aluminium and finally ultrasonically washed in distilled water for 15 minutes.

3.3 Experimental procedures

For all experiments performed in this section, working electrodes were polished for each experimental run, unless otherwise stated. For higher temperature experiments, temperature of the water bath was monitored with a mercury thermometer and that of the reaction solution with a digital thermometer. The

temperature of the two thermometers agreed by ±2 °C, to account for heat loss of water travelling from the water bath to the reaction vessel.

3.3.1 Reproducibility studies

LSV experiments were performed at 25 °C and 45 °C. Pure H_2SO_4 was diluted to a concentration of 0.1 M. Experiments were run at scan rates of 1, 2, and 5 mV/s. Individual experiments were first performed in a positive direction, negative direction and cyclically with a scan limit of between 800 and 1000 mV. Since LSV only allows for single scans, cyclic scans were performed by first running the forward scan and straight after completion, immediately reversing the scan. Experiments were performed in triplicates for all scan rates. A total number of 15 scans per scan rate were obtained. This can be thought of as 5 triplicates at that given scan rate. Solutions were changed after all 15 runs of a specific scan rate. Electrodes were polished for each and every triplicate run. At a certain temperature a maximum of 45 scans were obtained. 55 mL of H_2SO_4 was used for each scan rate run (i.e. every 15 runs). Effects of scan rates were also monitored. The total number of experiments was 3 × 5 × 3 × 2 × 2 = 180.

3.3.2 Iron Media studies

A. Linear Sweep Voltammetry

LSV experiments were performed in acid iron media that contained different proportion of ferric and ferrous ions. Sulfate salts of ferric and ferrous were dissolved in 0.1 M H_2SO_4 to make solutions of the following total iron concentrations, 0.5 g/L, 2 g/L, and 5 g/L. LSV sweeps were then performed at differing proportions of ferric to ferrous at a fixed total Fe concentration, which are 10:1, 5:1, 2:1, 1:1, 1:2, 1:5, and 1:10 Fe^{3+}/Fe^{2+}. Before the beginning of each LSV sweep, the electrode

was freshly renewed and polished as stated above. Thereafter solution at the correct ratio of Fe^{3+}/Fe^{2+} was mixed to a total volume of 55 mL. The LSV sweep was performed in the anodic direction for a total scan range of 0 to 1000 mV (later 800 mV) at a scan rate of 1 mV/s. Immediately after the anodic sweep, a sweep in the cathodic direction would then be performed for a potential range of 0 to -800 mV. The electrode was then polished and the next ratio solution used for the next sweep. This procedure was repeated for all seven Fe^{3+}/Fe^{2+} ratios, three total iron concentration and three temperatures (25, 45, 65 °C). All experiments were performed for both chalcopyrite samples from Durango, Mexico and Ontario, Canada, with the surface area of 0.24 and 0.2 cm^2, respectively, thus creating a total matrix of 7 × 3 × 3 × 2 = 126 LSV experiments.

To assess the effect of the starting potential for the cathodic direction sweeps, continuous LSV sweeps were performed from +800 mV to -800mV, i.e. starting from the anodic side and vice-versa from -800mV to +800mV starting from the cathodic side. These were performed at 25 °C for all total Fe concentrations for the 1:1 Fe^{3+}/Fe^{2+} only. Further experiments were performed whereby LSV sweeps were started from the open circuit potential (OCP). A freshly renewed electrode was subjected to a scan only once it had achieved its natural potential in the given system. These experiments were performed at 25 °C, for the 10:1, 1:1, and 1:10 Fe^{3+}/Fe^{2+} ratios for all total iron concentrations previously studied.

B. Chrono-amperometry

The passivation region current time behaviour was monitored by performing chrono-amperometric studies at different potential step intervals. These studies were performed in the potential range of 300 to 650 mV at potential step intervals of 50 mV. The conditions selected for these studies were 25 °C, 2 g/L total Fe concentration and 10:1, 1:1, and 1:10 Fe^{3+}/Fe^{2+} ratios. A pre-step voltage to 10 seconds was selected, and the actual specific step potential left to run for 60 seconds. The working electrode and the solution for a total potential range per

Fe^{3+}/Fe^{2+} ratios were changed, that is the electrode was polished and the electrolyte changed for every potential step.

4 RESULTS AND DISCUSSION

Chapter Summary

The following chapter summarizes the results and analyzes outcomes obtained from experiments that were performed as outlined in the previous chapter. The chapter starts with the reproducibility studies that were performed to commission and test the potentiostat. These studies where performed in H_2SO_4 solutions only in the anodic direction. From these studies it was observed that the experiments performed were reproducible to a high degree. This showed that the instrument was properly commissioned and electrodes properly prepared and further studies could then be performed. The reproducibility studies were also performed to investigate the effects of different scan rates on the sweeps. From these experiments it was observed that the lowest scan rate showed the highest and most pronounced current peaks during the anodic sweeps where these were observed. From this observation it was decided that subsequent studies would be performed at a scan rate of 1 mV/s. Subsequent studies were performed in Fe sulfate media at different total Fe concentrations, temperature and Fe^{3+}/Fe^{2+} ratios. Anodic and cathodic sweeps were performed for the Fe media studies. These experiments showed the classic behaviour well described in the literature, where four regions where observed for a typical anodic sweep. Following from these studies, certain aspects were investigated more closely. Cathodic sweeps are discussed for the initial parts of the chapter, however due to inconsistencies in the data obtained, it was decided that cathodic sweeps would be left out for the rest of the discussion as these were not deemed immediately relevant to the phenomena of interest (oxidative dissolution in ferric sulphate media). A selection of sweeps was selected for the purpose of the discussing the data. A comprehensive set of sweeps were obtained for the two different samples under a variety of conditions. Since these represent a large number, only plots of selected sweeps are shown in the discussion below, but all plots can be found in Appendix B.

4.1 Reproducibility experiments

Basic repeat experiments were performed to assess the level of reproducibility of results from the potentiostat. Since the potentiostat was purchased, it had not yet been commissioned and tested. Another motivation for these studies was to monitor the consistency of the potentiostat with regards to reproducing similar results over a length of time. Similar work to the present study, from literature has shown a lot of variability in reported data (refer to section 2.3.2 and 2.3.3), and this could in part be attributed to not checking the potentiostat as a potential source of error. The studies in this work were performed to examine slow scan rates. It is proposed from the objectives of the present work, that slower scan rates will provide more defined peaks which will in turn allow to identify where electron transfer reactions occur (also reported by Zhang et al. (2009) in their study) allowing to account for the slow establishment of surface currents or polarisation effects. All experiments were performed in 0.1 M H_2SO_4 at pH 1.04. Linear sweep voltammetry sweeps were performed and the measured current density (i) was plotted against potential (E).

4.1.1 Anodic sweep reproducibility studies

The first set of experiments were performed for positive potential sweeps from 0 to 1000 mV_{SCE}, at 25 and 45 °C for the two chalcopyrite working electrode samples at scan rates of 1, 2, and 5 mV/s. Triplicate sweeps were performed and these were repeated 5 times at each temperature, totalling 15 individual sweeps per scan rate. The working electrode was polished after every triplicate run and freshly renewed for each scan rate. Fresh acidic solution was used when switching to a new scan rate.

Sweeps for the electrodes at the temperatures measured showed similar trends throughout the whole potential range. Observing these sweeps for the total scan range showed a flat region from 0 to 800 mV_{SCE} and a region where current showed a steep rise until the end of the sweep (Figure 4.1). These types of sweeps were observed for the most of the triplicate repeats for a single scan rate at the given

temperature. The working electrodes showed different behaviour with respect to the origin of the chalcopyrite material; however, the sweeps shown in Figure 4.1 were consistent throughout the whole 15 sweeps that were performed for a given scan rate. The difference between the two electrodes for full potential scans were observed to be, that for the flat region (0 – 800 mV_{SCE}), the Ontario electrode (Figure 4.1B) showed a gently but continuously increasing current up until the region where current shows a steep rise. Around the same region the Durango electrode (Figure 4.1A) was observed to be completely flat with only a slight difference at a point where the sweeps turns to the steep region. This was observed only for the first scans of a triplicate. The current density axis scales for the two electrode samples were observed to be different. The Durango electrode was observed to have a final current density close to two orders of magnitude higher than the Ontario electrode at the same final potential (1000 mV_{SCE}).

Due to the scaling in the high current region, limited details in the flat region are visible; therefore the scale of the current density axis had to be adjusted due to the steep rise in current towards the end of the sweep. Thus, to be able to observe any differences in the low potential region between the triplicate sweeps and scan rates thereof, the sweeps were cut off at appropriate potentials levels (as shown in Figure 4.2). From this point onwards and for the rest of the chapter, the plots that will be discussed will be of an adjusted scale

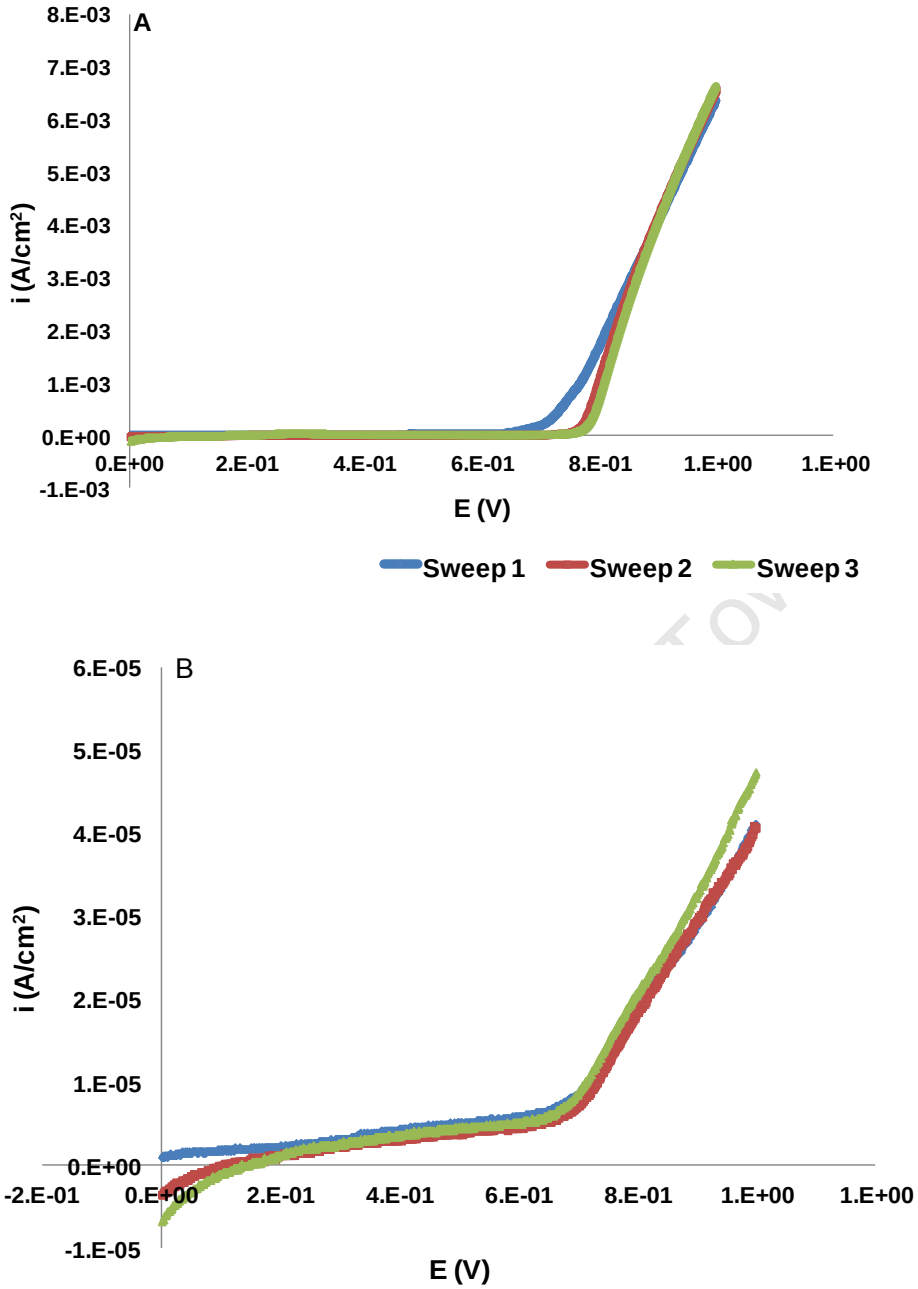

Figure 4.1. Sweeps of a single triplicate at 5 mV/s for (A) Durango and (B) Ontario electrode for a full 1000 mV scan range at 25 °C.

The following discussion first focuses on individual sweeps from a single triplicate run at one scan rate at 25 and 45 °C (Figure 4.2 for 25 °C). For most sweeps a small peak was observed within the 300-400 mV_{SCE} regions. Within a single triplicate run, peaks heights generally increase per run. Since the electrode was not polished before each sweep in a triplicate set, it is suggested that this observation is

due to the fact that in the case of the second and third sweep of a triplicate, the electrode surface has already been altered from the first scan of that same triplicate, with a surface layer formed that shows a different polarisation behaviour. It is worth noting at this point that not all scans exactly followed the trends depicted in Figure 4.1 and Figure 4.2.

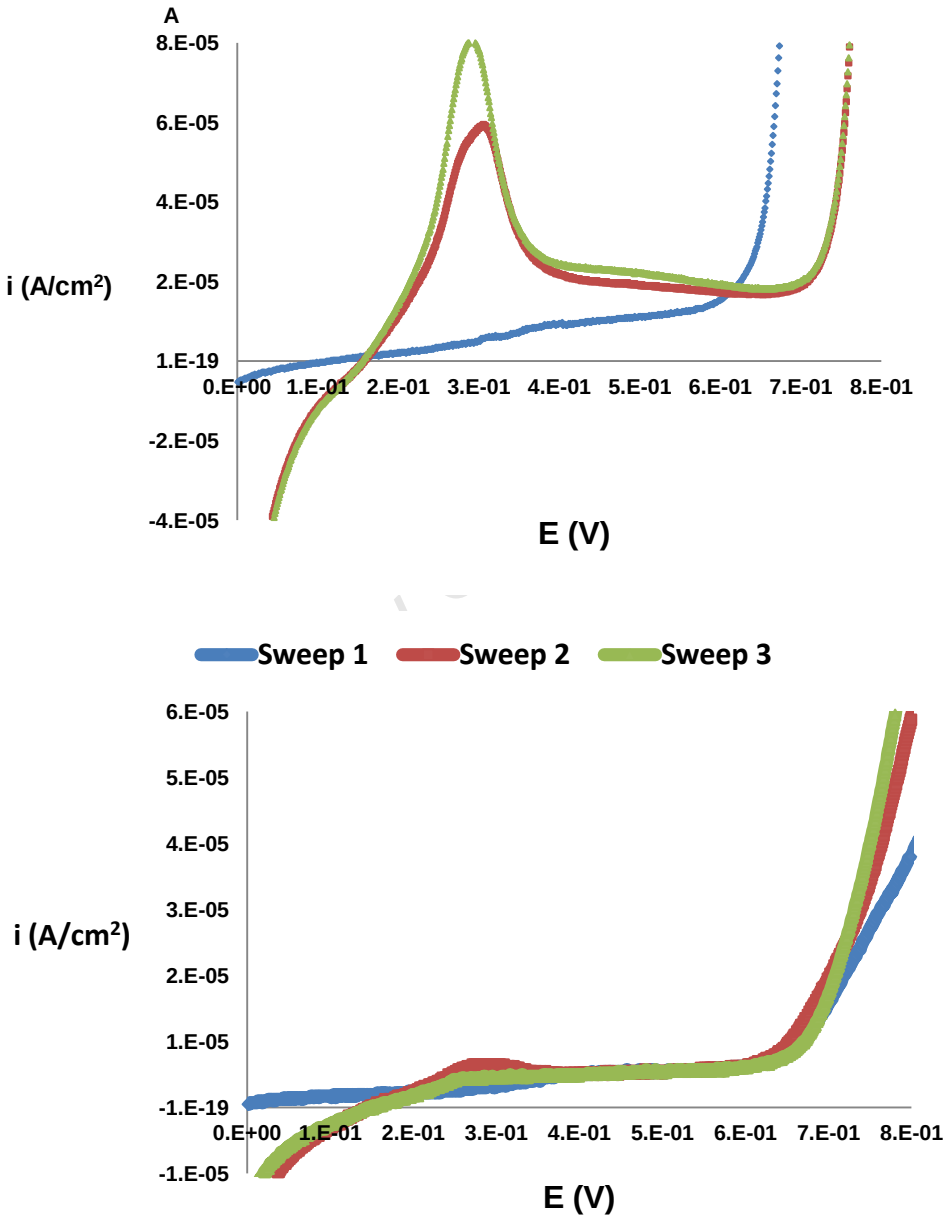

Figure 4.2. Sweeps shown in Figure 4.1 with the E and I axes scaled down to be able to observe the region abound 300-400 mV, where there is some visible activity at 25 °C. (A) Durango and (B) Ontario electrodes.

Changing the temperature to 45 °C (Figure 4.3), did not result in any changes to the trends and shape of the sweeps for the whole potential range studied (0 – 1000 mV_{SCE}) observed at 25 °C., but the increase in temperature resulted in the slope towards the end of the sweep (the tail end) becoming a steeper than at 25 °C. The peak height for the Durango sample decreased and was also observed to broaden with this increase in temperature. The Ontario electrodes did not show any peaks at 45 °C, but the scans were steeper than those of 25 °C. A similar trend was observed for all scans that were performed at this temperature.

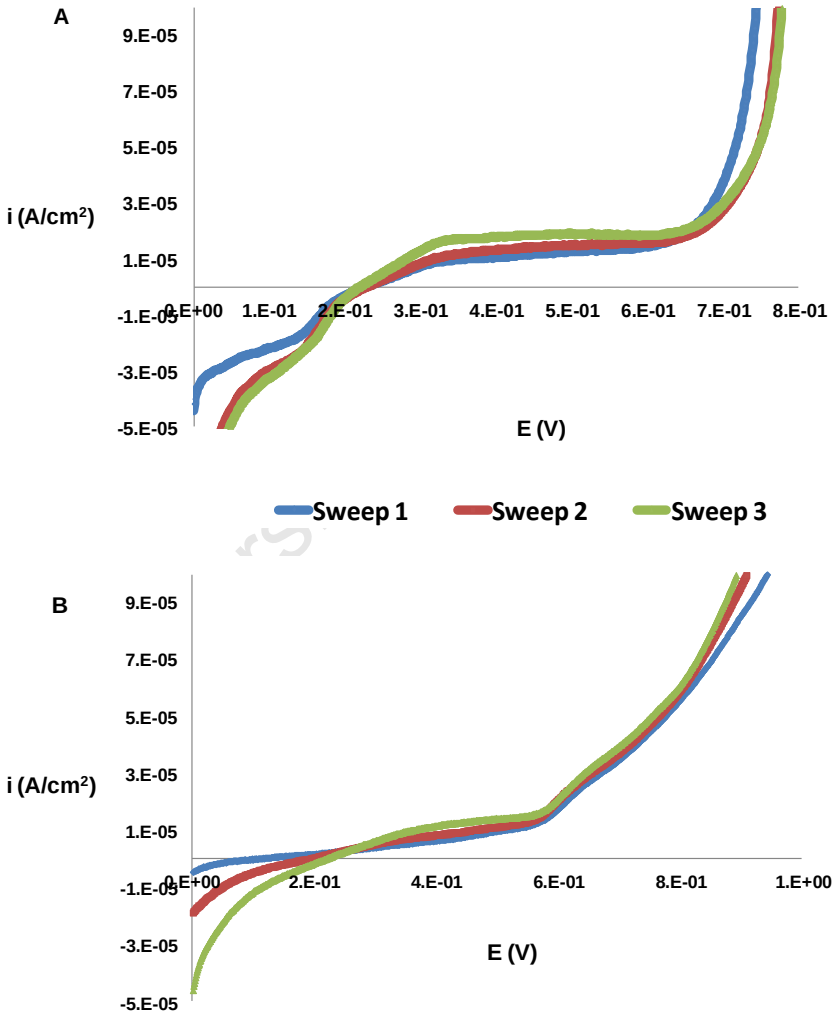

Figure 4.3. Sweeps for a single triplicate taken at 45 °C for (A) Durango and (B) Ontario electrodes.

The effect of scan rate was analysed for sweeps at the two temperatures to asses if there would be any difference in the peaks observed. It was observed for most sweeps of the Durango electrode that there was an increase in peak height and definition as scan rate decreased (Figure 4.4A, at 25 °C). The Ontario electrode in turn did not show any peaks with regards to effects of scan rate. The only variability in the sweeps for this electrode was observed at approximately 700 mV_{SCE}, where the sweep shows a steep rise in current. At these potentials it was observed that the plots separated, resulting in different final current densities (Figure 4.4(D), evident for 5 mV/s). From these observations, more especially for the Durango electrode, it was clear that the slowest scan rate at 25 °C brought about the most defined and highest peak for most of the repeats of the sweeps (as shown in Figure 4.4(A)). For sweeps at 45 °C, the peaks were observed to be broader for 1 and 2 mV/s scan rates, and the 5 mV/s sweep showed the highest peak compared to those at 25 °C. With this observation it is clear that an increase in temperature has an effect on the trends observed at 25 °C. Thus focusing only on the sweeps at 25 °C, a decrease in scan rate showed an increase in the peak height and definition. This can be explained as follows; at slower scan rates the current is allowed more time to establish a response to the change in applied voltage, thereby allowing polarisation effects to play themselves out for longer, as will be more clearly described later with chrono-amperometric studies. The Ontario sample electrode did not show any of the peaks observed for the Durango electrode and there was variability in the current density at the end of scan at different scan rates. This was probably due to the effects caused by the different mineralogy of the two samples. For the two different temperatures the point at which a steep rise in current commenced was observed to shift slightly.

For subsequent experiments (next section) in this work, the scan rate of 1 mV/s was chosen for all experiments.

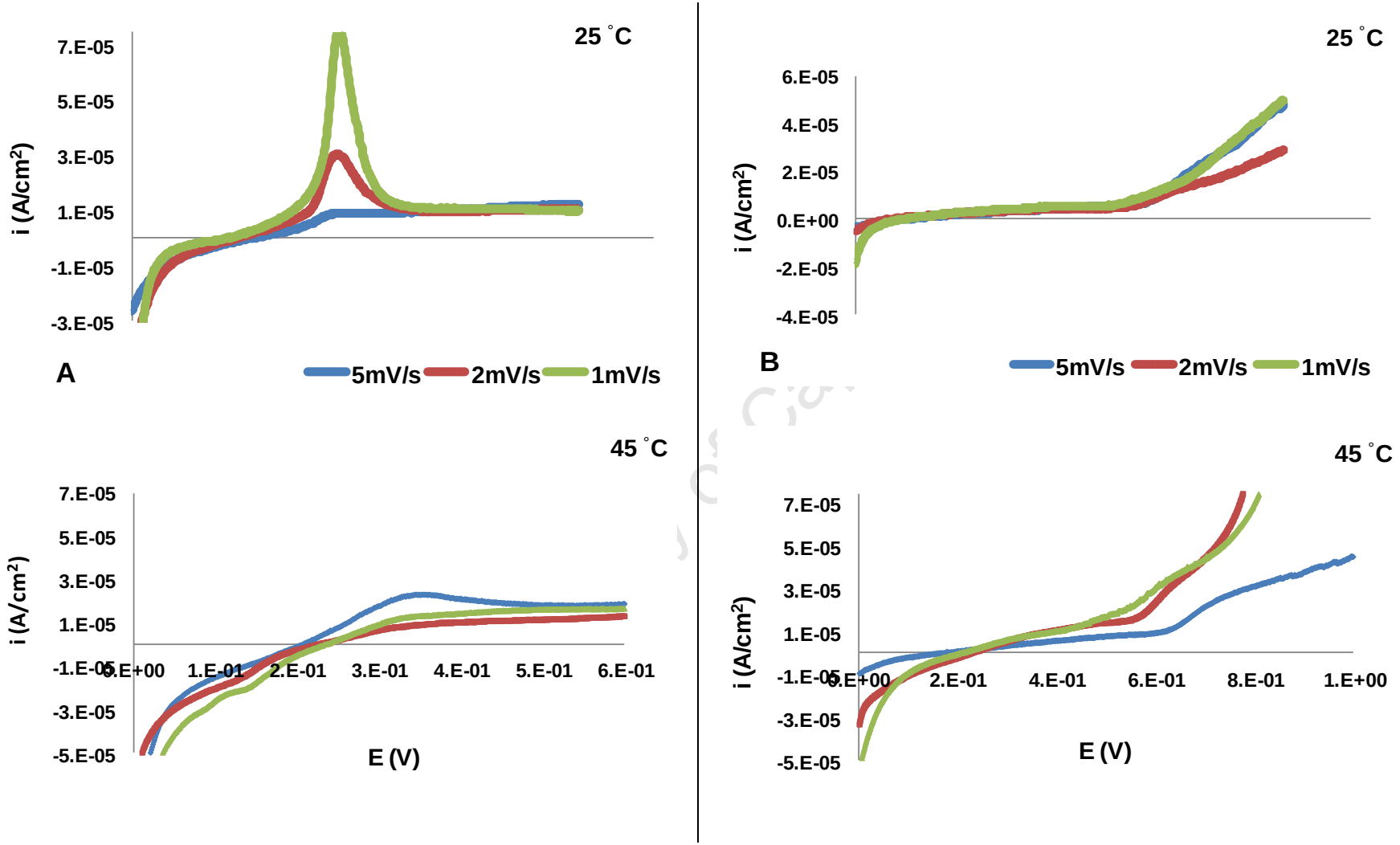

Figure 4.4. Differences that are shown by scan rates of the chalcopyrite electrodes at different temperatures. (A) Durango, (B) Ontario electrode.

4.2 Acidic iron media studies

Experiments in acid iron media were performed to depict real leach systems. These studies were the main focus of the present work. At first, visual observations of changes that were observed on the electrode surface during all sweeps are discussed. This is followed by an account of the general trends observed in these studies in response to changes in total iron concentrations, temperature and the Fe^{3+}/Fe^{2+} ratios. The effect of the different ratios on the main current peak are analysed in more detail. An electrochemical analysis of the data follows, where the potential at which the peaks occur were compared to the potentials where Fe^{3+}/Fe^{2+} redox reactions would occur and transformation using the Pourbaix diagram. A model is proposed to support for the redox reactions that are occurring during anodic sweeps. Finally chrono-amperometric studies are analyzed to elucidate the passivation phenomenon and the nature of LSV sweeps.

4.2.1 Visual observations on the electrode surfaces

For anodic sweeps the electrode was observed to turn from its shiny post-polishing appearance to a dull brown colour without any shine (Figure 4.5 (A, B and C)). This showed that the anodic sweep had some reactions occurring at the surface of the mineral that altered the composition of chalcopyrite. This was observed for almost all the sweeps performed throughout the whole concentration and temperature ranges. The degree of dullness was observed to increase with Fe concentration in solution and temperature. Throughout the ratios of Fe^{3+}/Fe^{2+} the degree of dullness of the electrode surface appeared to decrease with an increase in Fe^{2+} ion, but the differences were not significant compared to those observed for changing total iron concentration and temperature. After each anodic sweep a cathodic sweep was performed without re-polishing the electrode, for reasons mentioned above. At the end of the cathodic sweep, the electrode surface was observed to be totally covered

with a black colour. There were no trends observed with the degree of darkness i.e. the dark colour did not change with any of the parameter that were studied.

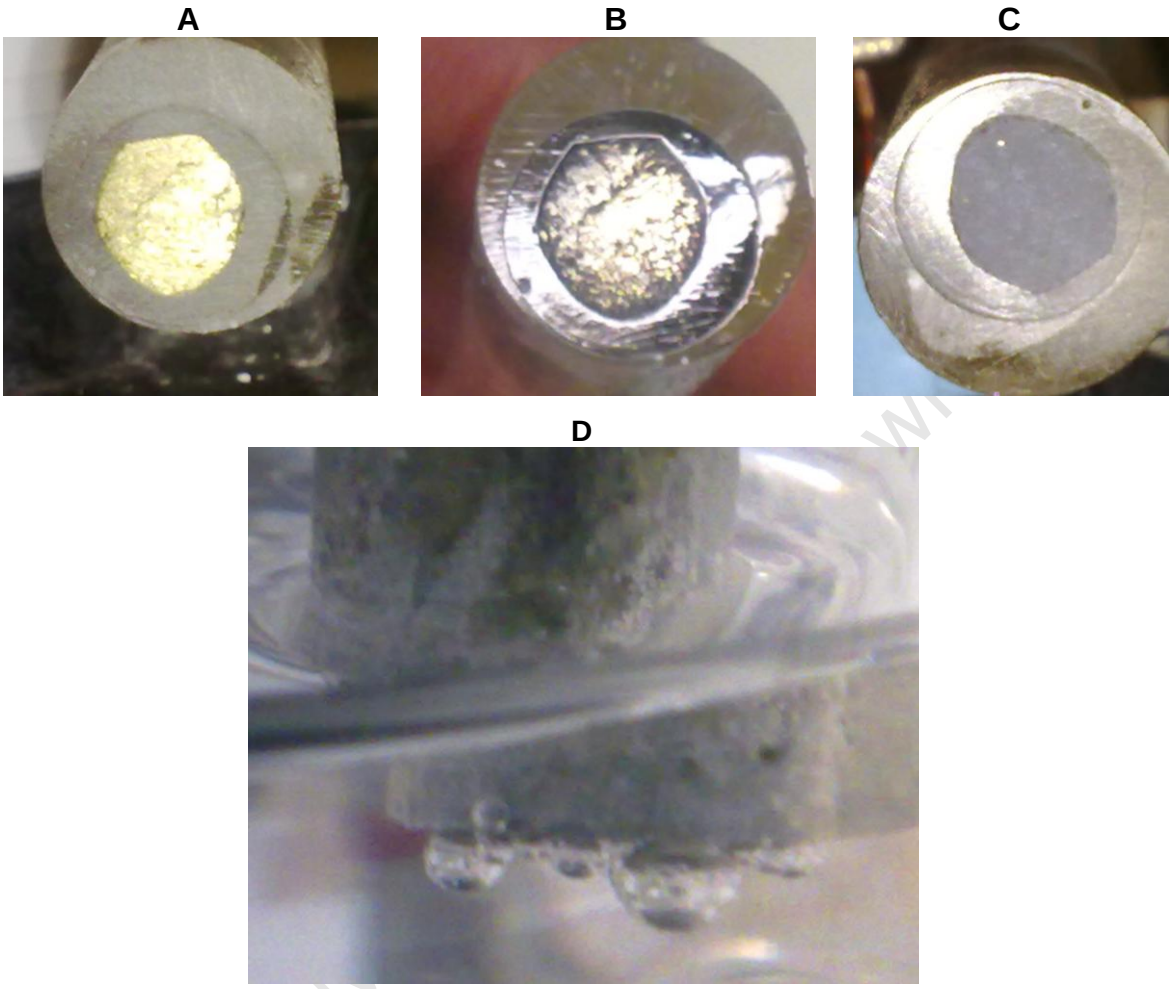

Figure 4.5. Changes in electrode surface from renewed up to the cathodic sweeps. (A) Freshly renewed surface, (B) surface after the anodic sweeps, (C) surface after the cathodic sweep and (D) bubbles that were observed during the cathodic sweep at the surface of the electrode.

At potentials greater than -600 mV, there were bubbles that were observed to form at the surface of the mineral (shown Figure 4.5 (D)). Formation of bubbles was influenced by temperature, such that these bubbles were observed mostly at 45 and 65 °C. It is assumed that around these potentials, reactions that occur are the electrolysis of water, or formation of H_2S and elemental copper. At the end of a cathodic scan, there was a foul metallic smell, which could further support the formation of H_2S gas. Thus a mixture of all of these reactions occurring at the same time on the electrode surface could be the reason for the darkening of the electrode surface. According to the Pourbaix diagram (Figure 2.2) the thermodynamically

stable products that can form at cathodic potentials are Cu^0, Cu_2S, Cu_5FeS_4 and H_2S (HS^-). The formation of these products can be further supported by reactions, (2.30 – 2.33), proposed by Elsherief (2002).

$$9CuFeS_2 + 4H^+ + 2e \rightarrow Cu_9Fe_8S_{16} + Fe^{2+} + 2H_2S \quad (4.1)$$

$$5\ CuFeS_2 + 12H^+ + 4e \rightarrow Cu_5FeS_4 + 4Fe^{2+} + 6H_2S \quad (4.2)$$

$$2\ CuFeS_2 + 6H^+ + 2e \rightarrow Cu_2S + 2Fe^{2+} + 3H_2S \quad (4.3)$$

$$2Cu_2S + 4H^+ + 4e \rightarrow 4Cu + 2H_2S \quad (4.4)$$

The two electrode samples from different locations were observed to follow more or less similar trends for the matrix of experiments reported in section 3.3.2. The Ontario sample was chosen for subsequent sections' discussion. This was because the Ontario sample showed clearer plots compared than the Durango sample electrode. The rest of the data plots can be obtained in the Appendix B.

4.2.2 General trends

Anodic sweeps of the chalcopyrite electrode with different ferric/ferrous ratios that were studied followed the common trend observed in literature (e.g. Hiroyoshi et al., 2004). At low potentials at the start of a sweep, there was the active region **1**, (see Figure 4.6), in which a steady increase in current density is observed as potential increases. The current increases to reach a peak maximum beyond which it decreases, **2**, known as the transient region (note that this is not so for 10:1 and acidic sweeps in Figure 4.6, and this will be discussed). The passivation region, **3**, is reached where current density shows no dependence on increasing potential and stays more or less constant at low, but non-zero values. The sweep then starts to increase steeply at higher potentials, known as the transpassive region, **4** (Figure 4.6). The cathodic sweep also showed a similar behaviour, whereby there was a

cathodic current density peak. The cathodic scan was started directly after the anodic sweep in the same solution without polishing the electrode. It can be observed that the current does not start at zero, even though the potential was set to zero at the beginning of the cathodic sweep, resulting in an apparent discontinuity around zero voltage (note that the joining of the curves at E = 0 is just a consequence of the software used for plotting; also for subsequent figures). This aspect is discussed further later in the section, but at this point attributed to the fact that there are already products and/or alterations that formed at the electrode surface during the anodic sweep and that certain reaction products may also now be present in the solution. According to anodic and cathodic sweeps performed, it is observed that the region where current density is not dependent on the increasing potential is observed for both, although for the cathodic sweep, it is shorter that the anodic sweep counterpart.

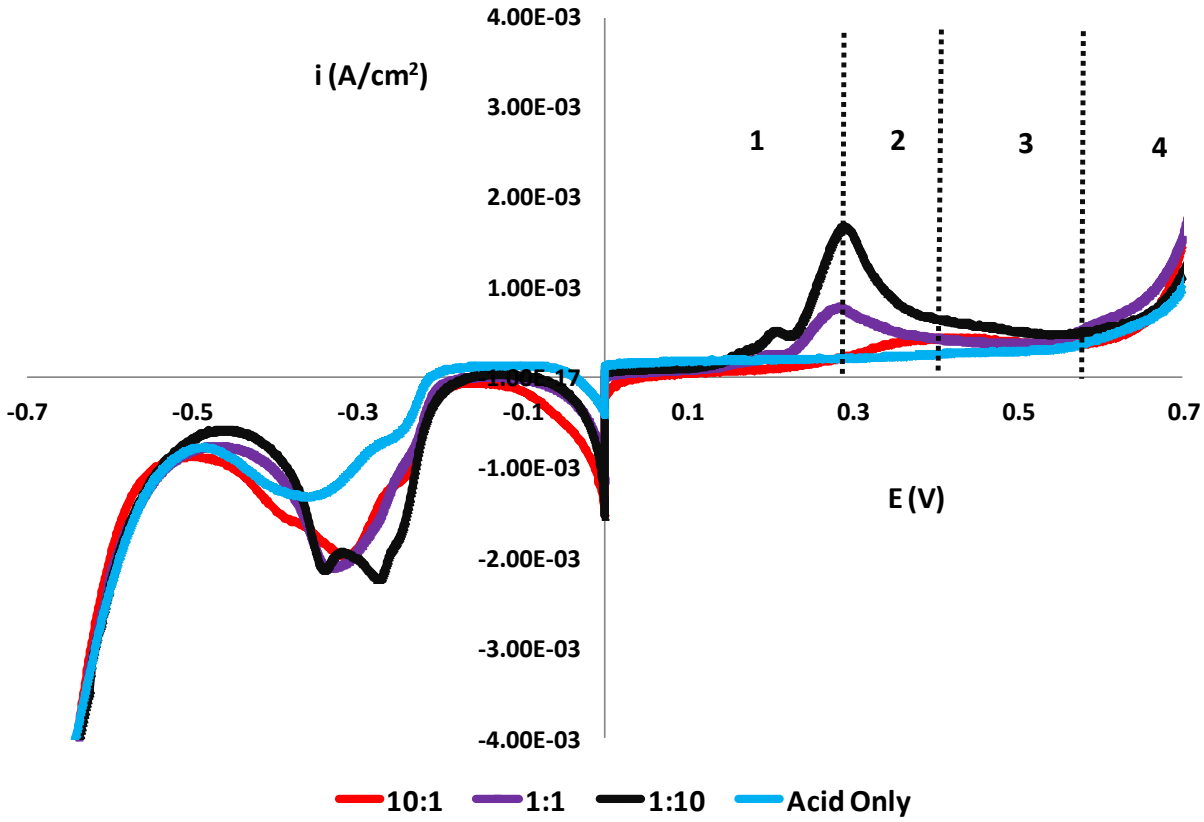

Figure 4.6. Typical sweeps obtained from anodic and cathodic sweeps for the Ontario chalcopyrite electrode for 0.5 g/L total Fe concentration at 25 °C. Only three ratios of Fe^{3+}/Fe^{2+} (10:1, 1:1, and 1:10) are shown, as well as the acidic scan which was used as a control. 1. Active, 2. Transient, 3. Passivation and 4. Transpassive regions of the anodic sweep. (The joining of the curves at E = 0 is a consequence of the MS Excel software that was used for plotting for clarity)

Analysis of the peaks observed during both anodic and cathodic sweeps showed that, in general, peak height increased with an increase in temperature for most Fe^{3+}/Fe^{2+} ratios. Studying a single ratio of the same concentration at the different temperatures, it was observed that as the Fe^{2+} ion concentration increased in solution, the height of the current peak also increased at the same time as temperature increased (Figure 4.6 and Figure 4.7). Total iron concentration also appeared to play a role in the height of the peak of the same Fe^{3+}/Fe^{2+} ratio, whereby the highest concentration showed the lowest current peak height, even at higher temperature (shown in Figure 4.8).

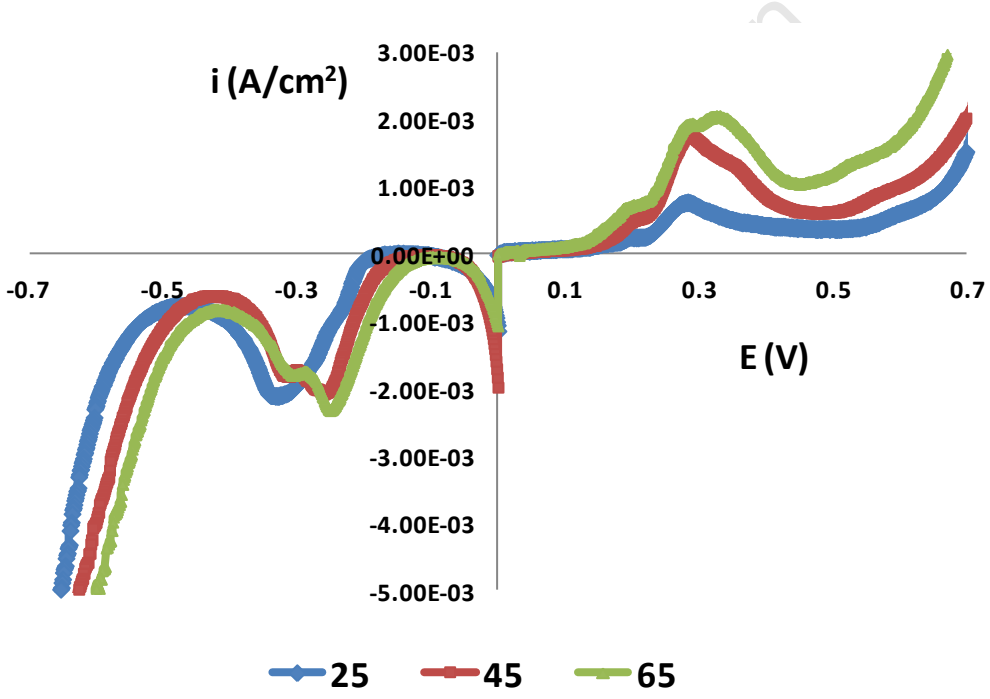

Figure 4.7. Anodic and cathodic sweeps from 1:1 Fe^{3+}/Fe^{2+} ratio at 0.5 g/L total Fe concentration at three different temperatures, 25, 45, 65 °C.

From the observation that peak height is affected by temperature, it can be suggested that temperature affects the active and transient region at the beginning of the sweep where the peak occurs. Since the highest peak is observed for the highest temperature, reaching higher current densities, this suggests that there is some activity occurring at the electrode-solution interface that needs some careful interpretation. Focusing on only the 65 °C sweeps throughout that whole concentration range, the passivation region of the sweeps shortened and even

disappears for some ratios. Some of the sweeps actually show a continuous increase throughout the passive region (Figure 4.8). In the case of the cathodic sweeps, there was no specific dependence of the peak height on temperature, instead the peak broadened as the temperature increased. The broadening of the cathodic peaks also resulted in a double peak being observed for these sweeps. At higher cathodic potentials, temperature also affected the steepness of the slope of the tail (E > 500 mV_{SCE} to the cathodic side), which increased as the temperature increased. This is the potential region where reactions 4.1 – 4.4 occur, as already mentioned earlier.

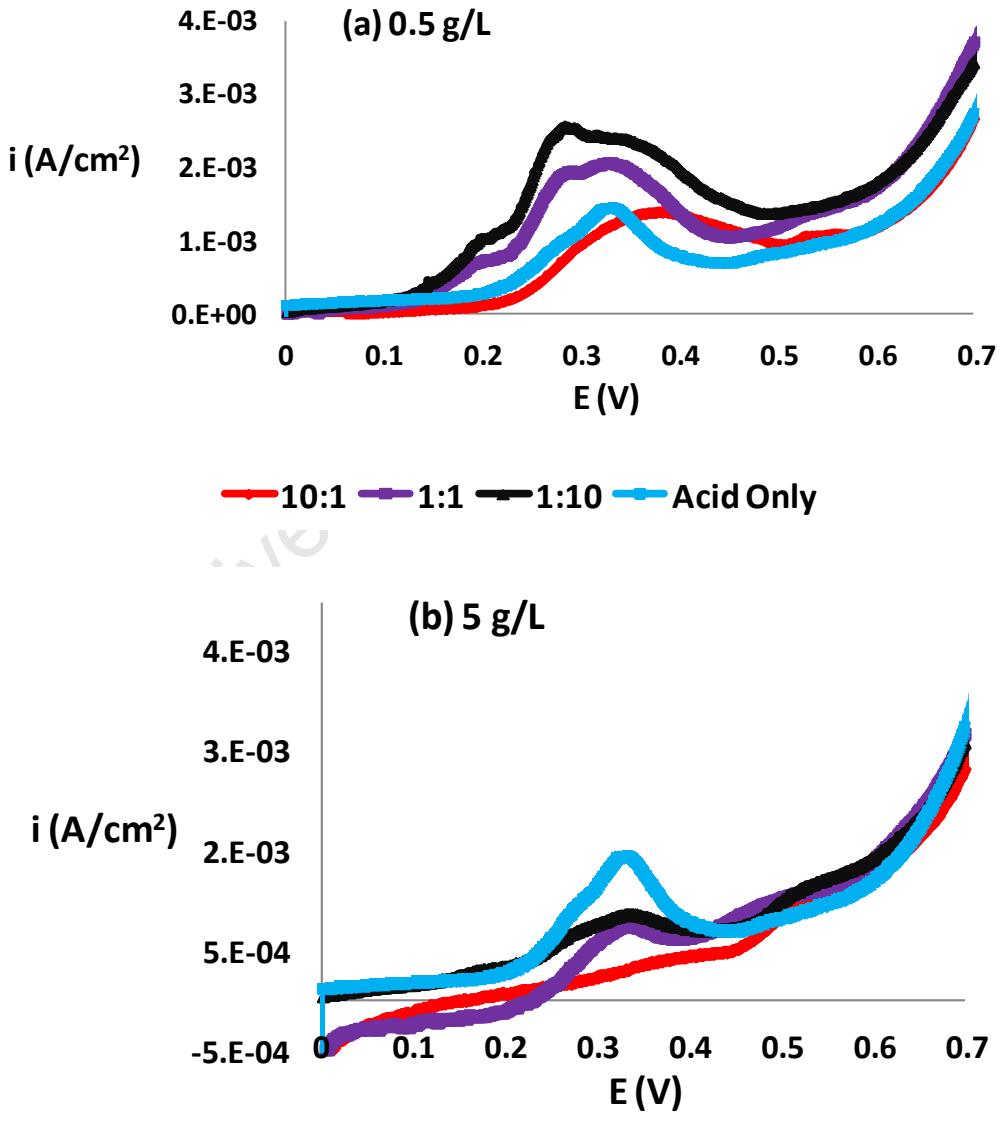

Figure 4.8. Shows the temperature effect on the passivation region for 0.5 and 5 g/L total Fe concentration (a and b, respectively), both at 65 °C for the anodic sweep only.

The effect of the total iron concentration at the different temperatures was primarily a change in the initial current density (at 0 mV) of the anodic sweeps (
Table 4.1). As the total Fe concentration increased from 0.5 to 5 g/L, the starting point shifted to cathodic currents, and this in turn became much more significant as the temperature was increased (Figure 4.8). Considering the 10:1 Fe^{3+}/Fe^{2+} ratio for the two concentrations in the figure, it is observed that the higher total Fe concentration results in a shift in the starting point of the sweeps to cathodic currents, cutting the potential axis at approximately 200 mV_{SCE}, which can essential be thought of as the open circuit potential (OCP) of the specific system, that is the potential at which there is no net current flowing through the electrode.

Table 4.1. Initial current density (in mA) at 0 V.

	0.5 g/L			2 g/L			5 g/L		
Fe^{3+}/Fe^{2+}	25 °C	45 °C	65 °C	25 °C	45 °C	65 °C	25 °C	45 °C	65 °C
10:01	-0.226	-0.101	-0.114	-0.101	-2.260	-0.376	-1.010	-0.709	-0.739
05:01	-0.001	-0.039	-0.051	-0.164	-0.239	-0.489	-0.664	-0.789	-0.701
02:01	-0.001	-0.089	-0.076	-0.114	-0.139	-0.314	-0.514	-0.651	-0.564
01:01	-0.001	-0.014	0.011	0.024	-0.089	-0.214	-0.414	-0.439	-0.551
01:02	0.024	-0.001	0.036	0.024	-0.026	0.024	-0.199	-0.301	-0.276
01:05	0.061	0.001	0.061	0.099	0.061	0.024	0.024	-0.039	0.061
01:10	0.061	0.036	0.024	0.124	0.061	0.086	0.061	0.061	0.049
Acidic	0.124	0.136	0.124	0.124	0.136	0.124	0.124	0.136	0.124

The start of these sweeps at cathodic currents also seemed to be affected by the ratio of Fe^{3+}/Fe^{2+} (discussed in the next section). In changing the direction after the anodic sweep, the cathodic sweeps showed that as temperature increased at a specific total iron concentration, the starting current density of the sweep also increased. This starting cathodic current was also slightly affected by the increase in temperature. As discussed earlier, at higher temperatures a short passivation region during the anodic sweep is observed, thus an increase in initial current densities for sweeps in the cathodic direction can be connected with the suggestion that the electrode surface was maximally altered at higher temperatures during the anodic direction sweep. This phenomenon is further tested and discussed in the next section (see Figure 4.11).

4.2.3 Ferric to ferrous ratio studies

The Fe^{3+}/Fe^{2+} ratios that were studied showed that, in general, as the proportion of Fe^{2+} ion increased in solution, the peak height also increased for anodic sweeps. This trend was observed for the 0.5 g/L total Fe concentration over the whole temperature range (Figure 4.9). The Fe^{3+}/Fe^{2+} ratios for the 2 and 5 g/L did not exactly follow this trend, however, instead ratios such as 5:1, 2:1, 1:2 and 1:5 of Fe^{3+}/Fe^{2+} seem to show greater peaks than those with the highest Fe^{2+} ion in solution. From the sweeps in Figure 4.8 it can be observed that the highest levels of Fe^{3+} ion in solution resulted in ill-defined peaks, which became more and more defined as the proportion of Fe^{2+} ions increased in solution. The peaks were observed around potential range of 280 – 330 mV_{SCE}, with differences observed for anodic peaks, for higher Fe^{3+} ion ratios. Anodic peaks with higher Fe^{3+} ion in solution were observed to be broader that those with more Fe^{2+} ion. The control acid-only sweeps showed no peak at 25 °C, and the lowest peaks at 45 and 65 °C, which also give evidence that the iron ions in solution have an effect on the anodic sweeps. The acid only sweeps also shown higher peaks when compared to the peaks at 2 and 5 g/L total Fe concentrations and higher temperature. All sweeps at different ratios converged in the passivation region at 25 °C, in which there was not much difference in the constant current density in this region. Slight differences in current density were observed as the temperature increased. The differences were observed where the potential range of the passivation region decreased as the temperature was increased, and the slope of the current density curve in the trans-passive region seemed to increase more rapidly with temperature increase. Total Fe concentration played a significant role in the starting point of the anodic sweeps, which in turn was affected by temperature.

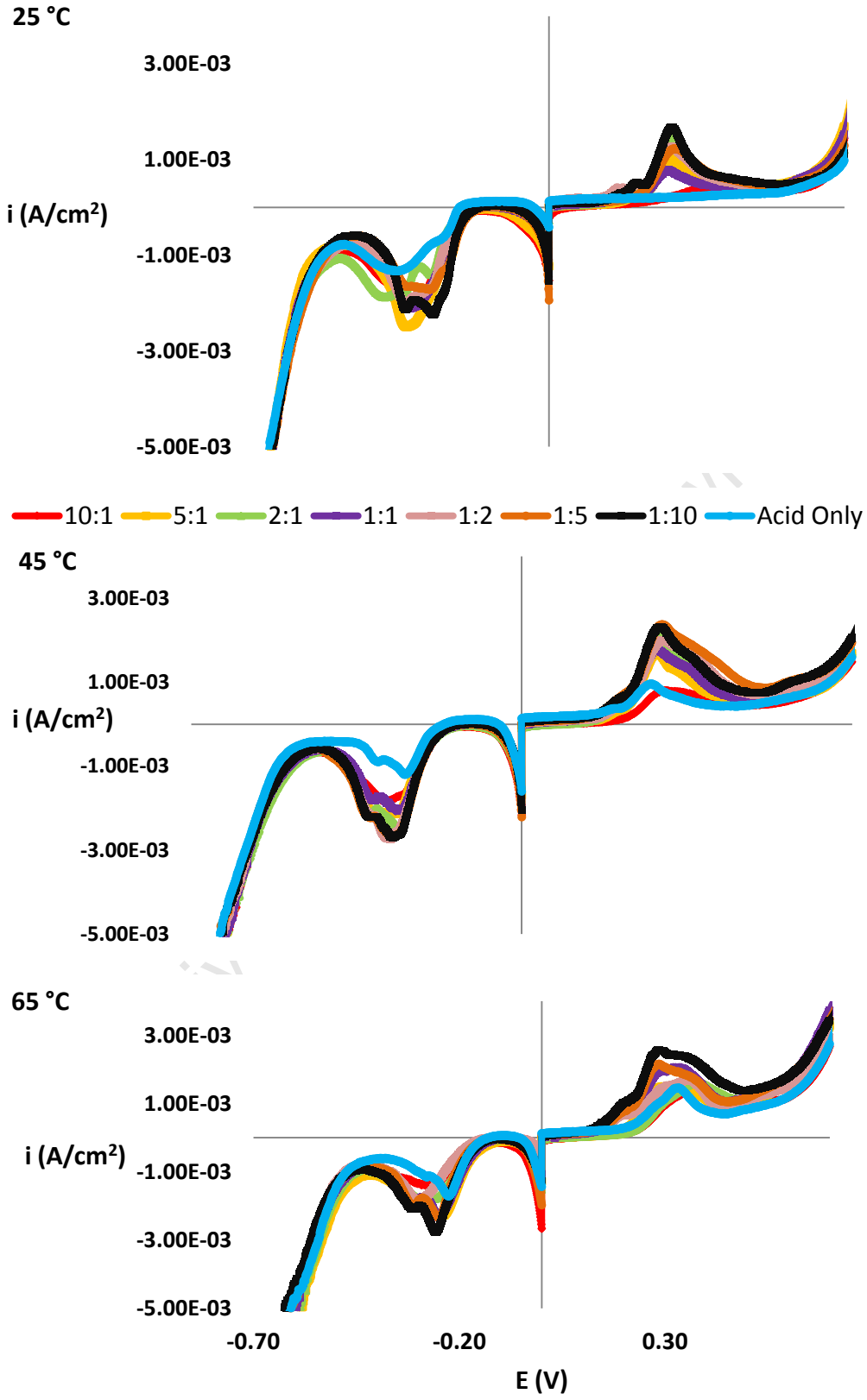

Figure 4.9. Anodic and cathodic scans for the 0.5 g/L total Fe concentration, for all Fe^{3+}/Fe^{2+} ratios studied, shown at three different temperatures (25, 45, 65 °C).

As the total Fe concentration increased, the initial current densities for sweeps in the anodic direction were observed to have a more and more negative initial current density (at zero mV) (Figure 4.10). As stated above, this increase in total iron concentration, different Fe^{3+}/Fe^{2+} ratios and temperature affected the OCP of the system. The Fe^{3+}/Fe^{2+} ratio also affected the initial current density of the sweep in the cathodic direction. Higher Fe^{3+} ions in solution tended to have higher initial current density for cathodic sweeps, and this trend was observed to decrease as the Fe^{2+} ion increased. As Fe^{2+} ion increased in solution the initial anodic sweep current density approached a start at zero (1:10 in Figure 4.10). Cathodic sweeps with regards to the Fe^{3+}/Fe^{2+} ratio did not show any observable trends that could be explained. There was a variation in the trends observed for each and every sweep at a specific temperature for a single concentration, as well as for all ratios. With these cathodic Fe^{3+}/Fe^{2+} ratio sweeps, the differences were observed whereby a sweep at a certain ratio was inconsistent with the positions of the observed peaks from one sweep to another. This observation can be attributed to the level of oxidation of the surface and reactions that occur during the anodic sweep, which was followed by the cathodic sweep without renewing the electrode, as already stated.

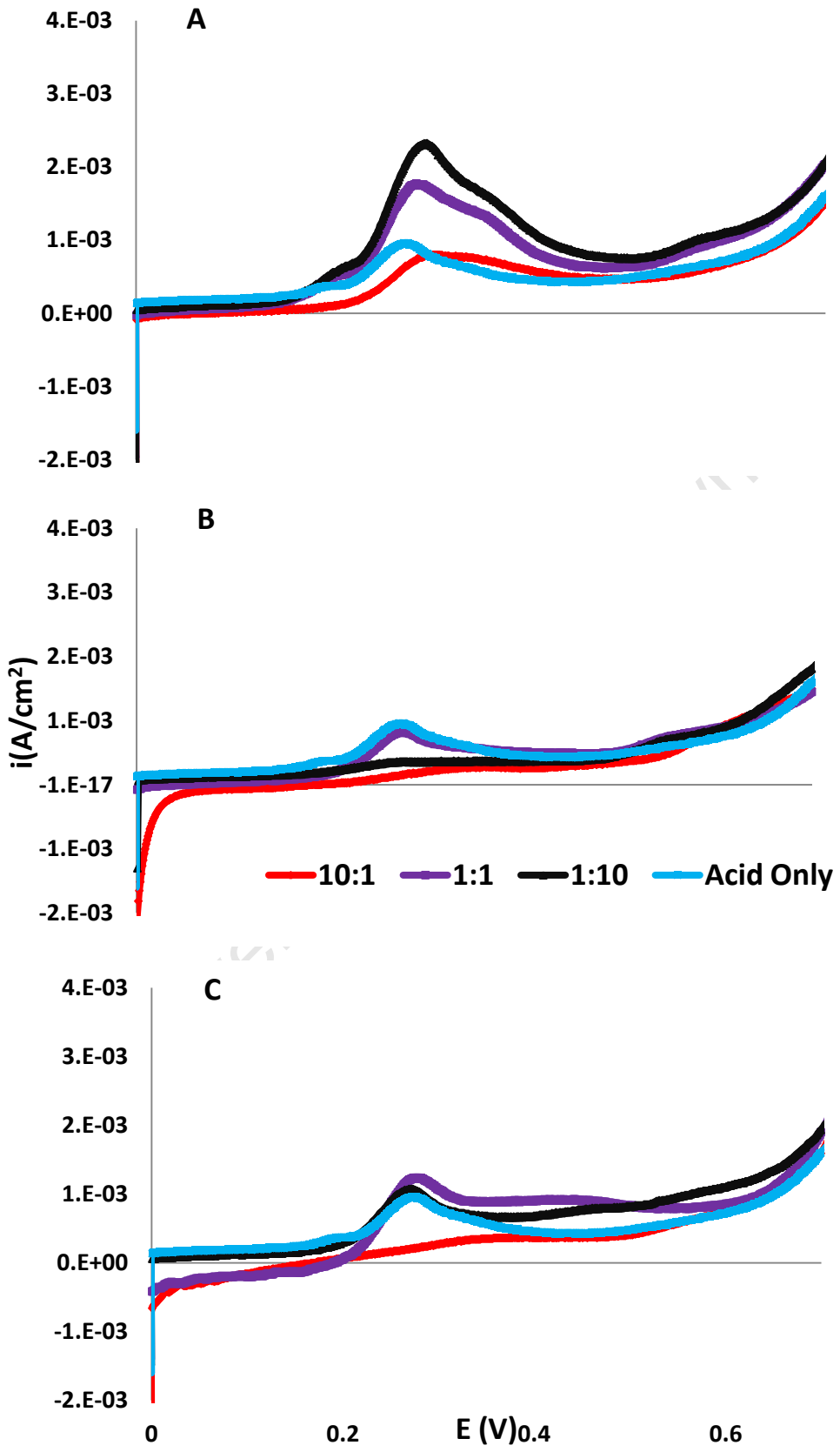

Figure 4.10. Comparisons between initial current density at the same temperature (45 °C) for different total Fe concentrations, A. 0.5 g/L, B. 2 g/L and C. 5 g/L.

The strongly negative current densities observed at the beginning of every cathodic sweep were further investigated to evaluate what the cause for this behaviour might be. This was tested by performing continuous sweeps from the anodic side to the cathodic side and vice-versa (Figure 4.11). The sweeps were started at 800 mV_{SCE} from one side, up until 800 mV_{SCE} in the opposite side. The sweeps were performed for the same ratio (1:1) at different total Fe concentrations. From these sweeps, there was a peak observed on the opposite side from where the sweeps were started, that is if a sweep was started in the anodic region towards the cathodic side, a peak would be observed in cathodic potentials.

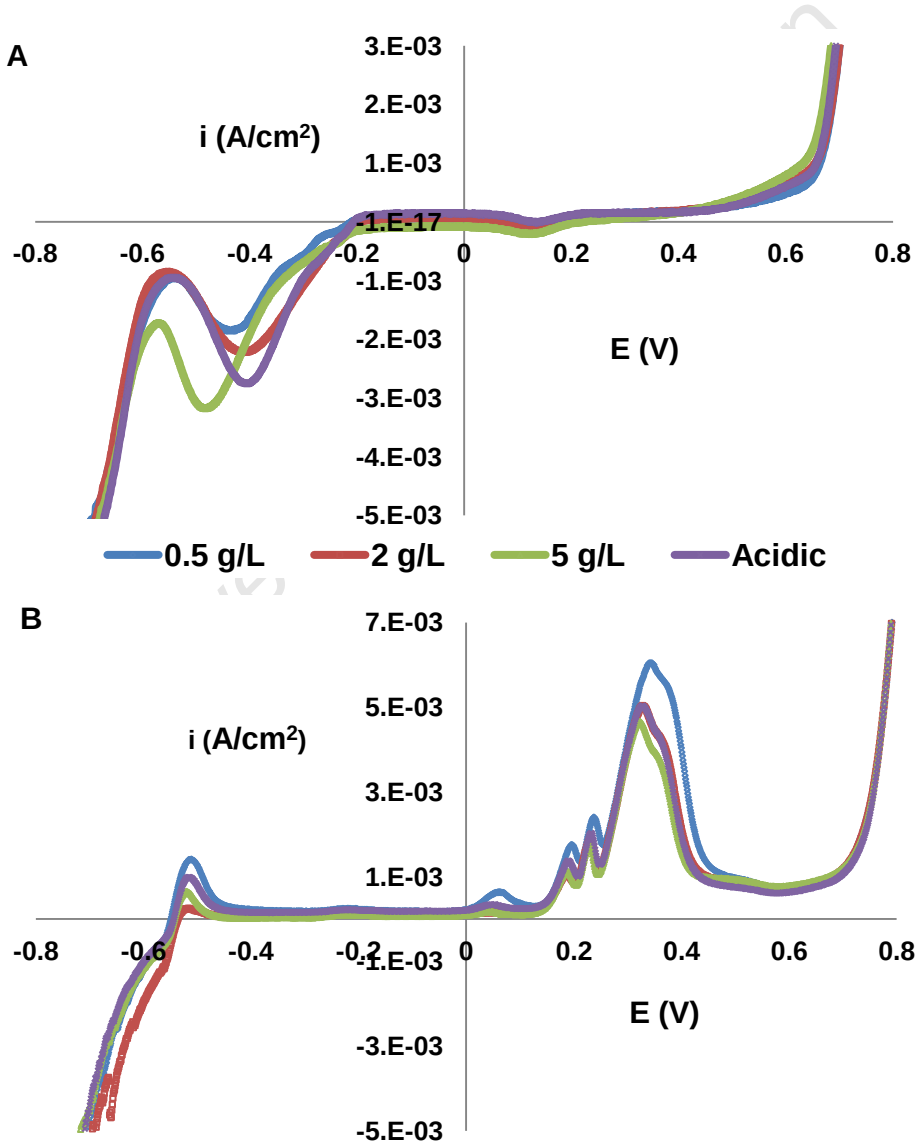

Figure 4.11. Continuous sweep for the Ontario chalcopyrite for the 1:1 ratio at the three different concentrations at 25 °C. (A) Anodic to cathodic direction, and (B) cathodic to anodic direction.

Essentially it can be observed from these sweeps that the previously observed trend, whereby the sweeps that were performed in the cathodic direction were observed to show a high negative starting point (Figure 4.9 for cathodic direction), diminishes with these sweeps. Thus this initial effect can be attributed to the fact the working electrode was not polished preceding the cathodic sweep. It would be valuable to test this observation by renewing and polishing the electrode straight after the anodic sweep. It can also be observed that the peak disappear when the sweep is started from one direction to the other. The peaks observed when the sweep is begun from the anodic side in the cathodic direction disappear when the opposite sweep is performed. From these sweeps, it can be postulated that the formation of a surface layer is accelerated at higher potentials, where the sweep is started, and is already established when the potential reaches lower levels. This is supported by a later study (section 4.2.5), which gives an indication that the active region of an LSV sweep is in effect transient and would most likely disappear with time.

To further analyze the significance of the heights of the current density peaks with regards to different Fe^{3+}/Fe^{2+} ratios, total iron concentration and temperature, the bar graphs shown in Figure 4.12 were plotted. The general trend observed for anodic current peak heights from these graph was that peak current densities increase with an increase in Fe^{2+} ion. The 0.5 g/L total iron concentration data showed this trend much better than that of the other two concentrations over the whole temperature ranges studied. Peak current densities for Fe^{3+}/Fe^{2+} ratios at a total iron concentration of 0.5 g/L showed a clear increasing trend as the Fe^{2+} ion increased (Figure 4.12, blue bars). This trend was more pronounced with increasing temperature. Between the two other total Fe concentrations, only subtle differences were observed, and trends for the Fe^{3+}/Fe^{2+} ratio did not follow any order with increasing temperature. For 25 and 45 °C for the 2 g/L experiments, it was observed that peak current densities decrease with increasing Fe^{2+} ion, but the opposite trend was observed for 65 °C. In contrast, the 5 g/L total iron concentration data showed the lowest peak current densities at 65 °C without any effect by Fe^{2+} ion. At 25 and 45 °C, there was a modest effect shown by an increase in Fe^{2+} ion, but fluctuations

were observed, whereby for 45 °C, the data showed the lowest peak at the highest Fe^{2+} ion ratio.

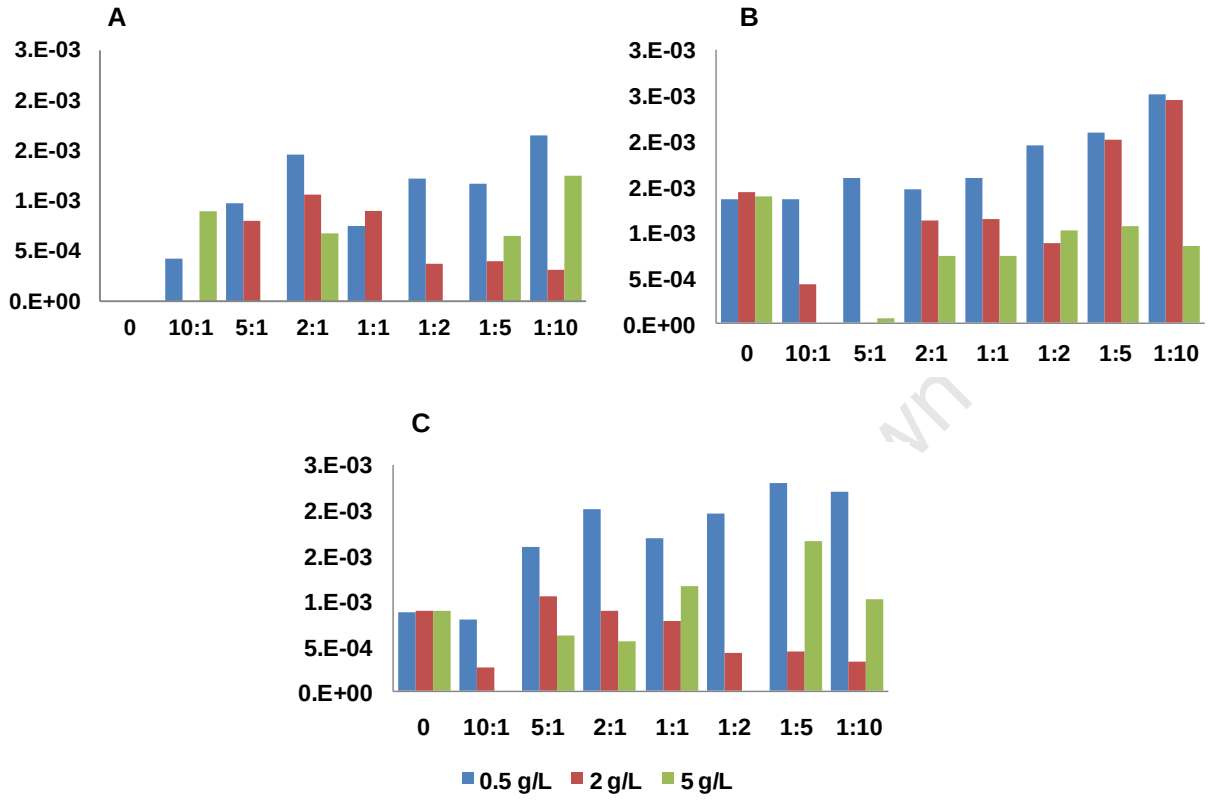

Figure 4.12. Current peak heights at a function of ratio of Fe^{3+}/Fe^{2+} for different total Fe concentration at different temperatures; A. 25 °C, B. 45 °C, and C. 65 °C.

These results showed that total iron concentration has an effect on the anodic sweep's peak current densities. This observation can be attributed to a school of thought that suggests that there is formation of iron-hydroxide (Fe-OH) (such as jarosite) species that precipitates during anodic chalcopyrite leaching (Córdoba et al., 2009; Nava, González, 2006). Taking the highest temperature, it can be observed that the highest total iron concentration demonstrates the lowest peak current densities relative to the acid-only sweeps (Figure 4.13). From this observation, it can be postulated that precipitation of the iron species occurs rapidly, inhibiting the oxidation of the mineral. This can also be observed by taking the Fe Pourbaix diagram (shown in Figure 4.14) where at pH ~ 1 and Eh ~ 0.4 V_{SCE}, Fe^{2+} and $Fe(OH)_3$ predominates, thereby affecting the peak that is due to oxidation of chalcopyrite.

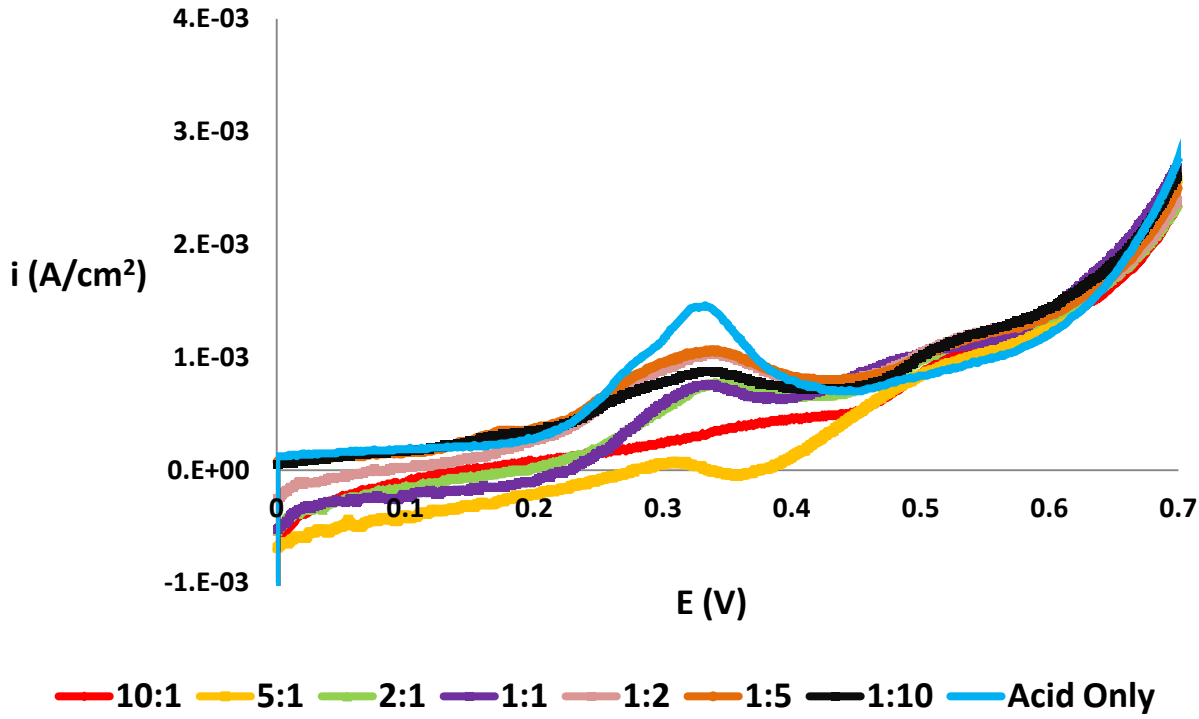

Figure 4.13. Sweeps at the highest total Fe concentration and temperature, 5 g/L and 65 °C.

With regards to the cathodic sweep current peaks, unlike the anodic sweeps discussed above, there was no specific trend observed that could be explicitly analysed. It was only observed that peak current densities increased as the temperature was increased. At 65 °C at the lowest total iron concentration, the highest peaks were observed and these increased with increasing Fe^{2+} ion, whereas the highest total iron concentrations showed peak heights that decreased. Given the lack of discernible trends, it was then decided that for the purposes of the present work that only anodic sweeps would be looked into from this point forward.

4.2.4 Electrochemical analysis of the Fe media studies

The potentials at which the current density peaks were observed during anodic sweeps of the chalcopyrite electrode in this study were compared to the calculated potentials for the Fe^{3+}/Fe^{2+} half reaction at 25 ^{0}C using the Nernst equation.

$$Fe^{2+} \rightarrow Fe^{3+} + e \qquad E^0 = 0.77\ V_{SHE}\ (\sim 0.52\ V_{SCE}) \qquad (4.5)$$

$$E = E^0 - \frac{0.0591}{n} \log_{10}\left(\frac{Fe^{3+}}{Fe^{2+}}\right) \qquad (Eq.4.1)$$

Table 4.2. Show the comparisons between potentials that are calculated from the Nernst equation compared to the anodic peak potentials at 25 °C. The potentials are reported versus SCE.

Ratio		Nernst E (mV)	Observed Peak E (mV)		
Fe^{3+}	Fe^{2+}	Calculated Potential	0.5 g/L	2 g/L	5 g/L
10	1	579	393	378	No peak
5	1	561	282	405	272
2	1	538	280	269	274
1	1	520	275	434	267
1	2	502	279	447	340
1	5	479	284	267	270
1	10	461	283	261	290

As can be seen from Table 4.2, potentials where the peak current densities were observed do not compare with the calculated Nernst potentials. As can be seen, the reversible potentials of the Fe^{3+}/Fe^{2+} half reaction are significantly higher and therefore disproves the speculation that the observed peaks belong to Fe^{3+}/Fe^{2+} redox reactions. Potentials at which a peak in current density occurred for the ratios of Fe^{3+}/Fe^{2+} studied can be analysed using the Pourbaix diagrams (Figure 4.14) and literature, in order to predict the reactions that might occur for the observed peaks. Since the present studies were performed at a pH = 1.09, the expected potential

where these peaks would generally occur could be at around 500 – 650 mV_{SHE} from the Pourbaix diagram (Figure 4.14,m, bottom).

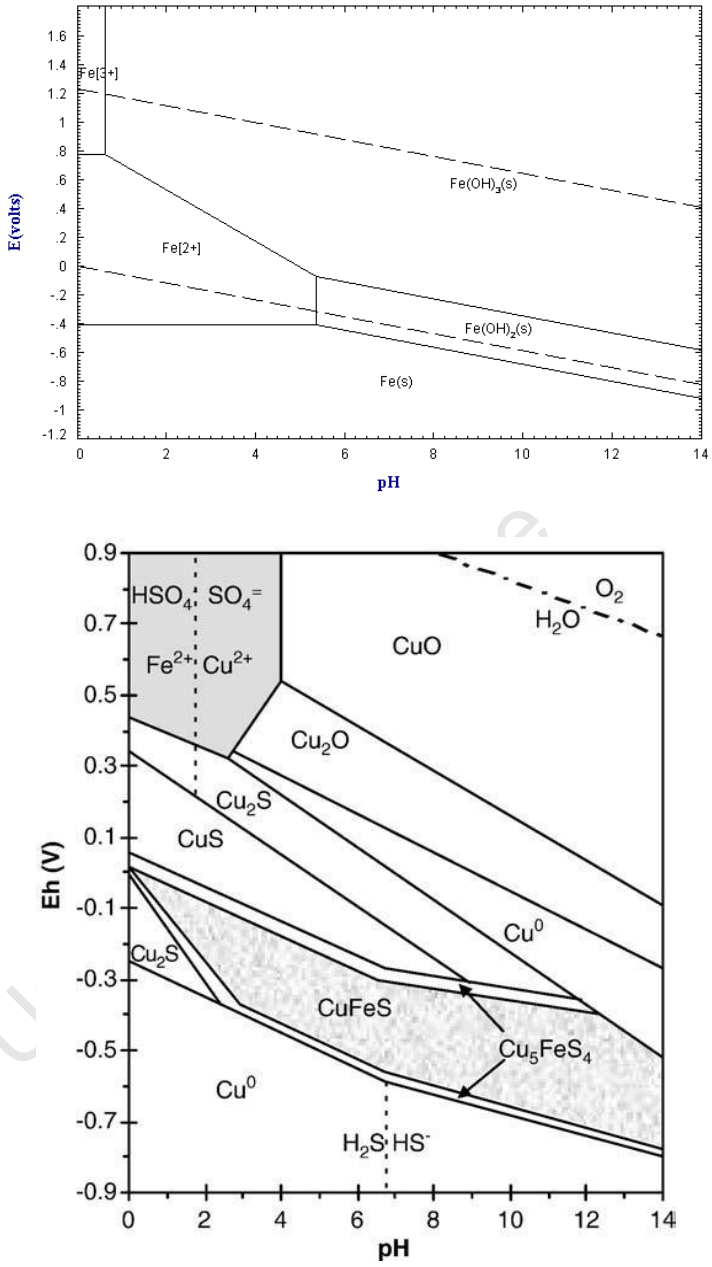

Figure 4.14. Pourbaix diagrams of (top) Fe and (bottom) Chalcopyrite (Garrels, Christ 1965).

According to the chalcopyrite Pourbaix diagram (Figure 4.14, bottom), around these potentials the dominant species in solution are Fe^{2+} and Cu^{2+} ions. Nonetheless, Fe^{3+} is present in solution and asFigure 4.14 (top) indicates it can precipitate at the

pH of the experimental conditions. Therefore precipitation might occur during anodic sweeps, as discussed earlier.

Furthermore, it is known that chalcopyrite oxidation to the final product, Cu^{2+}, requires potentials higher that 400 mV_{SHE} (Córdoba et al., 2008). Around these potentials, chalcopyrite is converted to Cu^{2+} ions, Fe^{2+} ions and other secondary copper sulfide intermediates (such as CuS, E^0 ~ 220 mV and Cu_2S, E^0 ~ 370 mV) at slightly lower potentials. It can thus be proposed that even though the observed peaks are mostly evident at potentials that show Fe^{2+} and Cu^{2+} to be stable on the Pourbaix diagram for chalcopyrite, it is possible that other secondary copper intermediates might be observed around the same potentials where current density peaks are observed. This is shown by wiggles on the sweeps that show miniature peaks before the main anodic peak. It is then reasonable to propose that around the main peak region, a number of redox reactions occur at the same time, which relate to mineral transformations, potentially modified by ferric iron reduction leading to the formation of Fe-OH species. This proposed phenomenon can be explained as follows; according to the Pourbaix diagram of chalcopyrite and Fe, the intermediates occur around similar potentials at the pH where these sweeps were performed as to where the main peak was observed. With all these reaction taking place at the same time around similar potentials each potentially at a certain rate slower than the sweep rate, the potentiostat cannot differentiate between the individual reactions. To further analyze this phenomenon, it would be useful to perform the sweeps at the lowest scan rates possible. This could assist in observing if better definition of these miniature peaks would not be obtained, thereby giving specific potentials that could be correlated with those observed from the Pourbaix diagrams.

A model of these discrete multiple redox reactions that occur is proposed in Figure 4.15. In this model, it is proposed that at potentials around the peaks region (A and B in Figure 4.15), where Fe^{3+}/Fe^{2+} redox reactions, potential precipitation of Fe species and oxidation of the mineral ore occur; that there are also regions (C in Figure 4.15) where these reaction might be in competition with each other. This might be a reason why it has been difficult to properly evaluate chalcopyrite electrochemical reactions and eventually find a suitable correlation between such studies and leaching studies.

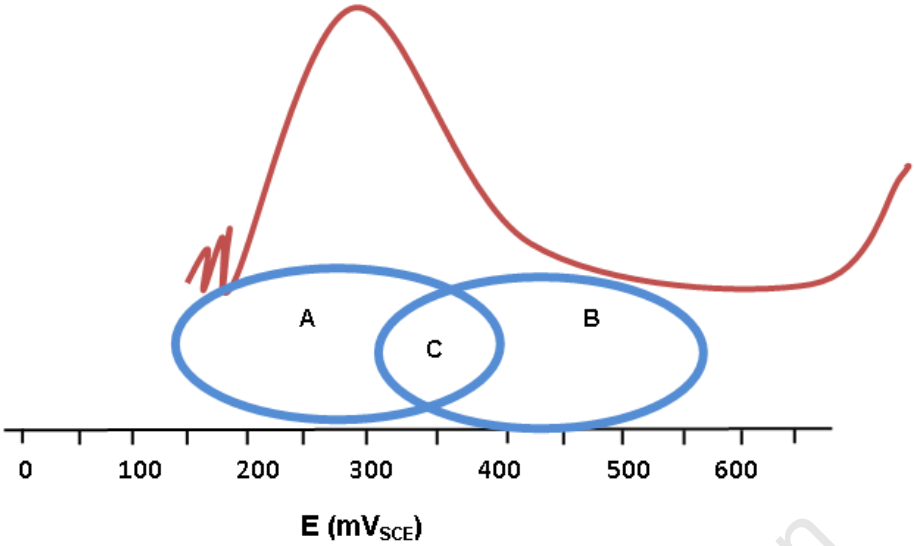

Figure 4.15. Represents a proposed model for the discrete sites that might be created during anodic sweeps for the chalcopyrite electrode. A and B represent sites where ferric/ferrous redox reactions occurs, precipitation of Fe-OH species, and mineral oxidation reactions. C represents a site where it is proposed that all these reactions occur.

To further analyze anodic current/potential peaks observed, studies were performed to monitor how the peak would be influenced by the open circuit potential (OCP) of the electrode established at the different Fe^{3+}/Fe^{2+} ratios. These studies were performed from the open circuit potential (OCP) of three Fe^{3+}/Fe^{2+} ratios (10:1, 1:1, 1:10) for the three total iron concentrations at 25 °C only. OCP runs were performed for 15 minutes on each ratio, thereafter the anodic sweep was performed, starting from the OCP observed (Figure 4.16). Fe^{3+}/Fe^{2+} ratios studied in these sweeps showed different OCPs, which decreased as ferrous ion increased. Anodic direction LSV sweeps performed from OCPs unexpectedly showed no significant difference between each other for the ratios studied (Table 4.3). These experiments were repeated a number of times to verify the observed trend, and demonstrated a high degree of reproducibility. The LSV sweeps started at the OCP when compared to the peaks of those that were previously started at 0 V, did not show any current peaks. For the 10:1 ferric/ferrous and 0.5 g/L total iron concentration, a potential peak at 393 mV_{SCE} would be expected by comparison to the a similar sweep that was performed in the sweeps that were started at 0 V, since it had an OCP less than that where the current density peak would occur (336 mV_{SCE}), however, no signs of a peak were observed. The 1:1 and 1:10 Fe^{3+}/Fe^{2+} ratios had an OCP that was above

the potential where a current density peak would occur. In the case of the 2 g/L, potential peaks were expected to be observed for the 10:1 and 1:1 Fe^{3+}/Fe^{2+} ratios as their OCPs were less than that of the observed potential where peaks occurred, however this was not the case. For the 5 g/L ratios, all OCPs were above the peak region.

Table 4.3. Open circuit potentials for the different Fe^{3+}/Fe^{2+} ratios taken at 25 °C, with the sweep following after 15 minutes.

	OCP (V)		
Ratio	0.5 g/L	2 g/L	5 g/L
10:1	0.314	0.358	0.388
1:1	0.276	0.340	0.447
1:10	0.277	0.295	0.337

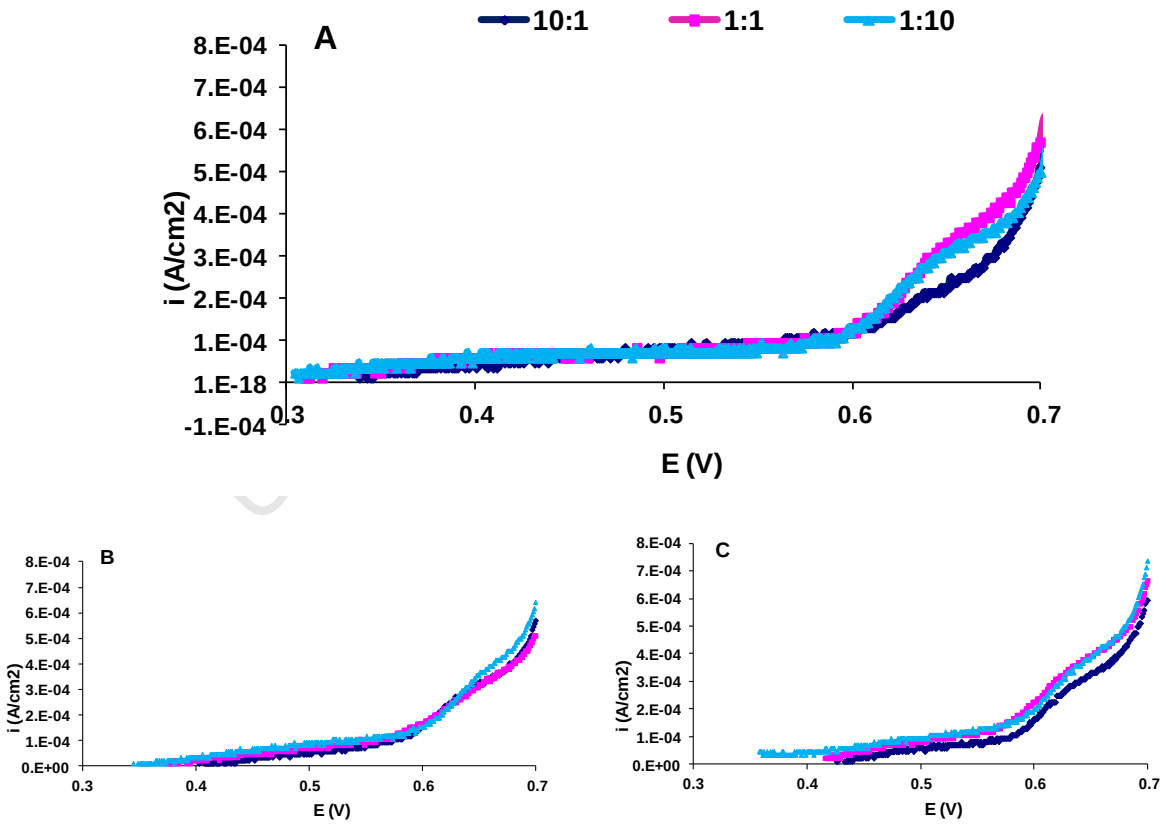

Figure 4.16. LSV Sweeps performed from the OCP, all at 25 °C. A. 0.5 g/L, B. 2 g/L and C. 5 g/L.

With OCPs being so close to the potential region where current density peaks occur, it appears that the time the electrode spends in the electrolyte might have an effect. For the Fe^{3+}/Fe^{2+} ratios at which peaks for the LSV sweeps were expected, in the sweeps that were begun at the OCP the lag time and possibly reactions that occurred prior to the current density peak in the studies performed from 0 V_{SCE} seem to affect these sweeps. Therefore differences observed between the sweeps started at the OCP and those started at 0 V_{SCE} could be attributed to about 5 – 7 minutes of lag time the electrode spends in the oxidizing media during the anodic scan, prior to reaching the OCP. Another explanation could be attributed to the reactions that occur prior to the main peak observed. The sweeps started at 0 V at higher total iron concentration and temperature showed initial negative currents (refer to Figure 4.10). As discussed earlier with potentials calculated from the Nernst equation, ferric is also likely to be reduced at low potentials near the surface. It was observed that for sweeps that have high Fe^{2+} ion in solution, an initial current density that approaches 0 A/cm^2 is observed, whereas those with more Fe^{3+} ion in solution show an initial current densities in the cathodic region. Thus, these initial Fe^{3+}/Fe^{2+}redox reactions could be considered to affect the anodic potential peak observed in the sweeps that were started at 0 V. Furthermore, the sweeps started at the OCP show more of a passivation type behaviour, in that, as discussed earlier, around this passivation-like region the sweeps show a similar current density convergence. Finally, the disappearance of the peak for sweeps started at the OCP could be described with reference to the discrete reaction sites model proposed in Figure 4.15. Since in this model other redox reactions were proposed to take place prior to the main anodic peak, it is then proposed that alterations to the mineral surface at these sites may as well play a role in the occurrence of the main anodic peak. As such, this is where difficulties of dealing with chalcopyrite as compared to other secondary sulfide minerals are encountered for most electrochemical work on chalcopyrite. In this regard, it is difficult to exclusively determine which factors affect the behaviour of the mineral during anodic dissolution, thereby in turn to predict the slow kinetics experienced by chalcopyrite during leaching.

4.2.5 Passivation and chrono-amperometric studies

The passive region on the linear sweep voltammetry (see Figure 4.8 - Figure 4.10) was observed to be affected by all conditions investigated, that is, total Fe concentration, temperature and Fe^{3+}/Fe^{2+} ion ratios. At 25°C, the passive region (region 3 in Figure 4.6) was observed to be as expected from literature, that is, the current density showed no or only marginal change with increasing potential. This behaviour was observed at potentials between 400 – 600 mV_{SCE} at 25 °C for all total Fe concentrations. As the temperature was increased to 45 and 65 °C, changes in the passive region were observed to increase instead of being constant around the passivation region. The Fe^{3+}/Fe^{2+} ion ratios also showed significantly different behaviour at higher temperatures. There was a 0.5 mA/cm^2 increase in base-line current density observed for each 20 °C increase in temperature (Figure 4.9, anodic side). The shortening of the passive region was also observed to be affected by the change in total Fe concentration. At 5 g/L total Fe concentration and 65 °C, the passive region seems to disappear completely, as the current density continued to increase steadily with increasing potential. These observed phenomena in the passive region have not been discussed in the literature before (Biegler and Horne, 1985; Warren et al., 1982; Biegler and Swift, 1979); where it is generally agreed that current density in the passive region is not dependent on potential due to the 'passive' layer that forms, rendering the surface of the electrode inaccessible to the oxidizing media, at certain potentials.

It thus becomes essential to study this 'passive' region much more closely so as to understand why for certain conditions it is observed to change. Methods different to LSV to study the nature of this region are then required.

A preliminary investigation into the passive region was set up by studying the current-time dependence at a given potential, and repeat this over short potential intervals across the passivation region, by the use of the chrono-amperometric electrochemical technique. The potential was stepped through intervals of 50 mV_{SCE} and current density monitored over a 60 second intervals before stepping to the next

level. Current densities measured are plotted against time at that constant step potential (Figure 4.17).

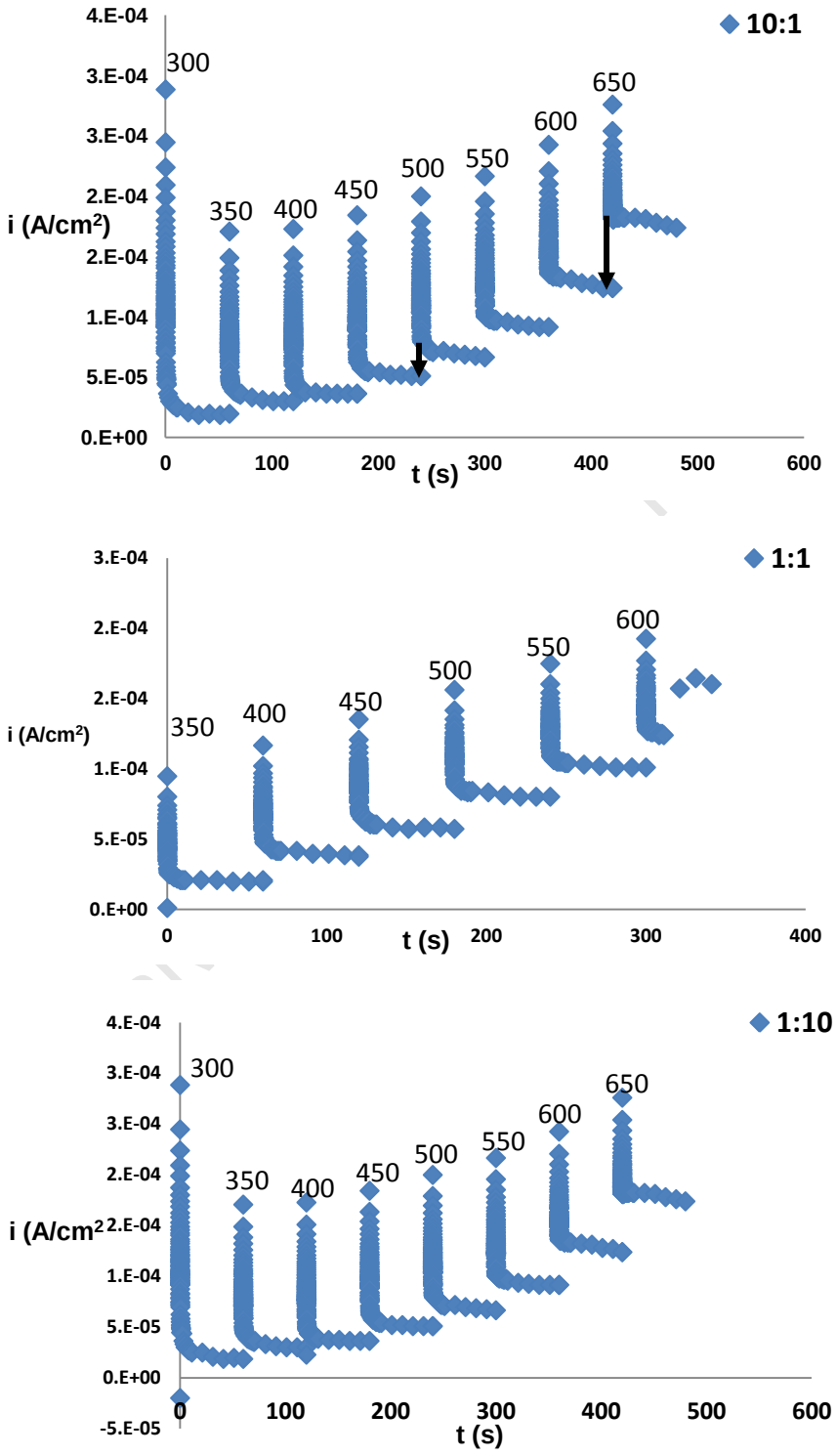

Figure 4.17. Chrono-amperometric runs for three Fe^{3+}/Fe^{2+} ratios at 25 °C and 2 g/L total Fe concentration, for potential steps between 300 mV to 650 mV. The steps are shown as continuous, but were actually run individually for every potential interval. The 1:1 ratio could not continue at step potentials of 300 and 650, hence the missing data points.

As can be observed from the figure above, as the potential is stepped up, a current density peak is observed, which then decreases rapidly over time at the potential held for 60 seconds. The current density spikes, then continuously decreases until it asymptotes a constant value at each given step potential. The current density gaps (marked with a downward arrow in Figure 4.17 for 1:10 Fe^{3+}/Fe^{2+}) between the potential steps are observed to be constant at lower potentials and increase slightly at higher potentials. The slightly higher increase in the gap at higher potentials (~600 mV_{SCE}) could indicate entry into the transpassive region. Since these studies were performed around the passivation region, it is proposed that, in accordance to literature and anodic LSV sweeps at 25 °C (i.e. non dependence of current density to potential at the passivation region), the tail ends of these chrono-amperometric potential steps should converge more or less to the same current density. However the tail ends of the current density appear to increase slightly from one potential step to the next. An increase in temperature to 45 °C showed a much more pronounced increase in the current density from one potential step to the next (Figure 4.18 (top), shown for a 5:1 Fe^{3+}/Fe^{2+}). General comparison between 25 and 45 °C total chrono-amperometric scans did not show significant differences in the converging of current density for each potential step. As observed in the 25 °C data, there was a higher current density gap at the tail end for higher potentials (> 500 mV_{SCE}).

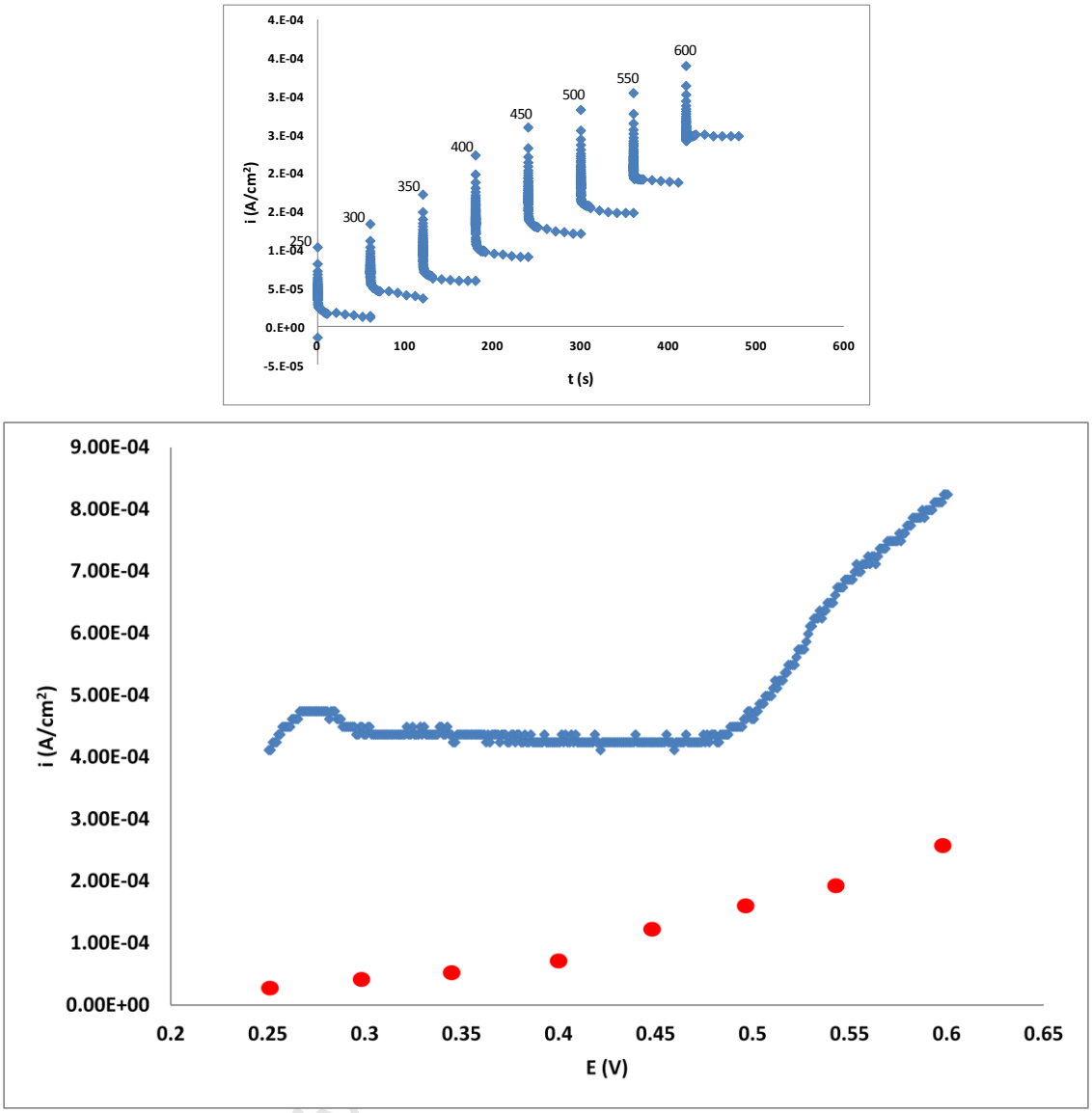

Figure 4.18. Chrono-amperometric scan (top) and LSV sweep for a 5:1 Fe^{3+}/Fe^{2+} at 45 °C, and 2g/L total Fe concentration (blue). Red points represent the end points of the chrono-amperometric scan mapped on the LSV sweep at the similar potentials.

Figure 4.18 also shows a LSV scan of the same Fe^{3+}/Fe^{2+} at the same total iron concentration and temperature (5:1, 2 g/L and 45 °C, respectively) and points representing the current density at the tail ends of each chrono-amperometric step (red points, in Figure 4.18). In the latter it can be observed that there is a linear increase in current density as the potential is stepped. This linear increase is more or less constant per potential step, *approx* 0.029 mA/cm^2. The current densities for the LSV sweep for the region studied was between 4.0 – 8 mA/cm^2. In the active region (250 – 300 mV) in the LSV, the peak observed does not agree with the data obtained from chrono-amperometric scan. From this observation it can be

postulated that the commonly employed LSV sweeps are a bit misleading with regards to the actual current density behaviour of the system while the potential is continuously increased during a LSV sweep. It is suggested that the peak observed during a typical LSV sweep is not a true representation of the changes in current as potential increases. Chrono-amperometric studies show that a short-lived peak occurs at every potential step, presumably due to surface polarisation effects, and hence rapidly stepping up in small potential steps will artificially boost the measured current by that needed to effect this polarisation. The study also showed that at each particular potential step, the decay in current actually reaches 'equilibrium', as shown by the points, current increase at a constant rate.

From comparing the LSV scan and that reconstructed from the 'equilibrium' values from the chrono-amperometric study, it can further be postulated that dissolution of chalcopyrite, as thought to occur in the pre-passivation and active region, is a transient process with respect to current density. This transient nature is also observed around the passivation region (350 – 500 mV_{SCE}) where it is expected that current is independent of potential, however, similar increases in the in current density per potential step are observed. Differences are only observed at higher potentials (500 – 600 mV_{SCE}); the start of the transpassive region, where the current density gaps start to increase and the current densities measured by LSV and chrono-amperometry show the same rapidly increasing trend and approach each other more closely.

5 CONCLUSIONS

The current study was set up as an initial study of the electrochemical behaviour of chalcopyrite under different conditions so as to set up methodologies and perform basic chalcopyrite electrochemical experiments. The following are the principal conclusions reached from the present study.

1. It was found from base reproducibility studies that the electrochemical behaviour of the mineral electrodes studied differs according to origin of sample and/or sample composition. For a single electrode under the conditions studied, it was observed that in triplicate runs that there was a significant difference between each run. From these observations it was clear that it is not possible to get an exact same sweep when repeating the experiment, but instead one that follows a similar trend from the previous.
2. Scan rate during a LSV affects the level of peak definition in the details observed during sweeps. Potentiostats, which run in a step-wise fashion, show more definition in the details of the peak; the slower a sweep is run, because there is more accessible time for the electrolyte and the working electrode to interact. Temperature changes seemed to affect this observation, therefore showing that temperature adds and extra effect to the whole system. On the other hand, the later chrono-amperometric studies indicated that this better definition may in fact relate to a temporal effect caused by the frequent potential step changes and hence be a somewhat an artificial effect.
3. Studies performed in acidic Fe media showed an increase in the current density peak in the active region as the temperature was increased from 25 – 45 – 65 °C. This agrees with the observation that leaching rate is increased by an increase in temperature. Temperature also affected the passivation region where it was observed that at 65 °C this region no longer showed a constant current density, but instead a continuous increase.
4. The 5 g/L total Fe concentration indicated decreases in current density peaks, suggesting that high concentrations may not be viable for such studies. The

optimum concentration indicated that it might fall somewhere between 0.5 and 2 g/L. At higher temperatures and high total Fe concentration the passivation region showed steadily increasing current densities instead of the usual constant value.

5. The Fe^{3+}/Fe^{2+} ratio indicated that inclusion of higher concentrations of Fe^{2+} ions in solution in the system increased the current density peak height in the active region. Since the potential was arbitrarily started at 0 V, increase in Fe^{3+}/Fe^{2+} ratio shifted the start of the sweeps to cathodic current densities, showing that as the concentration of Fe^{2+} in solution increased, the sweeps approached 0 A/cm^2 current density.
6. The difficulty in elucidating reactions that occur during chalcopyrite dissolution was explained by the "discrete sites model" discussed in Figure 4.15. It is concluded that multiple competitive electrochemical reactions occur around the same region during chalcopyrite leaching, hence conflicting explanations in the study of chalcopyrite dissolution
7. Chrono-amperometric experiments showed that LSV sweeps may not provide correct information with respect to how current behaves during a sweep. Thus LSV sweeps are suggested to be transient at different potentials during a typical LSV sweep. The peaks observed in LSV can be thought of as at least partially an artefact of the stepwise polarisation at the surface rather than just actual behaviour of the mineral.

Sweeps performed in the cathodic direction indicated a similar four region behaviour observed in sweeps in the anodic direction. Reactions that might occur relate to mineral transformations as suggested by thermodynamics in a Pourbaix diagram. High cathodic potentials made the electrode surface look like it was burnt. It was suggested that this could be due to reactions that occur at higher cathodic potentials, for example the H_2S evolution reaction and/or hydrolysis of water.

6 RECOMENDATIONS FOR FUTURE WORK

The present study was meant as an introductory study and the following are suggestion that can be proposed for future investigations.

6.1 General recommendations

1. To be able to study the changes observed between anodic and cathodic sweeps, a fresh surface and a new solution should be introduced after the anodic scan.
2. It is suggested that studies be performed at the slowest scan rate the potentiostat can maintain. These will be time consuming experiments, however they can also depict a real leaching system, where the mineral electrode can spend a significant length of time in the oxidizing media.
3. Study a wider range of total ion concentrations, so as to find the optimum concentration for chalcopyrite electrochemical studies. The effect of ferric/ferrous iron concentration and ratio has been extensively studied in leach studies, but a clear link to electrochemical experiments, however, remains elusive, and requires much more extensive study.
4. The inclusion of Fe^{2+} has been shown to have some effect on chalcopyrite electrochemical reaction. It is thus suggested that, this effect be investigated further. This can be done by continuously adding small amounts of Fe^{2+} to the system, and checking how it affects the system over time.
5. An extensive study on the surface of the electrode is suggested to supplement studies on the passivation behaviour of chalcopyrite. The surface of the electrode can be monitored under a microscope (SEM and/or TEM) during the duration of the study. This would require cutting a thin slice of the electrode after every sweep.

6.2 Recommendations for study in biotic environments

1. The cathodic reaction (ferric reduction) showed effects at lower potentials where sweeps with higher ferric ion showed a starting point at cathodic currents. This needs to be studied further, since for biotic experiments there would be a constant regeneration of ferric ion by the bacteria. This could then provide information on the rate determining step during a biotic experiment.
2. For experiments to be performed in biotic environments, it is suggested that since thermophiles have shown a greater advantage to chalcopyrite leaching, that such experiments be performed at higher temperatures. All recommendations suggested above should be taken into consideration when performing experiments in biotic environments. Most importantly it is suggested that these experiments be performed at the slowest scan rate possible, to eliminate any limitations from the instrument.
3. It is suggested that batch bioleach experiment also be performed over a longer period of time. The apparatus for such an experiment should allow for a three electrode setup, whereby for the duration of the batch experiment, LSV and chrono-amperometric scans can be performed at regular time intervals.
4. An emerging electrochemical technique called Electrochemical Impedance Spectroscopy should also be employed in these studies, to properly characterize the surface and activity at the electrode-solution interface.

REFERENCES

1. Antonijevic, M.M. and Bogdanovic, G.D. 2004, "Investigation of the leaching of chalcopyritic ore in acidic solutions", *Hydrometallurgy,* vol. 73, no. 3-4, pp. 245-256.

2. Bard, A.J. and Faulkner, L.R. 1980, Electrochemical methods : fundamentals and applications, John Wiley & Sons, Inc, New York.

3. Barret, J., Hughes, M.N., Kaeavaido, G.I. and Spencer, P.A. (eds) 1993, Metal Extraction by Bacterial Oxidation of Minerals, Ellis Horwood Limited. Bartos, P.J. 2002, *Resource Policy,* vol. 28, pp. 85-94

4. Batlett, R.W., Wilson, D.B., Savage, B.J. and Wesley, R.J. 1986, "Hydrometallurgy Reactor Design and Kinetics" in eds. Bautista, R.G., Wesley, R. and Warren, G.W., AIME, New York, pp. 277.

5. Betejtin, A. 1977, *Curso de Mineralogía,* 3rd edn, Mir, Moscú. Biegler, T. 1977, "Reduction Kinetics of Chalcopyrite Electrode Surface", *Journal of Electroanalytical Chemistry,* vol. 85, pp. 101-106.

6. Biegler, T. and Horne, M.D. 1985, "The Electrochemistry of Surface Oxidation of Chalcopyrite", *Journal of Electrochemical Society,* vol. 132, no. 6, pp. 1363-1369.

7. Biegler, T. and Swift, D.A. 1979, "Anodic electrochemistry of chalcopyrite", Journal of Applied Electrochemistry, vol 9, no. 5, pp. 545-554.

8. Bjorling, G., Faldt, I., Lindgren, E. and Toromanov, I. 1976, "A nitric acid route in combination with solvent extraction for hydrometallurgical treatment of chalcopyrite.", In Extractive metallurgy of copper, Yannopoulos,J.C. and Agarwal,J.C. ed, New York, AIME, vol.2, pp 725-737.

9. Brandl, H. 2005, 04/21-last update, "Microbial Leaching of Metals" *(Biotechnology, Vol 10, Chapter 8)* [Homepage of Dr. Frank Weinreich], [Online]. Available: http://www.wiley-vch.de/books/biotech/pdf/v10_bran.pdf [2010, 05/26].

10. Brierley, J.A. and Hill, D.L. 1993, "Biooxidation process for recovery of gold from heaps of low-grade sulfidic and carbonaceous sulfidic ore materials", U.S. Patent 5,246,486 edn, Unites States.

11. Brierley, J.A. and Brierley, C.L. 1986, "Microbial mining using thermophilic microorganisms." in *Thermophiles: general, molecular and applied microbiology*, ed. T.D. Brock, Wiley, New York, pp. 280-305.

12. Brierley, J.A. and Brierley, C.L. 2001, "Present and future commercial applications of biohydrometallurgy", *Hydrometallurgy,* vol. 59, no. 2-3, pp. 233-239.

13. Burkin, A.R. 2001, "Oxidative Leaching of alpha-Chalcopyrite and Mooihoekite in Acidic Solutions" in *Chemical Hydrometallurgy: Theory and Principles*, 1st edn, Imperial College, UK, pp. 327-387.

14. Clark, D.A. and Norris, P.R. 1996, "Oxidation of mineral sulphides by thermophilic microorganisms.", *Mineral Engineering,* vol. 9, pp. 1119-1125.

15. Córdoba, E.M., Muñoz, J.A., Blázquez, M.L., González, F. and Ballester, A. 2009, "Passivation of chalcopyrite during its chemical leaching with ferric ion at 68 °C", *Minerals Engineering,* vol. 22, no. 3, pp. 229-235.

16. Córdoba, E.M., Muñoz, J.A., Blázquez, M.L., González, F. and Ballester, A. 2008, "Leaching of chalcopyrite with ferric ion. Part I: General aspects", *Hydrometallurgy,* vol. 93, no. 3-4, pp. 81-87.

17. Das, T., Ayyappan, S. and Chaudhury, G.R. 1999, "Factors affecting bioleaching kinetics of sulfide ores using acidophilic micro-organisms", *BioMetals*, vol 12, no. 1, pp 1-10.

18. Davies, D.S., Lueders, R.E., Spitz, R.A. and Frankiewicz, T.C. 1978, "Nitric-sulphuric leach process improvements.", *107th Annual meeting of AIME*, ed. J.J. Miller, American Institute of Mining, Metallurgical and Petroleum Engineers, New York.

19. Dreisinger, D. and Abed, N. 2002, "A fundamental study of the reductive leaching of chalcopyrite using metallic iron part I: kinetic analysis", *Hydrometallurgy,* vol. 66, no. 1-3, pp. 37-57.

20. Dutrizac, J. 1981, "The dissolution of chalcopyrite in ferric sulfate and ferric chloride media", *Metallurgical and Materials Transactions B,* vol. 12, pp. 371-378.

21. Dutrizac, J.E. and MacDonald, R.J.C. 1974, "Ferric ion as a leaching medium", *Minerals Science and Engeneering,* vol. 6, pp. 59-100.

22. Dutrizac, J. 1978, "The kinetics of dissolution of chalcopyrite in ferric ion media", *Metallurgical and Materials Transisactions B*, vol. 9, no. 4, pp..431-439.

23. Edwards, K.J., Schrenk, M.O., Hamers, R. and Banfield, J.F. 1998, "Microbial oxidation of pyrite: Experiments using microorganisms from an extreme acidic environment", *The American Minerologist,* vol. 83, pp. 1444-1453.

24. Elsherief, A.E. 2002, "The Influence of Cathodic Reduction, Fe^{2+} and Cu^{2+} Ions on the Electrochemical Dissolution of Chalcopyrite in Acidic Solution", *Minerals Engineering,* vol. 15, pp. 215-223.

25. Enos, D.G. and Scribner, L.L. 1997, "Petentiodynamic Polarization Scan", Solartron Instruments, Famborough Hampshire, UK.

26. Fuentes-Aceituno, J.C., Lapidus, G.T. and Doyle, F.M. 2008, "A kinetic study of the electro-assisted reduction of chalcopyrite", *Hydrometallurgy,* vol. 92, no. 1-2, pp. 26-33.

27. Gamry Instruments 1990 - 2008, *PHE200™ Physical Electrochemistry Software*, Warminster, USA.

28. Garrels, R.M. and Christ, C.L. 1965, "Chalcopyrite" in *Solution, Minerals, and Equilibria* Harper & Row, NewYork, pp. 213-233.

29. Gehrke, T., Hallmann, R., Kinzler, K. and Sand, W. 2001, "The EPS of Acidithiobacillus ferrooxidans - a model for structure-function relationships of attached bacteria and their physiology", *Water Science & Technology,* vol. 43, no. 6, pp. 159-167.

30. Gómez, C., Figueroa, M., Muñoz, J., Blázquez, M.L. and Ballester, A. 1996, "Electrochemistry of chalcopyrite", *Hydrometallurgy,* vol. 43, no. 1-3, pp. 331-344.

31. Hackl, R.P., Dreisinger, D.B., Peters, E. and King, J.A. 1995, "Passivation of chalcopyrite during oxidative leaching in sulfate media", *Hydrometallurgy,* vol. 39, no. 1-3, pp. 25-48.

32. Hirato, T., Majima, H. and Awakura, Y. 1987, *The leaching of chalcopyrite with ferric sulfate*, " *Metallurgical and Materials Transactions B*", vol. 18, no. 3, pp. 489-496.

33. Hiroyoshi, N., Kuroiwa, S., Miki, H., Tsunekawa, M. and Hirajima, T. 2004, "Synergistic effect of cupric and ferrous ions on active-passive behavior in anodic dissolution of chalcopyrite in sulfuric acid solutions", *Hydrometallurgy,* vol. 74, pp. 103-116.

34. Hiroyoshi, N., Kuroiwa, S., Miki, H., Tsunekawa, M. and Hirajima, T. 2007, "Effects of coexisting metal ions on the redox potential dependence of chalcopyrite leaching in sulfuric acid solutions", *Hydrometallurgy,* vol. 87, no. 1-2, pp. 1-10.

35. Hiroyoshi, N., Hirota, M., Hirajima, T. and Tsunekawa, M. 1997, "A case of ferrous sulfate addition enhancing chalcopyrite leaching", *Hydrometallurgy,* vol. 47, no. 1, pp. 37-45.

36. Hiroyoshi, N., Kitagawa, H. and Tsunekawa, M. 2008, "Effect of solution composition on the optimum redox potential for chalcopyrite leaching in sulfuric acid solutions", *Hydrometallurgy,* vol. 91, no. 1-4, pp. 144-149.

37. Hiroyoshi, N., Miki, H., Hirajima, T. and Tsunekawa, M. 2001, "Enhancement of chalcopyrite leaching by ferrous ions in acidic ferric sulfate solutions", *Hydrometallurgy,* vol. 60, no. 3, pp. 185-197.

38. Hiroyoshi, N., Miki, H., Hirajima, T. and Tsunekawa, M. 2000, "A model for ferrous-promoted chalcopyrite leaching", *Hydrometallurgy,* vol. 57, no. 1, pp. 31-38.

39. Hunter, C.J. 2001, "A bacterially assisted heap leach", W.O. Patent 0144,519, Australia.

40. Hunter, C. 2002, "A method for the bacterially assisted heap leaching of chalcopyrite", World Patent 200270757, Australia.

41. International Copper Study Group 2010, *The World Copper Factbook 2010*, International Copper Study Group, Lisbon, Portugal.

42. Jackson, E. 1986, *Hydrometallurgical Extraction and Reclamation,* Ellis Horwood Limited, England.

43. Jáuregui, G.A. and Reyes, R.A. 1987, "Anodic electrooxidation of a copper concentrate", *Hydrometallurgy,* vol. 17, no. 3, pp. 281-294.

44. Jordan, H., Sanhueza, A., Gautier, V., Escobar, B. and Vargas, T. 2006, "Electrochemical study of the catalytic influence of Sulfolobus metallicus in the bioleaching of chalcopyrite at 70 °C", *Hydrometallurgy,* vol. 83, no. 1-4, pp. 55-62.

45. Kawatra, S.K. 2010, *Primary Metal Production*, CM2200 Lecture Notes edn, Michigan Technological University.

46. Kelly, R.M. and Deming, J.W. 1988, "Extremely thermophilic archaebacteria: Biological and engineering considerations.", *Biotechnology Progress,* vol. 4, pp. 47-62.

47. Kissinger, P.T. and Heineman, W.R. 1983, "Cyclic Voltammetry", *Journal of Chemical Education,* vol. 60, no. 9, pp. 702-706.

48. Konig, H. 1988, "Archaebacterial cell envelopes", *Canadian Journal of Microbiology,* vol. 34, pp. 395-406.

49. Lamya, R.M. and Lorenzen, L. 2005, "A study of factors influencing the kinetics of copper cementation during atmospheric leaching of converter matte", *The Journal of The South African Institute of Mining and Metallurgy,* vol. 105, no. 1, pp. 21-28.

50. Liddicoat, J. and Dreisinger, D. 2007, "Chloride leaching of chalcopyrite", *Hydrometallurgy,* vol. 89, no. 3-4, pp. 323-331.

51. Liew, F.C. 2009, [Homepage of TES-AMM Ausralia], [Online]. Available: http://www.tes-amm.com.au/downloads/TES-AMM_analysis_pyrometallurgy_vs_hydrometallurgy_April_2008.pdf [2010, 11/10].

52. Lu, Z.Y., Jeffrey, M.I. and Lawson, F. 2000, "An electrochemical study of the effect of chloride ions on the dissolution of chalcopyrite in acidic solutions", *Hydrometallurgy,* vol. 56, no. 2, pp. 145-155.

53. Lusinga, D. 2011, "*A multi criteria analysis and comparison of primary copper processing options"*, Cape Town, South Africa, University of Cape Town. (MSc-thesis)

54. Medvedev, D. and Stuchebruhov, A.A. 2001, "DNA Repair Mechanism by Photolyase: Electron Transfer Path from the Photolyase Catalytic Cofactor FADH−to DNA Thymine Dimer", *Journal of theoretical biology,* vol. 210, no. 2, pp. 237-248.

55. Meyer, G., Schneider-Merck, T., Böhme, S. and Sand, W. 2002, "A Simple Method for Investigations on the Chemotaxis of A. ferrooxidans and D. vulgaris", *Acta Biotechnologica,* vol. 22, no. 3-4, pp. 391-399.

56. Monk, P. 2002, "Fundamentals of Electro-analytical Chemistry", John Wiley & Sons Ltd, The Atrium, Southern Gate, Chichester.

57. Munoz, P., Miller, J. and Wadsworth, M. 1979, "Reaction mechanism for the acid ferric sulfate leaching of chalcopyrite", *Metallurgical and Materials Transactions B*, vol. 10, no. 2, pp. 149-158.

58. Nava, D. and González, I. 2006, "Electrochemical characterization of chemical species formed during the electrochemical treatment of chalcopyrite in sulfuric acid", *Electrochimica Acta,* vol. 51, no. 25, pp. 5295-5303.

59. Nemati, M., Lowenadaler, J. and Harison, S.T.L. 2000, "Particle size effects in bioleaching of pyrite by acidophilic thermophile Sulfolobus metallicus (BC)", *Applied Microbiology & Biotechnology,* vol. 53, pp. 173-179.

60. Parker, A.J., Paul, R.L. and Power, G.P. 1981, "Electrochemical aspects of leaching copper from chalcopyrite in ferric and cupric salt solutions", *Australian Journal of Chemistry,* vol. 34, no. 1, pp. 13-34.

61. Parker, A., Klauber, C., Kougianos, A., Watling, H.R. and van Bronswijk, W. 2003, "An X-ray photoelectron spectroscopy study of the mechanism of oxidative dissolution of chalcopyrite", *Hydrometallurgy,* vol. 71, no. 1-2, pp. 265-276.

62. Petersen, J. 2009, "Introduction to Hydrometallurgy and Hydrometallurgical Operations at Anglo Platinum", Short MSc Course, Anglo Plattinum Limited, Deapatment of Chemical Engineering, University of Cape Town.

63. Petersen, J. and Dixon, D.G. 2007, "Modelling zinc heap bioleaching", *Hydrometallurgy,* vol. 85, no. 2-4, pp. 127-143.

64. Petersen, J. and Dixon, D.G. 2003, "The dynamics of chalcocite heap bioleaching", *Proceedings of the 5th International Symposium Honoring Professor Ian M. Ritchie, vol. 1: Leaching and Solution Purification*, eds. C. Young, A. Alfantazi, C. Anderson, A. James, D.B. Dreisinger & B. Harris, PA: TMS Publishers, Warrendale, pp. 351.

65. Pradhan, N., Nathsarma, K.C., Srinivasa Rao, K., Sukla, L.B. and Mishra, B.K. 2008, "Heap bioleaching of chalcopyrite: A review", *Minerals Engineering,* vol. 21, no. 5, pp. 355-365.

66. Prasad, S. and Pandey, B.D. 1998, "Alternative processes for treatment of chalcopyrite —A review", *Minerals Engineering,* vol. 11, no. 8, pp. 763-781.

67. Prater, J.D., Queneau, P.B. and Hudson, T.J. 1970, " The sulphation of copper-iron sulphides with concentrated sulphuric acid.", *Journal of Metals,* vol. 22, pp. 23-27.

68. Rhodes, M. 2008, *Introduction to Particle Technology,* 2nd edn, John Wiley & Sons Ltd, Chichester.

69. Rodriguez-Leiva, M. and Tributsch, H. 1988, "Morphology of bacterial leaching patterns by *Thiobacillus ferrooxidans* on synthetic pyrite", *Archives of Microbiology,* vol. 149, no. 5, pp. 401-405.

70. Rohwerder, T., Gehrke, T., Kinzler, K. and Sand, W. 2003, "Bioleaching review part A: Progress in bioleaching: fundamentals and mechanisms of bacterial metal sulfide oxidation", *Applied Microbiology & Biotechnology,* vol. 63, no. 3, pp. 239-248.

71. Roine, A. and Anttila, K. 2009, *Eh - pH - DIAGRAMS (Pourbaix-diagrams)*, Instruction Manual for HSC Chemistry 7.0 edn, Outotec.

72. Sand, W., Gehrke, T., Jozsa, P. and Schippers, A. 2001, "(Bio)chemistry of bacterial leaching—direct vs. indirect bioleaching", *Hydrometallurgy,* vol. 59, no. 2-3, pp. 159-175.

73. Sanhueza, A., Ferrer, I.J., Vargas, T., Amils, R. and Sánchez, C. 1999, "Attachment of Thiobacillus ferrooxidans on synthetic pyrite of varying structural and electronic properties", *Hydrometallurgy,* vol. 51, no. 1, pp. 115-129.

74. Schippers, A. and Sand, W. 1999, "Bacterial leaching of metal sulfides proceeds by two indirect mechanism via Thiosulfate of via Polysulfides and Sulfur", *Applied and Environmental Microbiology,* vol. 65, no. 1, pp. 319-321.

75. Shrihari, R.K., Modak, J.M., Jayant, M., Kumar, R. and Gandhi, K.S. 1995, "Dissolution of particles of pyrite mineral by direct attachment of Thiobacillus ferrooxidans", *Hydrometallurgy,* vol. 38, no. 2, pp. 175-187.

76. Sokić, M.D., Marković, B. and Živković, D. 2009, "Kinetics of chalcopyrite leaching by sodium nitrate in sulphuric acid", *Hydrometallurgy,* vol. 95, no. 3-4, pp. 273-279.

77. Solari, J.A., Huerta, G., Escobar, B., Vargas, T., Badilla-Ohlbaum, R. and Rubio, J. 1992, "Interfacial phenomena affecting the adhesion of Thiobacillus ferrooxidans to sulfide mineral surfaces", *Colloids and Surfaces,* vol. 69, pp. 159-166.

78. Third, K.A., Cord-Ruwisch, R. and Watling, H.R. 2000, "The role of iron-oxidizing bacteria in stimulation or inhibition of chalcopyrite bioleaching", *Hydrometallurgy,* vol. 57, pp. 225-233.

79. Venkatachalam, S. 1991, "Treatment of chalcopyrite concentrates by hydrometallurgical techniques", *Minerals Engineering,* vol. 4, no. 7-11, pp. 1115-1126.

80. Vilcáez, J., Suto, K. and Inoue, C. 2008, "Bioleaching of chalcopyrite with thermophiles: Temperature–pH–ORP dependence", *International Journal of Mineral Processing,* vol. 88, no. 1-2, pp. 37-44.

81. Warren G. W 1978, "Electrochemical oxidation of chalcopyrite", Department of Metallurgy and Metallurgical Engineering, University of Utah. (PhD-thesis)

82. Warren, G., Wadsworth, M. and El-Raghy, S. 1982, "Passive and transpassive anodic behavior of chalcopyrite in acid solutions", *Metallurgical and Materials Transactions*, vol. 13, no. 4, pp. 571-579.

83. Watling, H.R. 2006, "The bioleaching of sulphide minerals with emphasis on copper sulphides — A review", *Hydrometallurgy,* vol. 84, no. 1-2, pp. 81-108.

84. Zhang, X.L., Jiang, Z.H., Yao, Z.P., Song, Y. & Wu, Z.D. 2009, "Effects of scan rate on the potentiodynamic polarization curve obtained to determine the Tafel slopes and corrosion current density", *Corrosion Science,* vol. 51, no. 3, pp. 581-587.

Appendix A

1.2 Potentiostat theory and techniques (PHE200 Gamry Sortware

Chronoamperometry

PHE200 Chronoamperometry experiment supports both single and double potential step experiments as shown by the figure below. In general, before beginning the experiment the electrode is held at a potential at which no faradaic process occurs, then the potential is stepped to a value at which a redox reaction occurs. Zero time is defined as the time at which the potential step is initiated. The chronoamperometry experiment can be used to accurately determine any one of the variables in the Cottrell equation (electrode area, diffusion coefficient, or sample concentration) as long as the other two variables are known and the contributions from adsorbed material are negligible. In some cases double potential step chronoamperometry experiments are used to determine the reversibility of a reaction by comparing the results from the two potential steps.

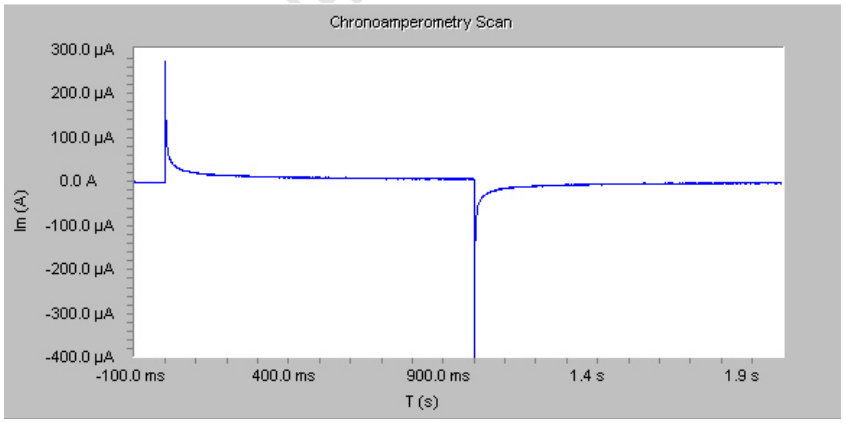

Figure A-1

Voltammetry

Voltammetry is used to study the mechanism, kinetics, and thermodynamics of chemical reactions. Both heterogeneous reactions occurring at the electrode surface and homogeneous reactions in solution can be studied. In the classical cyclic voltammetry triangle waveform, the potential is swept from an Initial E, to vertex E, and back to Final E, where Final E equals Initial E. Repeating this waveform for N times will perform N cycles of cyclic voltammetry. Linear sweep voltammetry is a simpler subset of cyclic voltammetry, consisting of a single unidirectional voltage sweep. In general, researchers will use Linear Sweep Voltammetry instead of cyclic voltammetry when there is no useful information on the return sweep of the cyclic voltammogram, such as in the case where the electron transfer is followed by a very fast irreversible reaction. In the PHE200, the more generic double vertex triangular waveform shown below. This applied waveform allows the user to set a second vertex potential (Scan Limit 2 in the software) which could be more positive than the initial potential. Setting ScanLimit2 and Final E to equal the Initial E can perform the classically defined triangle waveform for cyclic voltammetry. For the case of a simple one-electron transfer reaction, the resulting current vs. voltage plot will give the familiar "duck shape" waveform. In these cases, the reversible potential for the electron transfer can be evaluated from the half-wave potential for the redox process. In cases where the chemistry of the system is more complicated, cyclic voltammetry can be used to determine the mechanisms and kinetics involved.

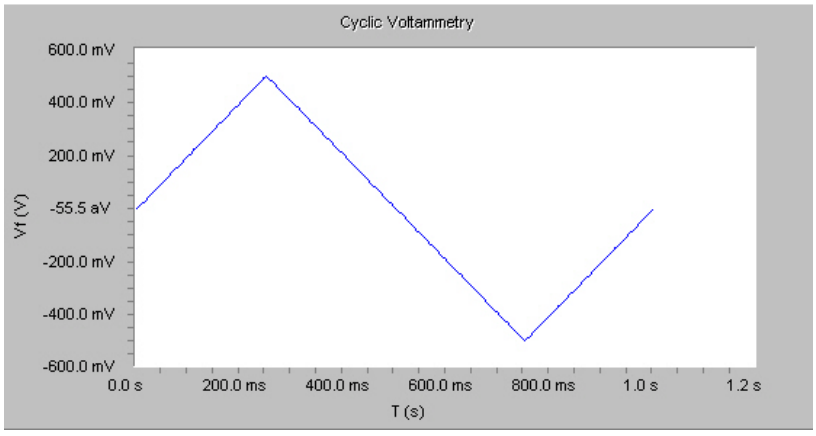

Figure A-2

Scan Rate

The Scan Rate parameter defines the speed of the potential sweep during data acquisition. The Scan Rate is entered in units of mV/sec. A practical bound on the Scan Rate is 1000 mV/sec. Higher Scan Rates may run, but can yield inaccurate data due to the inability of the software to acquire data points fast enough. This parameter when combined with the step size parameter determines time between data points and thus the data acquisition rate used in the experiment.

Time (seconds/point) = [Step Size (mV/point)] / [Scan Rate (mV/second)]

The maximum data acquisition rate is dependent on the speed of the computer, the configuration of Windows and the other software currently executing. As a guideline, one should avoid sample times below 100 µs. Note that for scans faster than 1 ms that the acquired data will only be displayed once the experiment has completed. This reduces the chance that the computer will limit the acquisition speed.

Step Size

The Step Size parameter determines the spacing between the data points in mV. A typical Step Size setting is between 1 and 5 mV. This parameter combines with the scan range on any given cycle to determine the number of data points. The total number of data points must be less than 64000 for all cycles.

 # Points = [Scan Range (mV)] / [Step Size (mV)]

Initial Time Delay

The Initial Delay phase of the experiment is the first step to occur in the experimental sequence. This phase of the experiment is used to stabilize the open circuit voltage of the sample prior to any applied signal and to measure that open circuit potential (E_{oc}). The initial delay is turned *on* or *off* with the Initial delay parameter *check box* in

the “setup dialog”. This is the time that the sample will be held at the open circuit prior to the scan. The units for time are seconds. The minimum time is one second. The maximum time is 400,000 s (more than 4 days). Below 1000 seconds, the time resolution is 1 s. Between 1000 and 10,000 s, the resolution is 10 s and above 10,000 s it is 100 s.

In many cases, you really do not want to delay for a fixed time. What you really want is to delay until E_{oc} stops drifting. The *stability* parameter allows for setting a drift rate that represents a stable E_{oc}. If the absolute value of the drift rate falls below the *stability* parameter, the initial delay phase of the experiment ends immediately, disregarding the programmed initial delay time. A *stability* setting of zero is entered to assure that the delay will last for the full time. The units of *stability* parameter are mV/s. A typical value is 0.05 mV/s. The upper limit in this parameter is 8 V/s, well above the range of practical stabilities with real cells. The lower limit of the *stability* parameter is set according to patience. A stability of 0.01 mV/s means that a 1 mV drift takes 100s. The software will always take data long enough to resolve a 1 mV change in the potential at the requested drift rate. No open circuit voltage measurement will take place if the initial delay is turned off. In this case, the open circuit voltage is defaulted to 0.0 volts.

Appendix B

Linear Voltammetry Sweeps

Table B-1. Index for all the linear sweep voltammetry sweeps represent in the following Appendix.

	Sample Origin		Total Fe Concentration (g/L)			Temperature (°C)		
	Durango, Mexico	Ontarion, Canada	0.5	2	5	25	45	65
Figure B-1	√		√			√		
Figure B-2	√		√				√	
Figure B-3	√		√					√
Figure B-4	√			√		√		
Figure B-5	√			√			√	
Figure B-6	√			√				√
Figure B-7	√				√	√		
Figure B-8	√				√		√	
Figure B-9	√				√			√
Figure B-10		√	√			√		
Figure B-11		√	√				√	
Figure B-12		√	√					√
Figure B-13		√		√		√		
Figure B-14		√		√			√	
Figure B-15		√		√				√
Figure B-16		√			√	√		
Figure B-17		√			√		√	
Figure B-18		√			√			√

Each figure in the following appendix represents sweeps performed at for Fe^{3+}/Fe^{2+} ratios (10:1, 5:1, 2:1, 1:1, 1:2, 1:5, 1:10) for three total iron concentration (0.5, 2, 5 g/L) at three different temperatures (25, 45, 65 °C). Also represent in the figure are acidic scans, i.e. those that do not contain any iron.

Durango, Mexico Chalcopyrite sample sweeps

0.5 g/L Total Fe Concentration

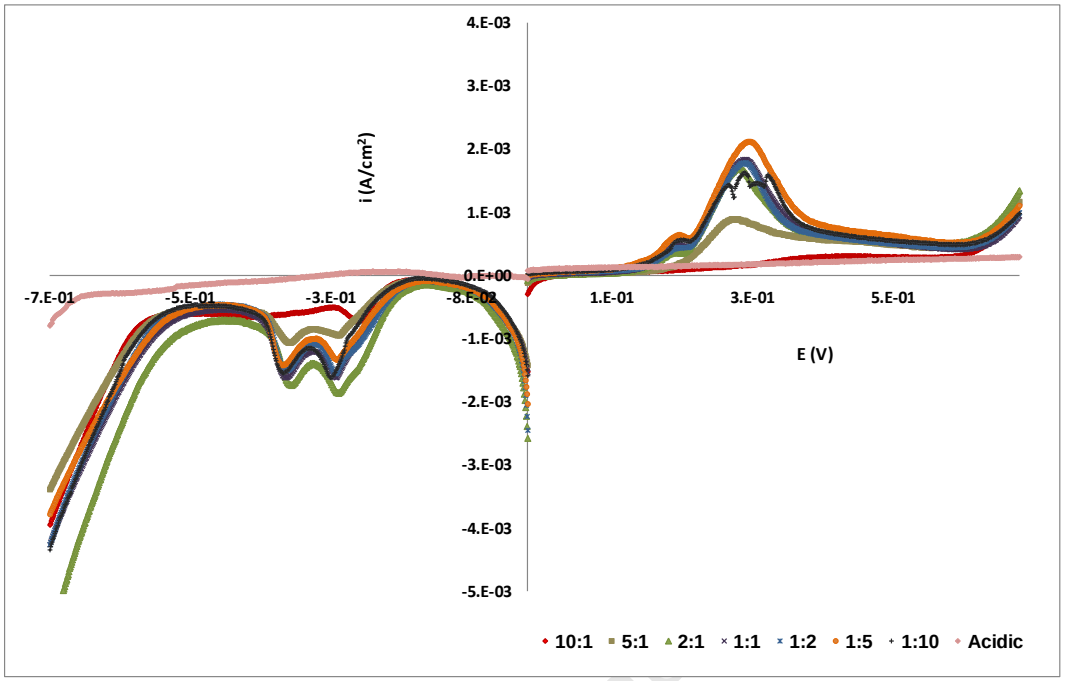

Figure B-1. 25 °C

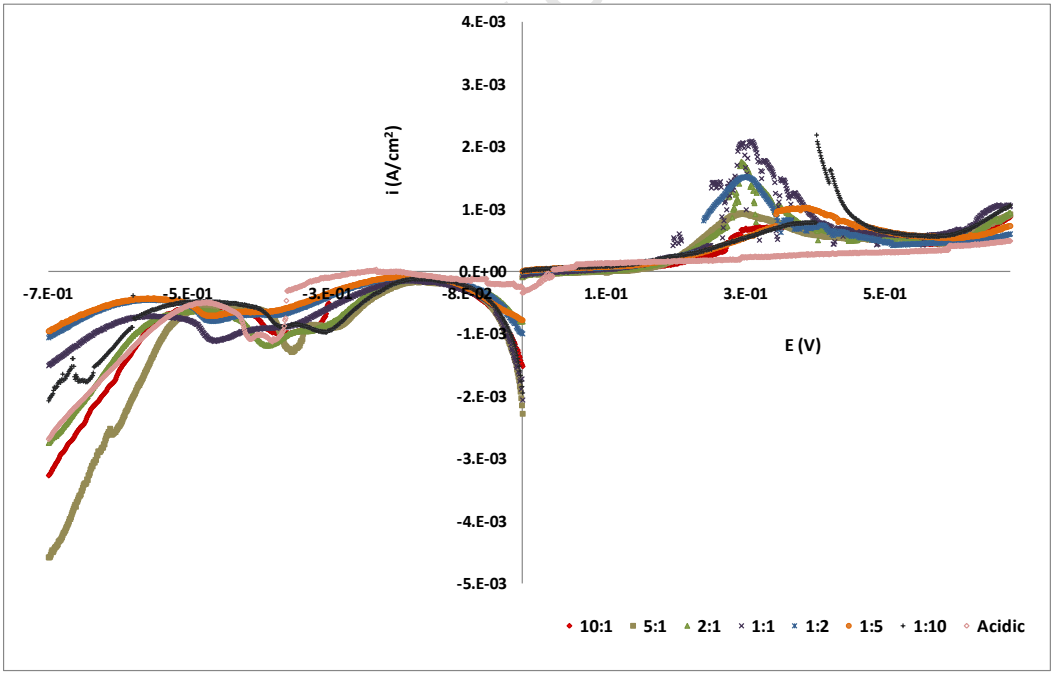

Figure B-2. 45 °C

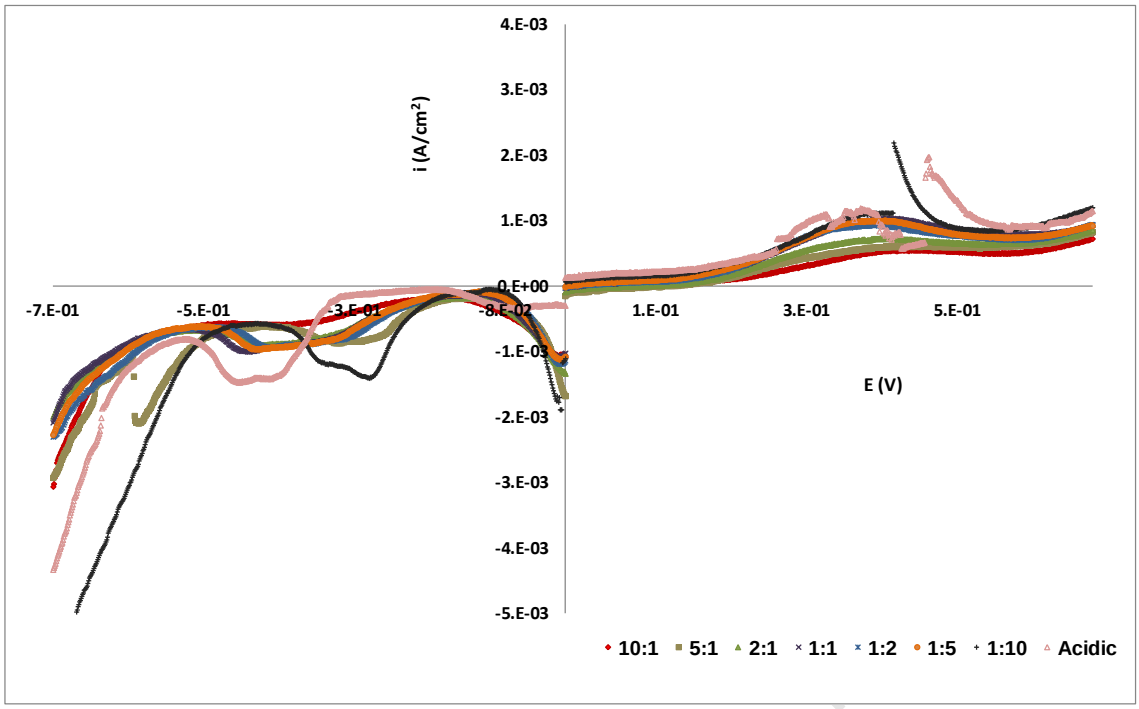

Figure B-3. 65 °C

2 g/L Total Fe Concentration

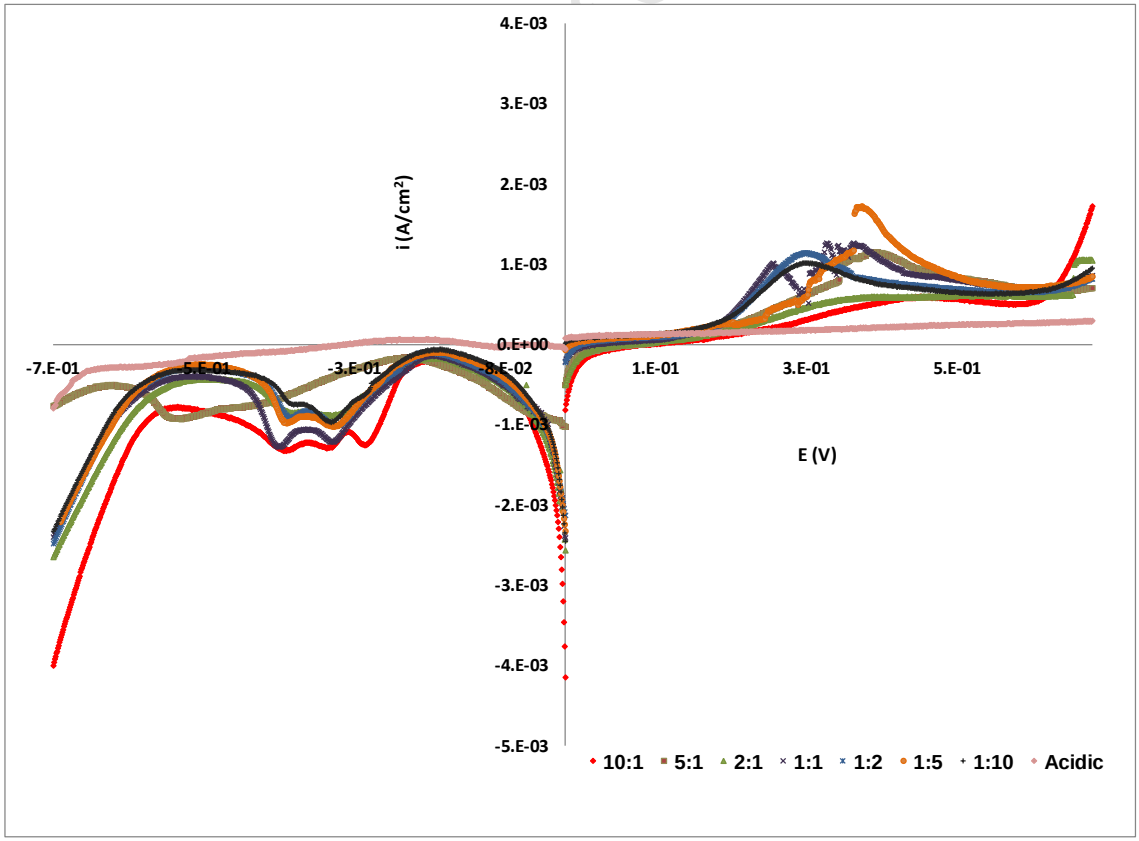

Figure B-4. 25 °C

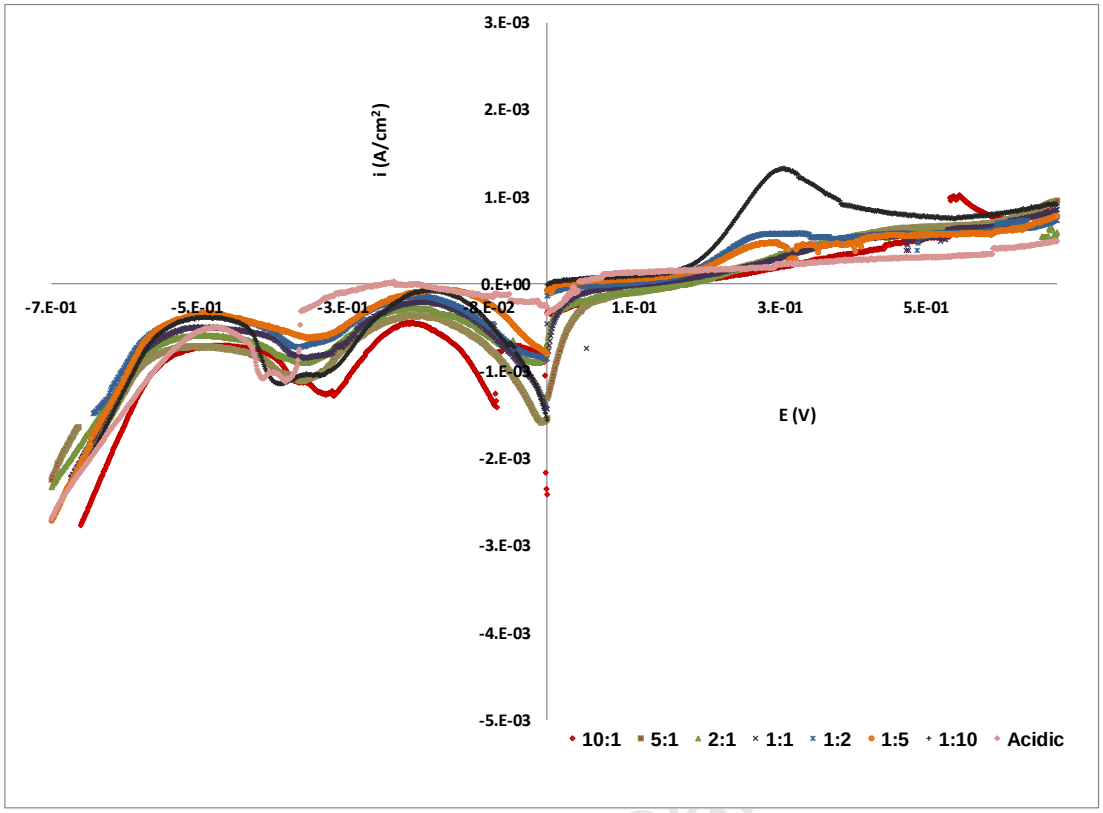

Figure B-5. 45 °C

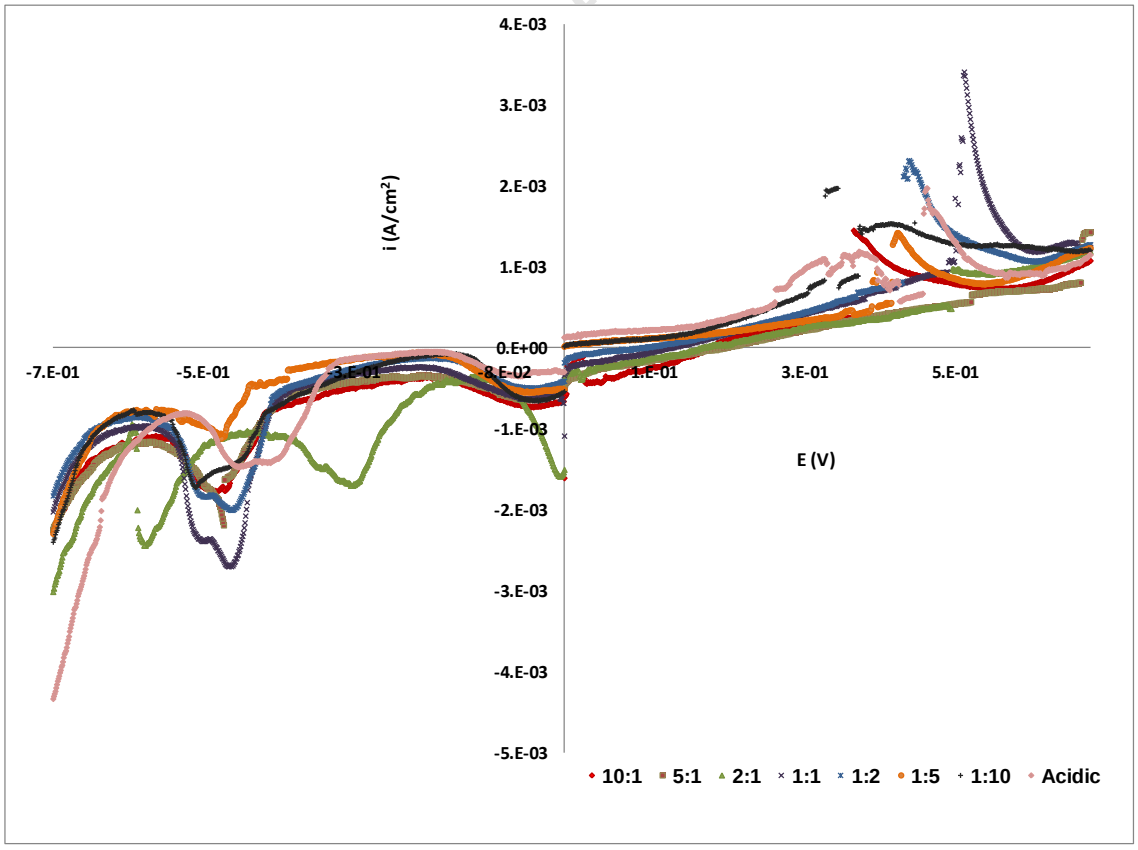

Figure B-6 65 °C

5 g/L Total Fe Concentration

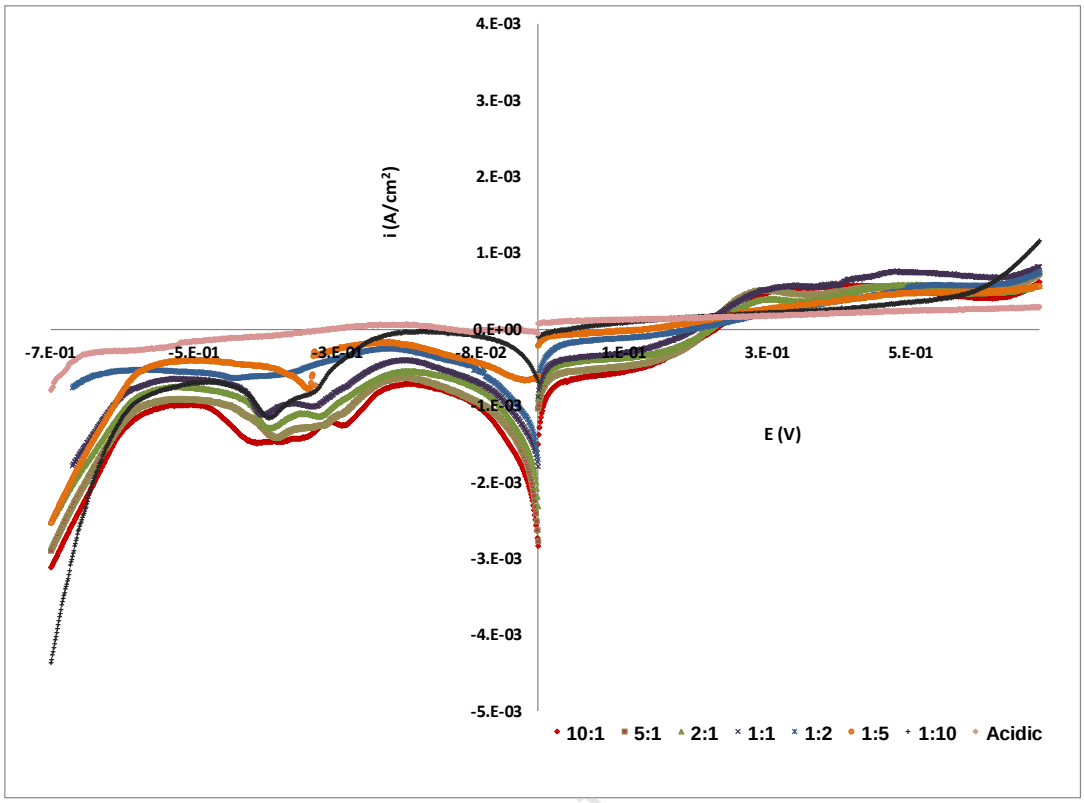

Figure B-7 25 °C

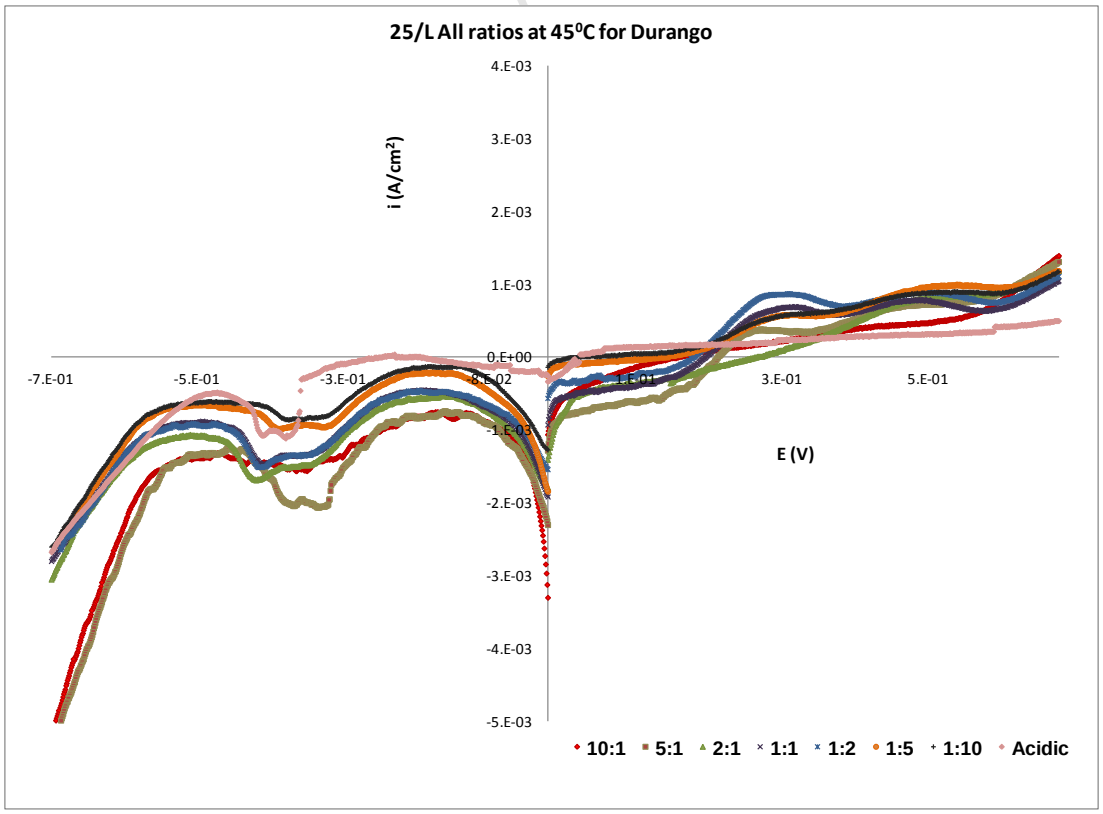

Figure B-8 45 °C

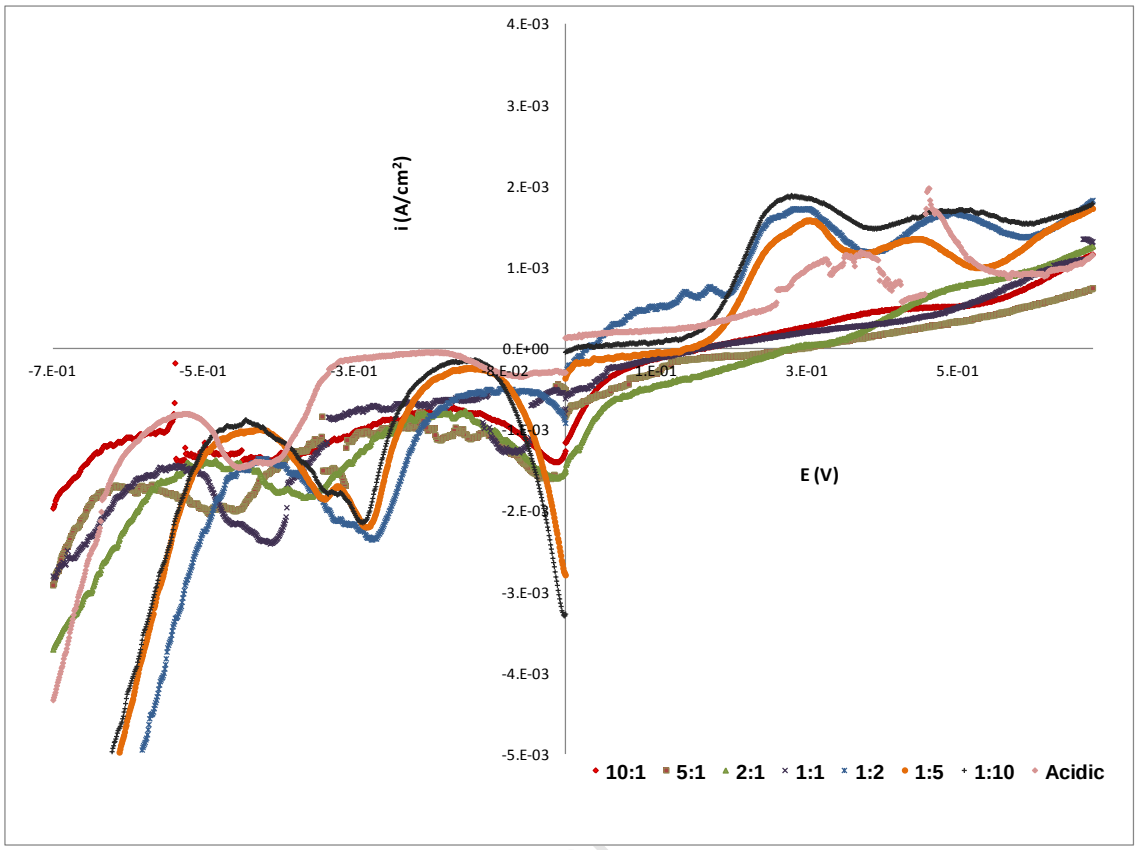

Figure B-9 65 °C

Ontatio, Canada Chalcopyrite sample sweeps

0.5 g/L Total Fe Concentration

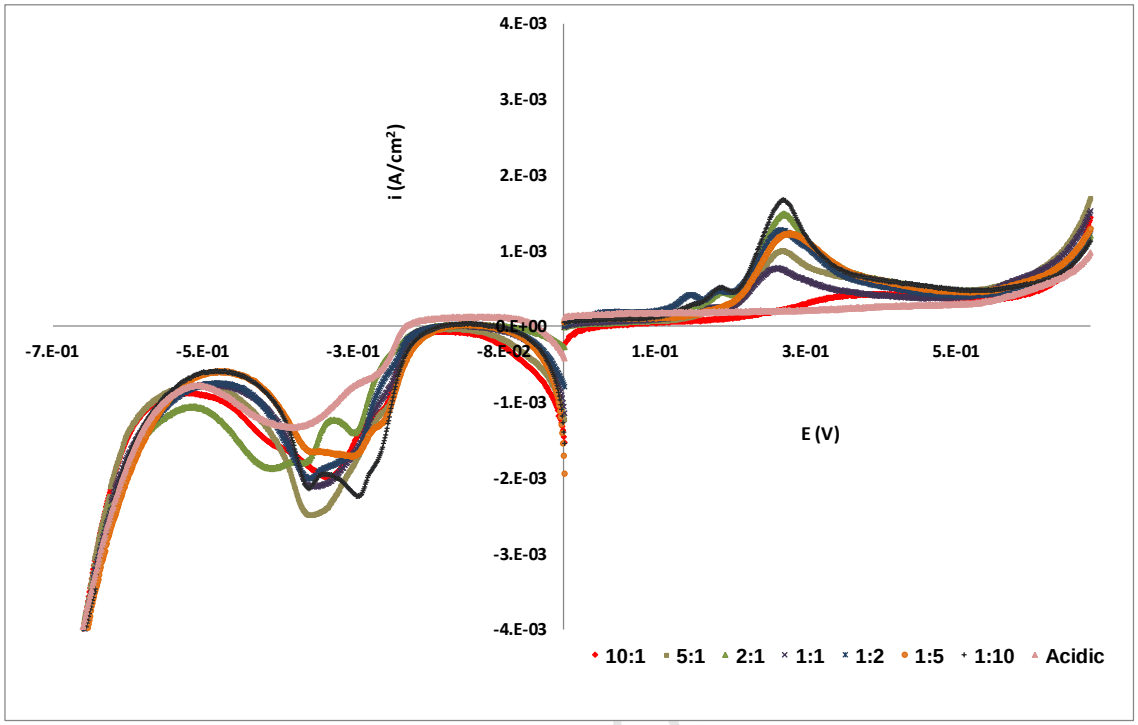

Figure B-10. 25 °C

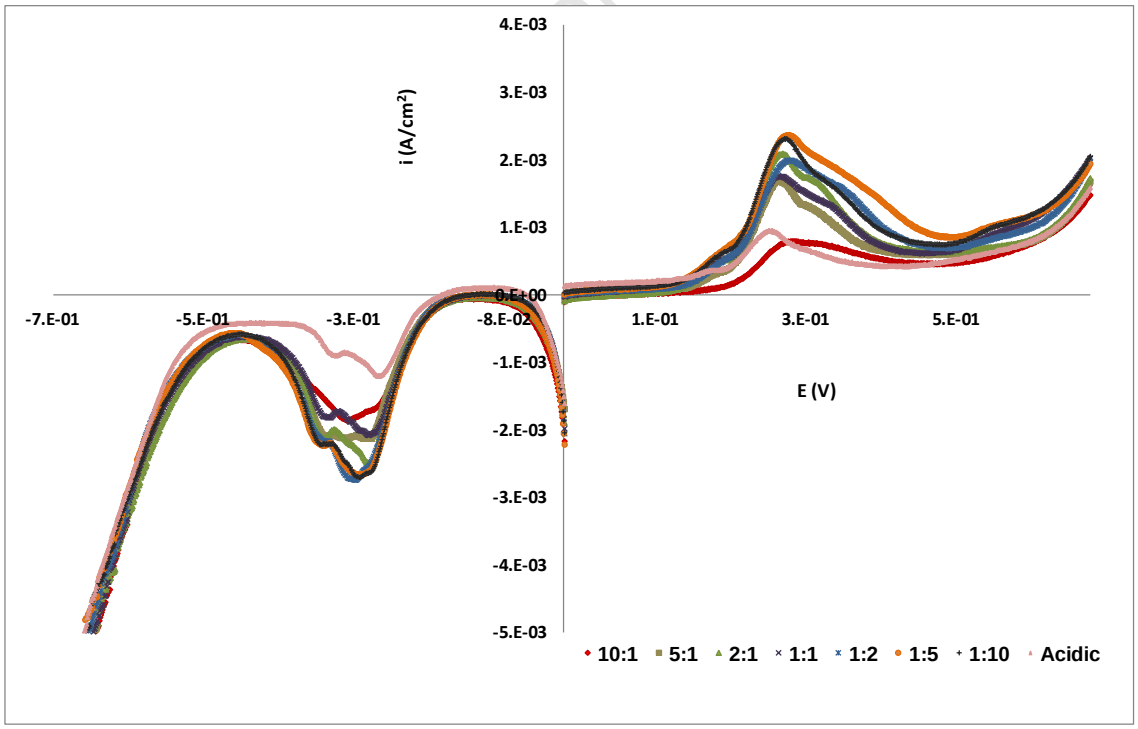

Figure B-11. 45 °C

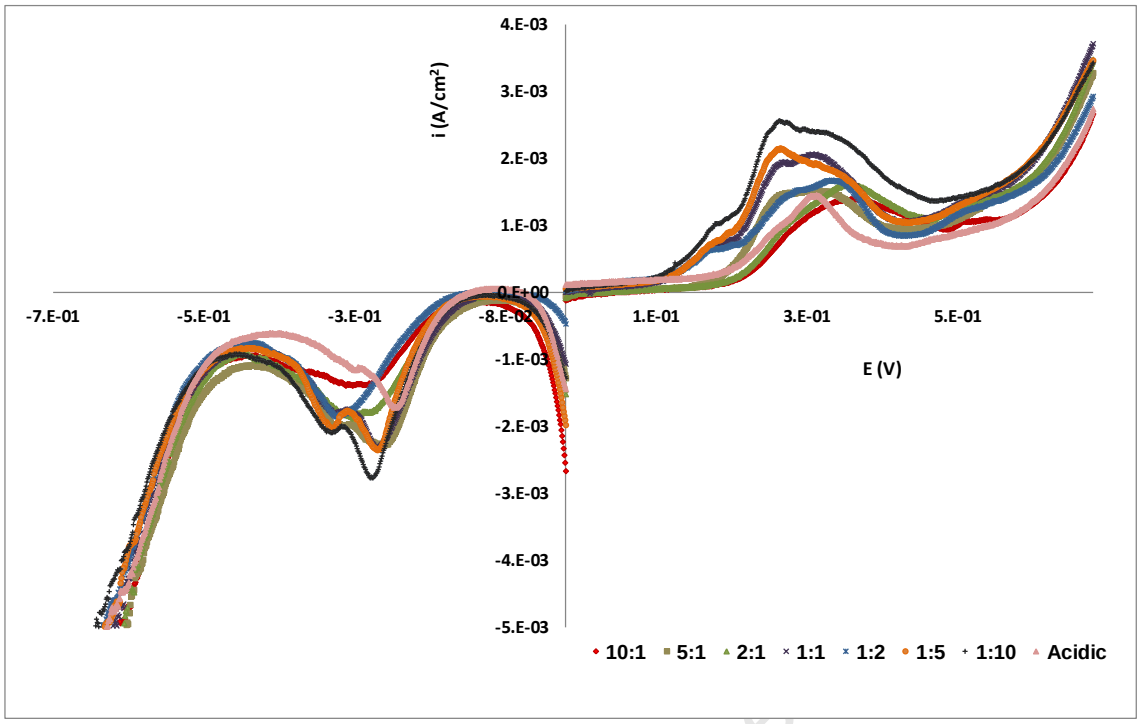

Figure B-12. 65 °C

2 g/L Total Fe Concentration

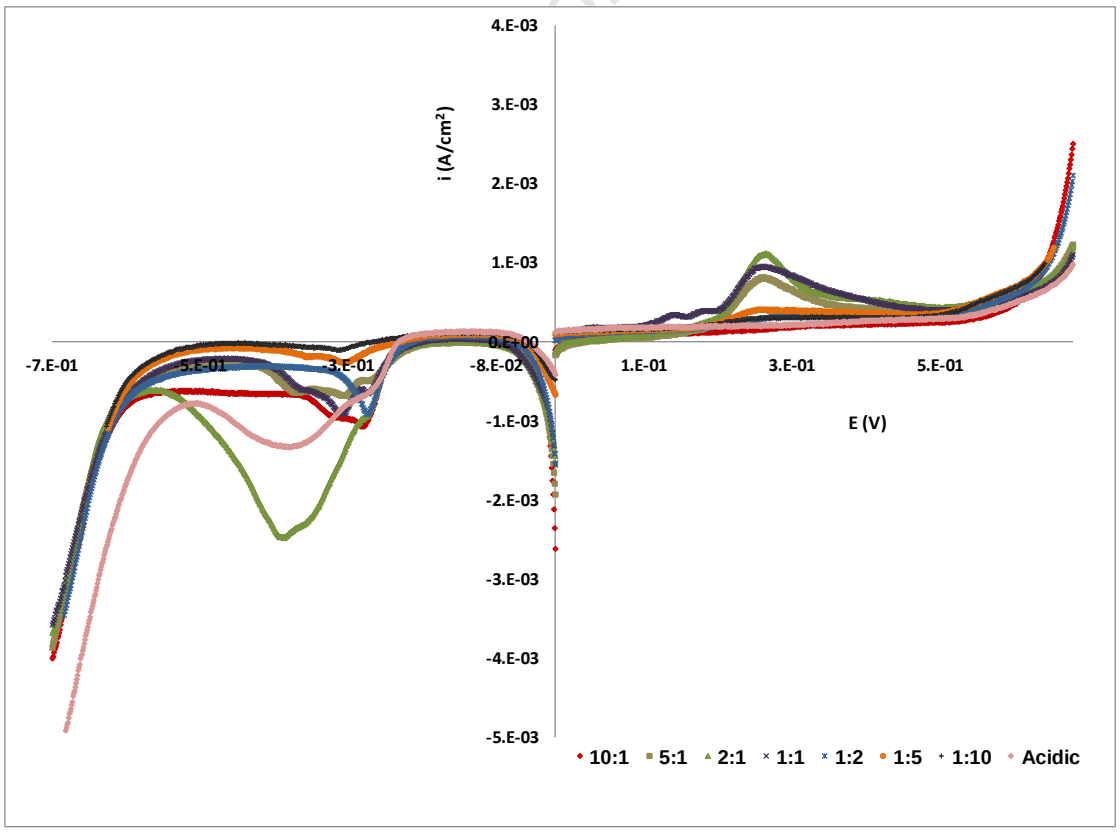

Figure B-13. 25 °C

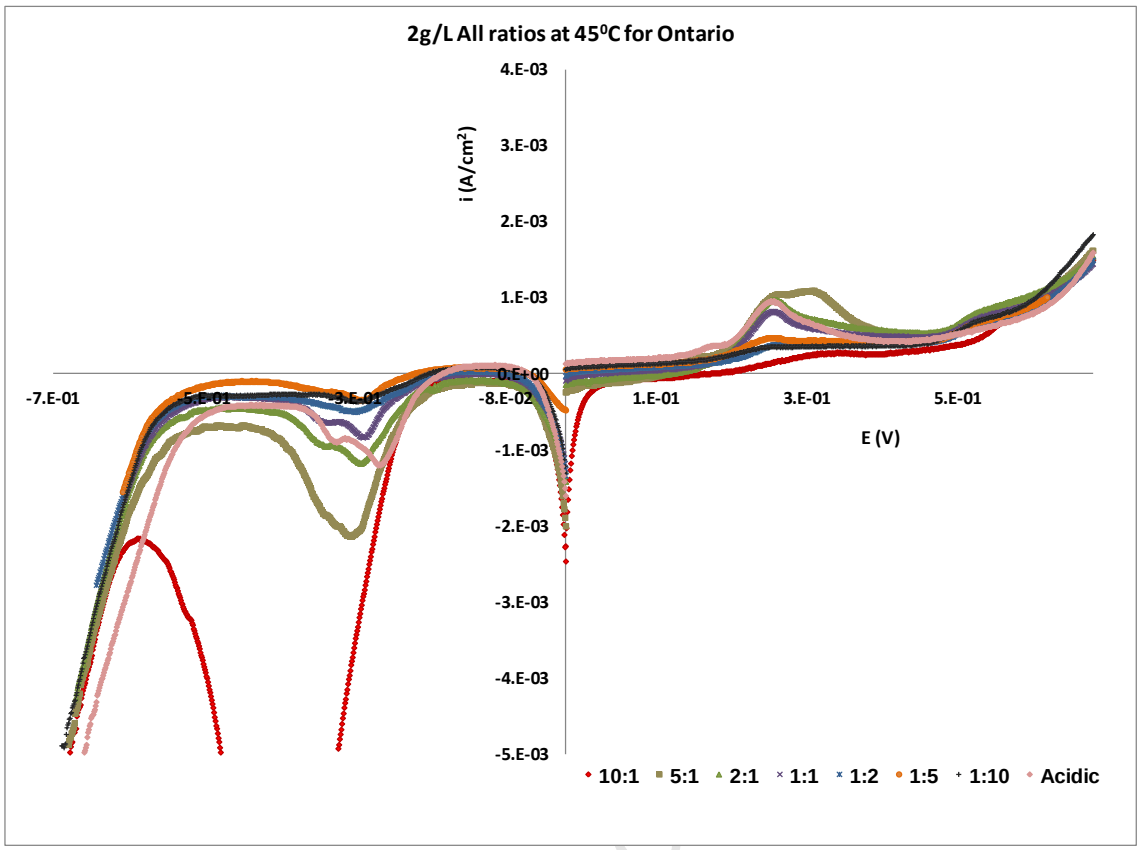

Figure B-14 45 °C

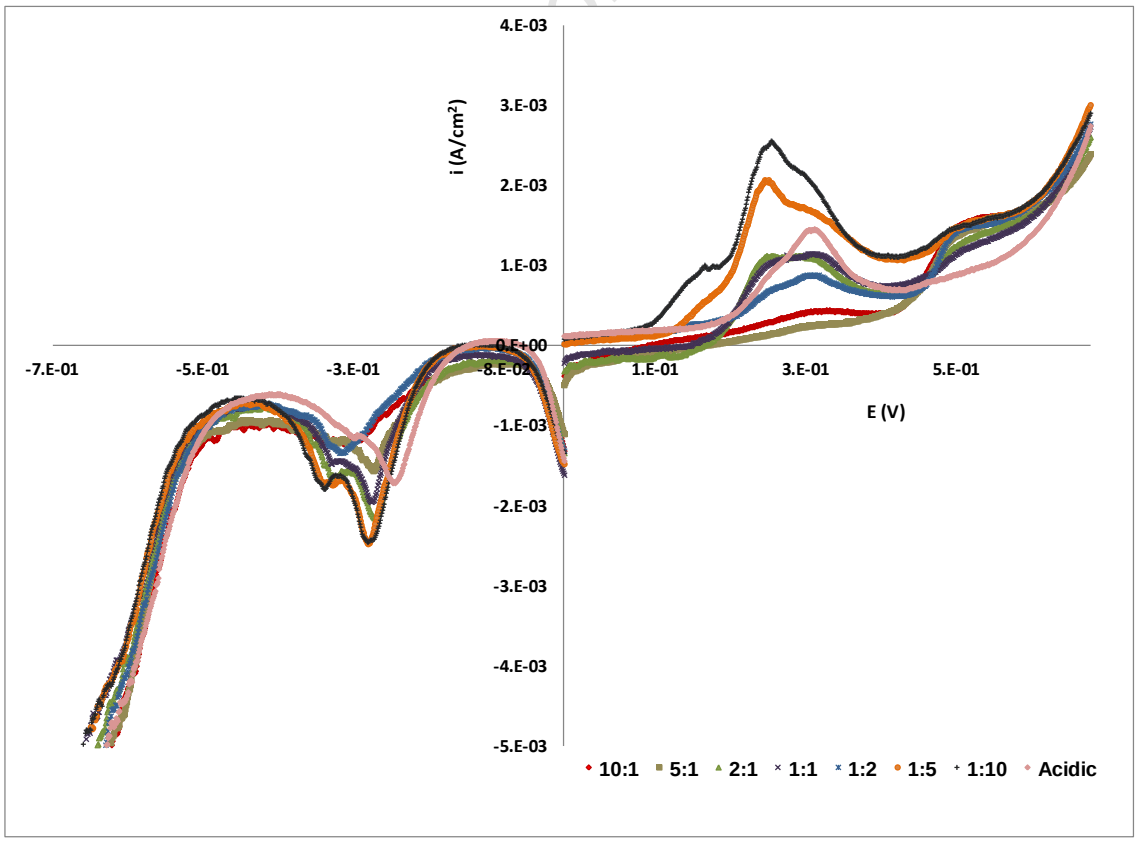

Figure B-15. 65 °C

5 g/L Total Fe concentration

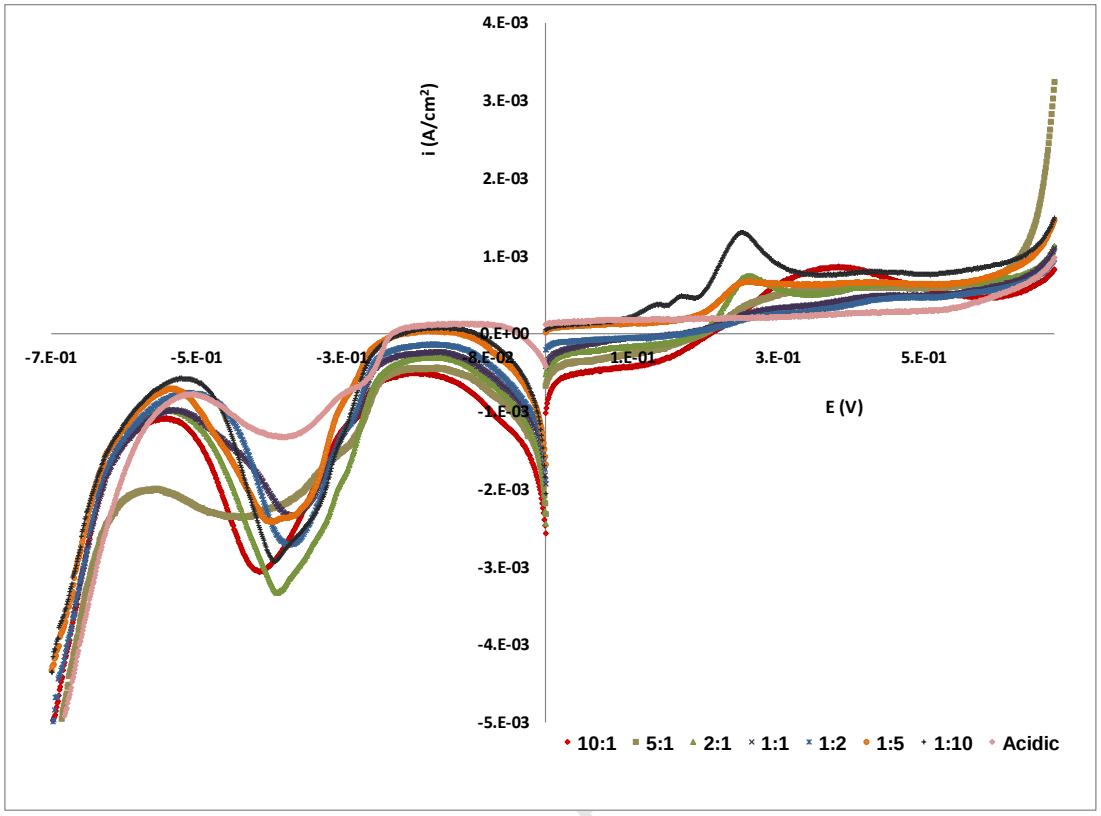

Figure B-16. 25 °C

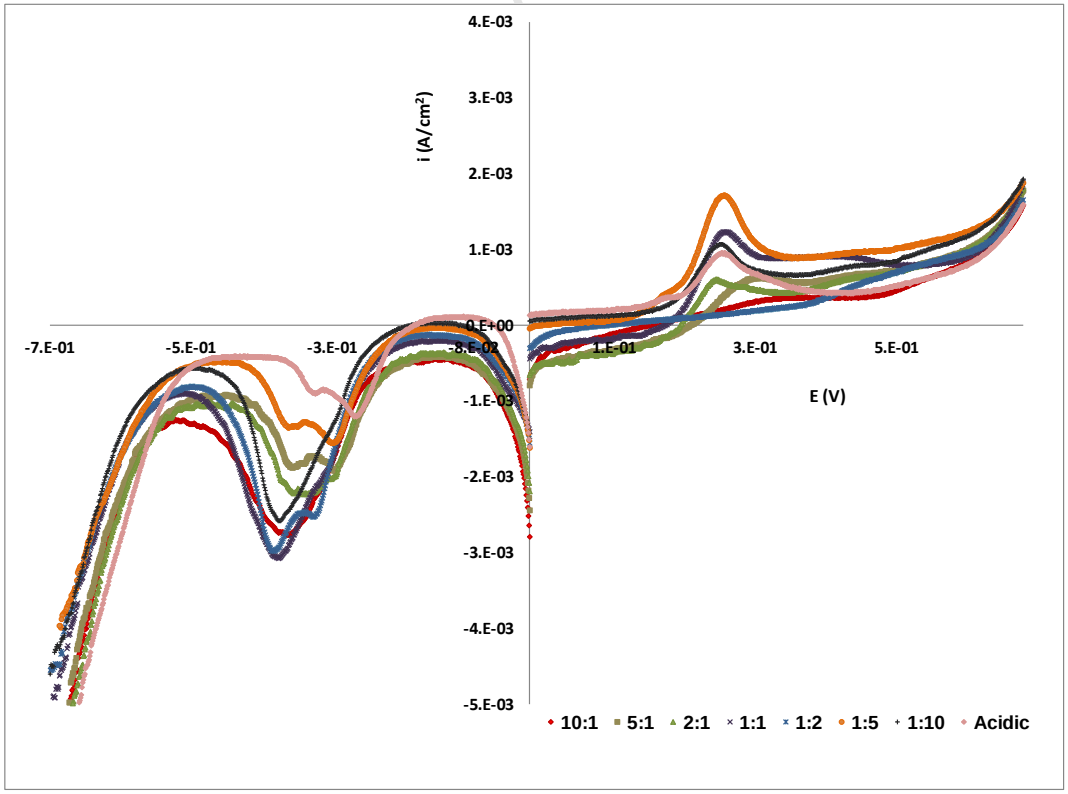

Figure B-17. 45°C

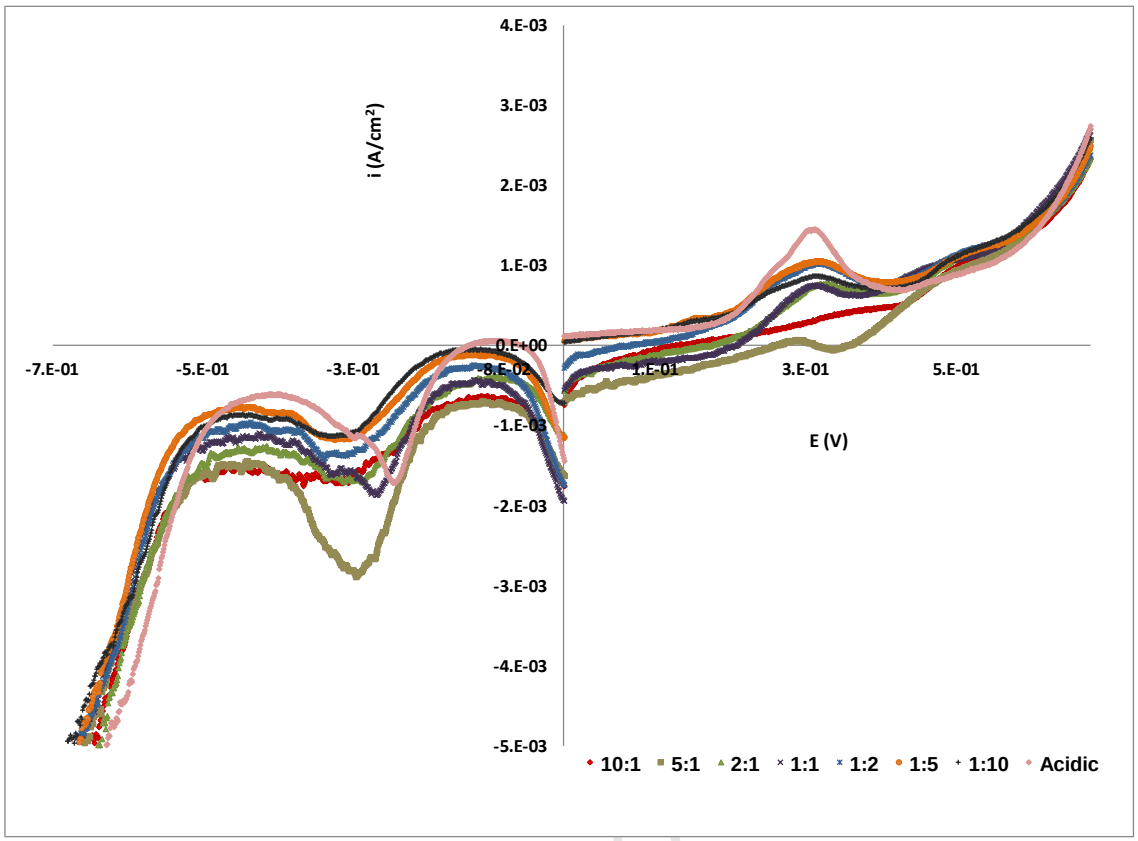

Figure B-18. 65°C